Universitat Autònoma de Barcelona

ER+ metastatic breast cancer targeted therapy: biomarkers of response and mechanisms of resistance to PI3K and FGFR inhibitors

Mònica Sánchez Guixé

Universitat Autònoma de Barcelona

Facultat de Medicina

Departament de Bioquímica I Biologia Molecular

Programa de Doctorat en Bioquímica, Biologia Molecular i Biomedicina

ER+ metastatic breast cancer targeted therapy: biomarkers of response and mechanisms of resistance to PI3K and FGFR inhibitors

Thesis presented by Mònica Sánchez Guixé for the degree of Doctor of Philosophy (PhD) in Biochemistry, Molecular Biology and Biomedicine by Universitat Autònoma de Barcelona

Barcelona, 2019

PhD candidate

Mònica Sánchez Guixé

Thesis tutor

Dr José Ramon Bayascas Ramírez

Thesis director

Dr Violeta Serra Elizalde

Thesis co-director

Dr Mariona Graupera Garcia-Milà

Thesis co-director

Dr Jordi Rodon Ahrnet

Strangers passing in the street

By chance two separate glances meet

And I am you and what I see is me

And do I take you by the hand

And lead you through the land

And help me understand the best I can

Echoes – Pink Floyd

A la meva família

Però sobretot:

A la iaia Maria, qui ja ha marxat

I a la Joanna, qui acaba d'arribar

Acknowledgements

Arribats aquests moments fa especial il·lusió pensar en tota la gent que ha sigut partícip del meu camí cap al doctorat. Ha sigut molta gent, d'abans i durant. Espero que aquestes paraules arribin a tothom qui m'ha ajudat a fer-me com a científica, persona, amiga i companya.

Primer de tot, voldria agraïr a la meva directora de tesi, Violeta Serra. Sense la seva determinació i anàlisi al detall aquesta tesi no hagués estat possible. En segon lloc, agraïr als meus co-directors, Mariona Graupera i Jordi Rodon, els quals han estat peces claus en el raonament experimental i l'anàlisi de dades. Gràcies per els vostres consells i revisions. M'agradaria també agraïr el meu tutor, José Ramon Bayascas, per el seu suport i ajuda cada cop que l'he necessitat.

Seguidament, i molt important, voldria agraïr a la meva companya de projecte, Cinta Hierro. Moltes gràcies per els teus ànims i la teva positivitat, realment són útils en moments difícils. Ha sigut un plaer intercanviar idees i complementar-nos en coneixements clinico-mol·leculars.

Voldria també agraïr a la comissió de seguiment del doctorat, que m'ha ajudat a agafar perspectiva i identificar punts febles i millorar: Héctor G. Palmer, José Miguel Lizcano i Josep Lluis Parra.

Agraïr també als meus companys del laboratori de teràpies experimentals (ETG), on he trobat un munt de gent molt especial i un gran equip. Primer de tot, a la Laia Monserrat, qui m'ha ajudat substancialment en la part experimental. Ha sigut un plaer planejar experiments amb tu, seràs una gran científica. A la Marta Palafox, de quien aprendí tan solo aterrizar en el laboratorio, y de quien sigo aprendiendo. A l'Albert Gris, per tots els consells i estar disposat sempre a donar-me un cop de mà. A tots en conjunt, el PI3K team: m'encanta fer brainstorming amb vosaltres, sou genials!

No me quiero olvidar de las manos técnicas del laboratorio: Marta Guzman, Olga Rodriguez, Judit Grueso i Mireia Parés. Muchas gracias por todo lo que me habéis enseñado. Siempre estáis dispuestas a ayudar y a afrontar los problemas con altura y determinación. Trá, trá!

Quiero tambien agradecer a la otra mitad del laboratorio: el BRCA team. A Marta Castroviejo, muchas gracias por todos los consejos, sobretodo en el último tramo del doctorado. A l'Alba Llop, admiro el teu pensament crític i la teva manera de fer ciència, ets una font d'inspiració. A la Cristina Cruz, els teus consells i ànims són molt útils, tothom necessita que li diguin que fa una feina ben feta de tant en quant, i tu sempre t'enrecordes. A Benedetta Pellegrino, ha sido un placer tenerte en el laboratorio, las risas que nos hemos echado son inolvidables. A Giulia, conocerte ha sido un placer, eres una gran persona. A Flaminia Pedretti, siempre es agradable hablar contigo, y Andrea Heredia, que el poco tiempo que lleva con nosotros ya ha demostratdo ser una gran persona.

No quería olvidarme tampoco de Alberto Cedro, que estuvo brevemente en el laboratorio pero considero que ha sido una gran ayuda para entender los análsis de comparaciones múltiples. Gracias por tus conocimientos, y por la ayuda prestada.

Voldria agraïr també al laboratori del meu primer secondment: el laboratori de Mariona Graupera, Angiogenesis Tumoral en IDIBELL. Va ser un plaer estar allà amb tots vosaltres. Especialmente querría agradecer a Erika Monelli, por sus consejos y ayuda en el laboratorio.

I would like to thank the host laboratory for my second secondment: the laboratory of Len Stephens and Philip Hawkins at Babraham Institute, Cambridge, UK. Thanks for all the advising and suport. It was a great experience to be there. També voldria agraïr a David Barneda, qui em va guiar i ajudar en l'anàlisi de mostres dels PIPs i sobretot durant el perillós procés de derivatització dels fosfolípids. Aquestes coses sempre fan respecte.

I want to as well thank all the PHD (PI3K biology in Health and Disease) consortia, specially to all the ESR colleagues: Piotr Kobiałka, Piotr Jung, Fernanda Ramos, Silvia Arucci, Elena Rebollo, Paula Samsó, Abhishek Derle, Albert Mackintosh, Cristina Courrèges, Vasugi Nattarayan, Jasmina Zanoncello, Charis Kampyli, Erhan Keles and Iosif Serafemidis. We had a great time together, it was an amazing expierence to meet you all guys! Però sobretot a

la Laia Muixí, una project manager estupenda. Segueix així, fas que tothom s'ho passi molt bé sempre, un plaer haver-te conegut.

Agraïr també a tots els companys i amics del VHIO: a la «guardería del VHIO», per tots els ànims que heu donat en moments difícils, em feu saber que no estic sola i que aquesta experència és compartida entre tots nosaltres. Les birres afterwork han ajudat moltíssim! Sobretot voldria agraïr a dues companyes de procés final de tesis: Estefania i Gemma, gràcies per fer-me costat fins al final. També a la gent amb la que vaig compartir l'estància a Albufeira a la Summer School in Translational Research. Als membres del VHIO running, que encara que no m'apunti tant com voldria, sé que sempre m'animeu. I a todo el VHIO birras, y a los que se esfuerzan para organizar los VHIO findes. Gracias a todos, os aprecio muchísimo.

Tambien, querría agradecer de forma especial a mis amigos de toda la vida, y con ello me refiero a las grandes constantes en mi vida desde que me fui de Blanes: Melisa, Juanmi, Momo, Mauro, Poke, Huke, Uri, Isma, Alberto y Álvaro. No importa donde me vaya la próxima vez, siempre que vuelvo estáis ahí para echar unas birras y eso es de agradecer.

Voldria també agraïr les grans amistats que m'ha brindat la ciutat de Barcelona: la Rosie, una de les grans amistats de la meva vida, podria dir. Vam connectar un dia i desde llavors no ens hem separat. Et tinc sempre molt en compte. Miguel, un placer haberte conocido, eres un gran conversador y gran científico. Tu honestidad te horna. Priscila, muchas gracias por todos los momentos de apoyo moral, tan necesarios para la vida de un doctorando. Quedar contigo y conversar ha sido de gran ayuda para seguir adelante con éste proceso.

No querria olvidarme de todas aquellas amistades surgidas en Noruega, el lugar donde he aprendido más cosas de toda mi vida. Khadija, eres otro gran pilar en mi vida, gracias por todas ésas conversaciones tan profundas. El tiempo pasa, la distancia aparece, pero nosotras seguimos como siempre. Y seguimos gritando igual! A la gente del Fishmarket, Ona, Georgina, Patri y Diana, fuisteis parte de mi gran aventura! Quien diria que se puede aprender tanto tan sólo vendiendo pescado. Ése mercado ha sido uno de los grandes puntos de inflexión de mi vida. A todas las demás amistades recogidas por el camino: Guille, Coralie, Aurora, Belén, Antonio, Mikel y África, que aunque la vida nos lleve a tantos lugares distantes del planeta, seguimos igual de cercanos en la amistad. A Lolo, has sido parte de

mi vida durante estos últimos 5 años, no lo olvidaré. Siempre tendrás una amiga con la que contar. Se te echa de menos pero también se te desea lo mejor en la vida.

As well I would like to thank the special friendships from Sweden: Lauma, Zane and Cristina. I have great memories from you. It is great to keep in touch with you girls, we were a very good team in Lund.

Per últim i més important, a la meva família: mama, papa, Dani i Alba. Sempre m'he sentit molt orgullosa de tots vosaltres. Per molt lluny que la vida em porti sempre sentiré que tinc una gran familia al darrere que em fa costat en cada decisió que prengui. A l'Anna i en Marc, és genial tenir-vos també a vosaltres, gràcies per formar part de Can Guixé. I a la petita Joanna, que espero sàpiga i entengui algún dia tot el que l'estimo. I sobretot als meus avis, que encara que ja no hi siguin, han format part de la meva vida i els recordo molt. Estic segura que si la iaia Maria hagués nascut avui dia hagués estat capaç d'aconseguir qualsevol cosa que es proposés.

De tot cor, gràcies a tothom que m'ha fet fer a mi mateixa, us tinc sempre present.

Summary

Endocrine therapy has been one of the major advances in the treatment of breast cancer (BC) for the past 30 years. However, patients eventually relapse due to mechanisms of resistance. These involve several pathways related to proliferation and growth, including the PI3K/mTOR and FGFR pathways.

The PI3K pathway is frequently altered in BC, especially in the luminal setting where 30-40% of patients harbor *PIK3CA* mutations. Specific inhibitors targeting key nodes in the PI3K pathway have been developed, such as mTOR and PI3K inhibitors (PI3Kinh). Clinical trials combining these inhibitors with endocrine therapy showed improved responses, leading to FDA approval of some of these inhibitors for metastatic ER+ BC. However, mechanisms of resistance are a major concern. In this sense, alterations downstream PI3K or in parallel pathways are recurrent in the metastatic disease, and it is important to understand if they confer resistance to PI3K inhibitors. Another common alteration in luminal BC is the amplification of the 11q13 amplicon, containing important genes for proliferation such as *CCND1*, *FGF3/4/19*, *PAK1* and *RPS6KB2*, whose impact on PI3K sensitivity is unknown.

FGFR1 amplification is found in 10% of metastatic luminal BC. Specific inhibitors against FGFR1/2/3 (FGFRinh) have shown limited efficacy in the *FGFR1*amp BC. This is in contrast with the clinical efficacy observed previously with Multi-targeted Tyrosine Kinase Inhibitors (MTKI, targeting FGFR, VEGFR and PDGFR families), albeit these agents showed severe adverse effects.

In this study, we investigated mechanisms of resistance to PI3Kinh and biomarkers of response to FGFRinh. In the first part, we determined the antitumoral activity of alpelisib, an α-specific PI3Kinh, in a cohort of 24 genetically annotated Patient-Derived Xenografts (PDX). We observed an aggregation of genetic alterations downstream PI3K and 11q13 amplifications among the resistant models and validated these with in vitro models as mechanisms of resistance to alpelisib, including overexpression of cyclin D1 and high FGF-signaling. In addition, in 2 out of 3 PDX models with putative mTORC1 activating alterations,

we observed higher efficacy of an mTORC1/2 inhibitor (mTORC1/2inh) compared with a PI3Kinh.

In the second part of this thesis we analyzed the antitumor activity of an FGFRinh, rogaratinib, in a cohort of 17 PDX harboring amplifications in *FGFR1/4* and/or *FGF3/4/19* (11q13 amplicon). Amongst the potential biomarkers of response tested (FGFR1-4 gene copy number, *FGFR1-4* gene expression, and FGF ligand co-amplification and expression), we identified that high mRNA of FGFR1-4 could predict for FGFRinh response. We compared rogaratinib efficacy with a MTKI, lucitanib, and we observed higher efficacy of lucitanib across 7 models. We further analyzed the mode of action of rogaratinib *vs.* lucitanib and we observed an increased blockade of proliferation and vascularization under lucitanib treatment. However, when testing an antiangiogenic therapy in two rogaratinib-resistant models, similar levels of efficacy as with lucitanib monotherapy were achieved, suggesting that lucitanib efficacy was due to the blockade of the vascularization in both models.

In conclusion, we established that PDX models harboring genetic alterations consistent with mTORC1 activation (e.g. *TSC1*del) are resistant to PI3Kinh but sensitive to an mTORC1/2inh and that cyclin D1 overexpression, high FGF and both alterations together result in resistance to PI3Kinh. We further determined that high mRNA of FGFR1-4 predicts for FGFRinh response and that a MTKI exhibits higher efficacy than specific FGFRinh due to a higher blockade of proliferation and vascularization. These results will help for a better patient selection in future clinical trials for ER+ BC targeted therapy.

Resum

La teràpia endocrina és un dels majors avenços en el tractament de càncer de mama (CM) dels últims 30 anys. Tot i això, les pacients acaben recaient degut a mecanismes de resistència, com ara les alteracions de la via de PI3K/mTOR i de FGFR.

La via de PI3K està freqüentment alterada en CM, especialment en el conjunt luminal on el 30-40% de les pacients tenen mutacions al gen *PIK3CA*. S'han desenvolupat inhibidors específics d'mTOR i de PI3K (PI3Kinh), i alguns han sigut aprovats per la FDA per a CM ER+ metastàtic. Tanmateix, mecanismes de resistència han estat limitant la resposta. En aquest sentit, alteracions posteriors o en paral·lel a PI3K, com la amplificació de la regió 11q13, són recurrents en CM metastàtic i és important esbrinar si aquestes confereixen resistència a PI3Kinh.

L'amplificació de *FGFR1* es troba en 10% dels casos de CM metastàtic. Inhibidors específics contra FGFR1/2/3 (FGFRinh) han mostrat una eficàcia limitada en el conjunt d'amplificats de *FGFR1*. D'altra banda, els inhibidors multi-tirosina quinasa (MTKI, específics per a les famílies de FGFR, VEGFR i PDFGR) han mostrat una millor eficàcia però amb més toxicitat.

En aquest estudi, hem investigat mecanismes de resistència a PI3Kinh i biomarcadors de resposta a FGFRinh. En la primera part, hem determinat l'activitat antitumoral d'alpelisib, un PI3Kinh específic per a la isoforma α, en una cohort de 24 xenògrafts derivats de tumor de pacient (PDX). Hem detectat una agregació d'alteracions posteriors a PI3K i amplificacions en l'11q13 entre els models resistents i les hem validat en models in vitro, incloent la sobreexpressió de ciclina D1 i FGFs. A més, 2 de 3 models PDX amb alteracions possiblement activadores d'mTORC1 han mostrat una eficàcia superior amb l'inhibidor d'mTORC1/2 (mTORC1/2inh) en comparació amb l'PI3Kinh.

En la segona part d'aquesta tesi hem analitzat l'activitat antitumoral d'un FGFRinh, rogaratinib, en una cohort de 17 PDXs que contenen amplificacions en *FGFR1/4* i/o *FGF3/4/19* (l'amplicó 11q13). D'entre els potencials biomarcadors de resposta analitzats (nombre de còpies de gen de *FGFR1-4*, expressió gènica de FGFR1-4, i co-amplificació i expressió de lligands FGF), hem identificat que alts nivells de mRNA de FGFR1-4 prediuen la resposta a FGFRinh. Hem comparat l'eficàcia de rogaratinib amb un MTKI, lucitanib, on

hem observat una millor eficàcia. A més, hem observat un elevat bloqueig de proliferació i vascularització amb lucitanib. Testant teràpia antiangiogènica en dos models resistents a rogaratinib, hem observat nivells similars d'eficàcia al lucitanib, suggerint que la resposta a lucitanib és deguda al bloqueig vascular en ambdós models.

En conclusió, hem determinat que models que contenen alteracions activadores d'mTORC1 (e.g. *TSC1*del) són resistents a PI3Kinh però sensibilitzen a mTORC1/2inh i que la sobreexpressió de ciclina D1, FGF i ambdues alteracions generen resistència a PI3Kinh. Tanmateix, hem determinat que nivells alts d'mRNA de FGFR1-4 prediuen la resposta a FGFRinh i que els MTKI presenten millor eficàcia degut a un elevat bloqueig de la proliferació i la vasculatura. Creiem que aquests resultats ajudaran a millorar la selecció de pacients en futurs assajos clínics de teràpia dirigida a CM ER+.

Abbreviations

AI	Aromatase Inhibitor
AKT	AKT Serine/Threonine Kinase 1
AMP	Adenosine Monophosphate
AMPK	AMP-activated protein kinase
ATP	Adenosine Triphosphate
BC	Breast Cancer
bFGF	Basic Fibroblast Growth Factor
CAF	Cancer-associated Fibroblasts
CCND1	Cyclin D1 gene
CDK4	Cyclin Dependent Kinase 4
CDK6	Cyclin Dependent Kinase 6
CDK4/6inh	Cyclin Dependent Kinase 4 and 6 inhibitor
CI	Confidence Interval
CNTL	Control
CoA	Co-Activator
CSC	Cancer Stem Cell
CSF-1R	Colony Stimulating Factor 1 Receptor
DCIS	Ductal Carcinoma In Situ
DNA	Deoxyribonucleic Acid
E_2	Estrogen
eBC	early Breast Cancer
ECM	Extracellular Matrix
EMT	Epithelial-Mesenchymal Transition
ER	Estrogen Receptor
Erα	Estrogen Receptor α isoform
ERE	Estrogen Receptor Element
Erk	Extracellular Signal-Regulated Kinases

ESR1	Estrogen Receptor 1 gene
ERBB2	Erb-B2 Receptor Tyrosine Kinase 2 gene
FC	Fold-change
FDA	Federal Drug Administration
FGF	Fibroblast Growth Factor
FGFR	Fibroblast Growth Factor Receptor
FGFRinh	Specific pan-FGFR inhibitor
FKBP12	12 KDa FK506-binding protein
FOXO	Forkhead box subclass O
FRS2	FGFR substrate 2
GAB1	GRB2-Associated Binding protein 1
GR	Glucocorticoid Receptor
GRB2	Growth factor Receptor-Bound-2
HCC	Hepatocellular Carcinoma
HDAC	Histone Deacetylase
HPSGs	Heparan Sulphate Proteoglycans
HR	Hormone Receptor*
HER2	Human Epidermal growth factor Receptor-type2
IDC	Invasive Ductal Carcinoma
Ig	Immunoglobulin domain
IGF	Insulin Growth Factor
IGF1R	Insulin Growth Factor Receptor 1
IGFR	Insulin Growth Factor Receptor
ILC	Invasive Lobular Carcinoma
INPP4B	Inositol Polyphosphate 4-Phosphatase type II
IRS	Insulin Responsive Element
LKB1	Liver Kinase B1
LCIS	Lobular Carcinoma In Situ
MAPK	Mitogen Activated Kinase

mAb	monoclonal Antibody
mBC	metastatic Breast Cancer
MEK	Mitogen-activated protein kinase kinase
MLL3	Myeloid/Lymphoid Or Mixed-Lineage Leukemia Protein 3
mRNA	messenger RNA
MTKI	Multitarget Tyrosine Kinase Inhibitor
mTOR	Mammalian Target of Rapamycin
mTORC1	mTOR Complex 1
mTORC2	mTOR Complex 2
NDRG1	N-myc downstream-regulated gene 1
OS	Overall Survival
P70	70kDa Polypeptide
PAK1	P21 Activated Kinase 1
PAM	PI3K/AKT/mTOR
PARP	Poly [adenosine diphosphate-ribose] polymerase
PD1	Programmed cell Death protein 1
PDGFRα	Platelet Derived Growth Factor Receptor α
PDGFRβ	Platelet Derived Growth Factor Receptor β
PDK1	Pyruvate Dehydrogenase Kinase 1
PDL1	Programmed cell Death protein Ligand 1
PDO	Patient-Derived Organoid
PDX	Patient-Derived Xenograft
PFS	Progression Free Survival
PgR	Progesterone Receptor
PI3K	Phosphoinositide 3 Kinase
PI3Kinh	Phosphoinositide 3 Kinase inhibitor
PI3Kα	Phosphoinositide 3 Kinase α isoform
PI3Kβ	Phosphoinositide 3 Kinase β isoform
PI3Kγ	Phosphoinositide 3 Kinase γ isoform

PI3Kδ	Phosphoinositide 3 Kinase δ isoform
PIK3CA	Phosphatidylinositol-4,5-Bisphosphate 3-Kinase Catalytic Subunit Alpha
PIM	Serine/Threonine-Protein Kinase Pim
PIP	PtdIns(4)P
PIP2	PtdIns(4,5)P_2
PIP3	PtdIns(3,4,5)P_3
PKC	Protein kinase C
PLCγ	Phospholipase C γ
PtdIns	Phosphatidylinositol
PTEN	Phosphatase and tensin homologue deleted on chromosome 10
Rb	Retinoblastoma protein
RET	Rearranged During Transfection
RTK	Receptor Tyrosine Kinase
RNA	Ribonucleic acid
ROG	Rogaratinib
RPS6KB2	Ribosomal Protein S6 Kinase B2 gene
RSK3	Ribosomal Protein S6 Kinase A2
RSK4	Ribosomal Protein S6 Kinase A4
RTK	Tyrosine Kinase Receptors
S6K	Ribosomal protein S6 Kinase
S6K1	P70 Ribosomal protein S6 Kinase Alpha
S6K2	P70 Ribosomal protein S6 Kinase Beta
SERD	Selective Estrogen Receptor Degrader
SERM	Selective Estrogen Receptor Modulator
SGK1	Serum/Glucocorticoid Regulated Kinase 1
SGK3	Serum/Glucocorticoid Regulated Kinase 3
SOS	Son of Sevenless
STAT	Signal Transducer and Activator of Transcription
STK11	Serine/Threonine kinase 11

TK	Tyrosine Kinase
TKI	Tyrosine Kinase Inhibitor
TNBC	Triple Negative Breast Cancer
TSC1	Tuberous Sclerosis Complex Subunit 1
TSC2	Tuberous Sclerosis Complex Subunit 2
VAF	Variant Allele Frequency
VEGF	Vascular Endothelial Growth Factor
VEGFR	Vascular Endothelial Growth Factor Receptor

Index

Introduction

1. Breast cancer background

1.1. The healthy breast

1.1.1. Anatomy and function

The mammary glands or breasts are organs which serve as a nourishing source for the offspring of the mammals. They are present in the female individuals of the species, and produce a secretion that contains the basic nutrients for the complete development of the offspring: the milk[1].

These organs undergo postnatal development when they are stimulated through steroidal hormones, which are regulated by the ovaries that influence the reproductive function. The female breasts have different stages through life: at 20 years of age, they reach their developmental maturity; and at the age of 40, they begin an atrophic process, even before menopause is presented. In each menstrual cycle, the breasts undergo structural changes under the influence of the ovarian hormones. During pregnancy and lactation, major changes occur in order to fulfill the function of milk production: they increase in volume (increased glandular tissue) and they start producing milk. The milk production is stimulated through the secretion of prolactin from the pituitary gland and somatomammotropin from the placenta. When the female arrives at the menopause, several hormonal changes occur inducing the breast glandular tissue to regress and involute, being replaced by stroma[1].

The mammary glands are composed of 15 to 20 irregular lobes of branched tubuloalveolar glands (**Figure 1**). These lobes are all connected to the mammary papilla, or nipple, and are surrounded by fibrous bands of connective tissue. There is abundant fat tissue in the fibrotic tissue that connects with the dermis, and little fat in the connective tissue between the lobes. Each one of these glandular lobes produce milk, and connect to a duct which serves as a channel to the milk to go through into the nipple[1].

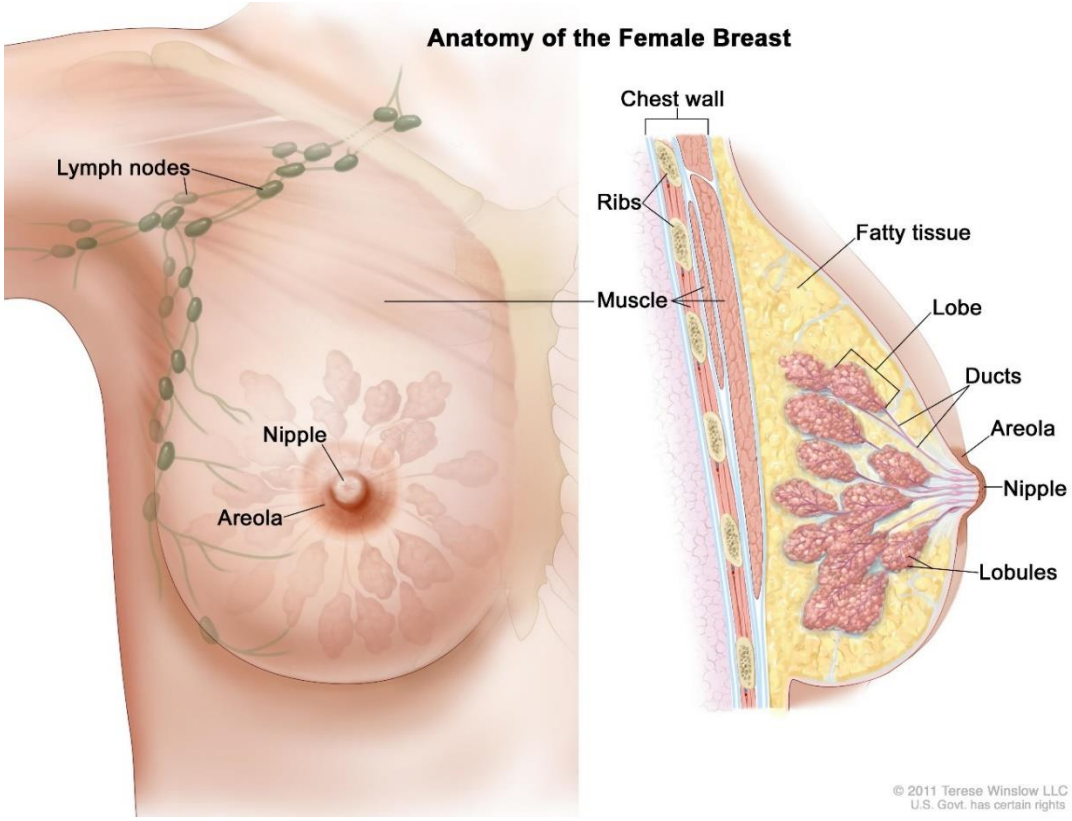

Figure 1. Anatomy of the Female Breast. The nipple is the end of all the ducts in the breast. Each duct connects with a glandular lobe, which produces milk. Abundant fat tissue is present in the surrounding area around the lobes. The axillary lymph nodes are located close to the glandular tissue of the breast. *Image taken from the National Cancer Institute © 2012 Terese Winslow LLC, U.S*

1.1.2. Hormonal regulation of the breast

At puberty, there is an enhanced production of estrogens and progesterone by the ovaries initiating the development of the mammary gland. In each menstrual cycle, there are minor changes in the morphology of the glandular tissue. During pregnancy, there is a continuous production of estrogens (stimulated by the placenta and the corpus luteum) and progesterone, which will further produce the development of the mammary gland. At parturition, there is a reduction of circulating estrogens and progesterone hormones, as well as a degeneration of the corpus luteum and placenta. An increased secretion of prolactin and adrenal cortical steroids stimulate the secretion of milk. When the infant initiates the act of suckling, there is a generation of impulses from receptors in the nipple, which will provide the hormonal feedback regulation to continue producing milk. Also, these impulses cause the release of oxytocin which stimulates the myoepithelial cells, causing them to contract and eject milk. The mammary glands turn to an inactive state when the act of suckling ceases[1].

After menopause, the mammary gland becomes atrophied and involutes. The secretor cells of the alveoli degenerate and disappear due to the decrease of ovarian hormones in the body. Connective tissue is also degenerated and the number of stromal cells and collagen fibers lessens drastically[1].

1.2. Carcinogenesis in breast cancer

Breast cancer is a pathological uncontrolled cellular growth originating in the breast tissue, commonly from the ducts or the lobules. Breast cancer cells maintain similarities to the cells of the organism from which they are originated. DNA and RNA are similar, but not identical, causing the possibility to be ignored by the immune system[2].

Normal cells become cancerous through genetic modifications. These genetic alterations can occur spontaneously or they may be induced by environmental factors such as: nuclear radiation, electromagnetic radiation (microwaves, X-rays, Gamma-rays, Ultraviolet-rays, etc.), viruses, bacteria and fungi, parasites (due to tissue inflammation) irritation, heat, chemicals in the air, water and food, mechanical cell-level injury, free radicals, evolution and aging of DNA and RNA, etc. All of these factors can produce mutations that may start cancer. Cancer develops if the immune system is not able to detect cancer cells and/or the amount of cells produced is too great for the immune system to eliminate[2].

1.2.1. The genetics behind cancer

Many genes can start carcinogenesis if mutated. There are two main types[3-5]:

- Oncogenes are mutant genes able to induce cancer in animals. They derive from proto-oncogenes (previous to the mutation). These genes participate in cellular growth controlling proliferation pathways. Mutations in oncogenes are gain-of-function mutations. There are three main types of genetic modifications in proto-oncogenes that can transform them into oncogenes:
    - *Point mutations*: these are nonsynonymous mutations that substitute one amino acid for another (missense mutation) and creates a constitutively activated protein.

- *Gene amplification*: duplication or amplification of a region in the DNA that contains a proto-oncogene.

- *Chromosomal translocation*: refers to the fusion of different DNA regions that result in a fused gene/protein or a gene that is controlled by another promotor and becomes constitutively activated.

- Tumor-suppressor genes code for proteins that inhibit cell proliferation. Generally, mutations induce loss of function of these proteins. There are different types of mutations that can cause tumors suppressors loss-of-function; these are the most common:

  - *Point mutations*: Non-synonymous mutations that can either substitute one amino acid for another (missense mutation) or either create a premature STOP codon (nonsense mutation).

  - *Frame-shift mutations*: A gene loses its reading frame due to a small insertion or deletion of nucleotides (Indels). This gives an alternative reading frame from the Indel region creating a new sequence of amino acid that normally contain a premature STOP codon.

  - *Deep deletions*: Complete deletions of a whole gene or most of it, causing the absence of the protein in the cell.

Generally, mutations are more likely to cause loss-of-function rather than gain-of-function. But gain-of-function mutations need to be just in one allele to be oncogenic, while in the loss-of-function mutations, the other allele can conserve the function; only another deleterious mutation can lead to the complete absence of the protein function.

These alterations are somatic events, although some germ-line mutations can predispose for the development of cancer. Usually, a single genetic change is not sufficient for the development of a malignant tumor, but rather a multistep process of sequential alterations across time in many oncogenes and tumor suppressor genes.

Importantly, not all mutations in a cancer cell contribute to carcinogenesis. They can be classified in two major groups: *driver* and *passenger* mutations. Driver mutations confer growth advantage and have been positively selected during the evolutionary process of cancer. Passenger mutations are those alterations which do not contribute to cell growth or are of any advantage for cancer, but they were present in an ancestor cancer cell containing a driver mutation[6].

Driver mutations can occur in genes from several important pathways for cell proliferation, such as: *ligand/receptor* signaling, elements from the downstream *proliferation pathways* and the *cell cycle*. Growth factors, or ligands, are secreted by cells in order to send a signal to activate proliferation. They bind to a receptor present in the cell membrane of another or the same cell. This receptor will send a signal, through phosphorylation and conformational changes in a cascade of proteins, to activate the cell cycle in the nucleus. The cell cycle will perform a sequence of events enabling the cell to replicate its DNA giving two daughter cells with the same genetic information. In cancer, mutations in genes belonging to these pathways, such as *PIK3CA* in ER+ BC[7], can become oncogenic drivers[8].

Different type of tumoral cells can arise in a tumor; this is the so-called *tumor heterogeneity*. Different clones tend to exist in a single tumor. Each clone differs genetically from the other. This happens in an evolutionary way: from the initial cell and through sequential cell divisions, genetic mutations are appearing and different lineages with different background appear. This gives the advantage to the tumor to adapt at different environmental conditions: hypoxia, immune system attack and, importantly, treatments[9].

1.2.2. Tumor microenvironment

In a tumor, besides the initial clone and subclones of cancer cells, different cell types coexist to stimulate growth and progression of the tumor (**Figure 2**) [9, 10]:

- Cancer Stem Cells (CSC): These are progenitor cancer cells that have the capacity to adapt fast to environmental changes and can differ in sensitivity to different treatments.
- Cancer-associated Fibroblasts (CAFs): A sub-population of fibroblasts with a myofibroblastic phenotype. These CAFs remain in the tumor perpetually activated, unlike

the process of wound healing, where they are activated just to repair the tissue. These CAFs have relevant roles on cancer progression through remodeling the Extracellular Matrix (ECM), inducing angiogenesis, recruiting inflammatory cells, and directly stimulating cancer cell proliferation via the secretion of growth factors, immune suppressive cytokines, and mesenchymal-epithelial cell interactions.

- Immune and inflammatory cell: The immune system has the capacity to detect the early steps of carcinogenesis, attack and eliminate cancer cells. But eventually, the cells in the tumor learn to escape this system, and continue growing. Immune cells and inflammatory cells coexist in the tumor environment, producing a complex communication network involving cytokines and other receptor-ligand processes.

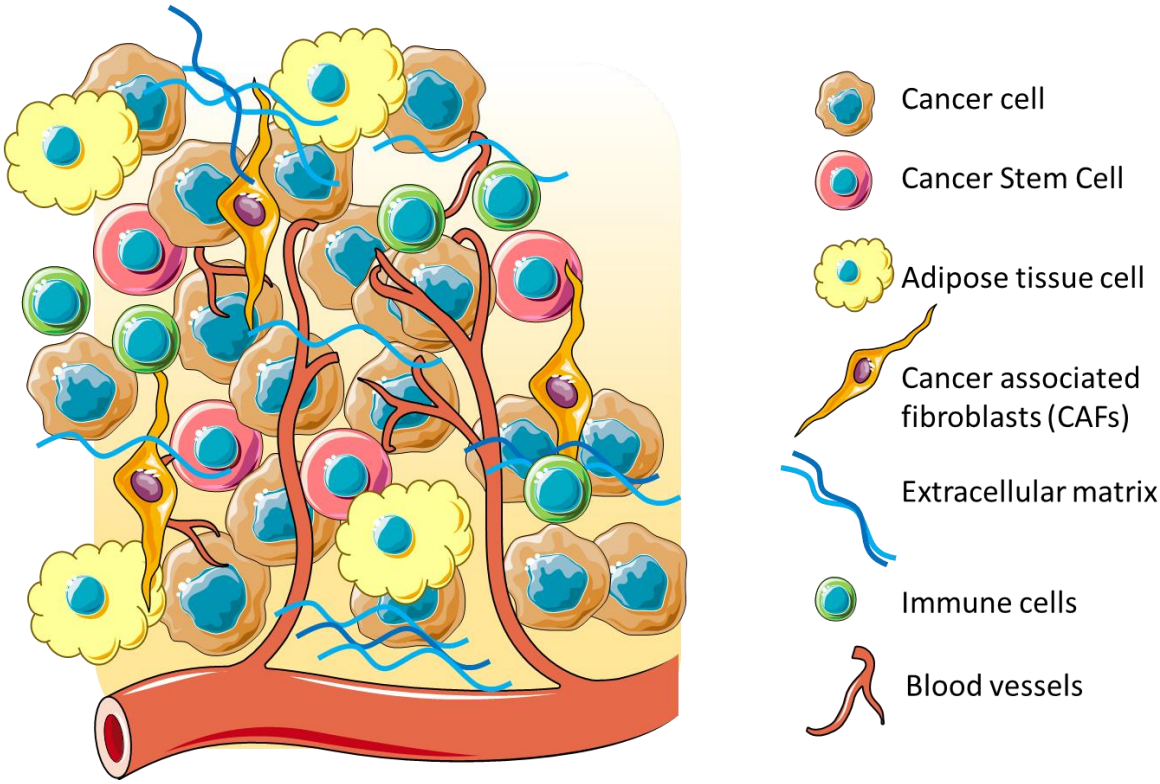

Figure 2. The tumor microenvironment. Tumoral cells coexist with other cell types to assist tumor growth. Cancer stem cells divide and produce the bulk of tumoral cells; Adipose tissue cells provide chemoattractants and proinflammatory signals; Cancer Associated Fibroblasts (CAFs) secrete several types of growth factors; immune cells, attracted by cytokines, aim to detect and destroy cancer cells; blood vessels provide nutrients necessary for growth; all these cells are sustained in extracellular matrix, containing fibrous proteins, such as collagen.

- The blood and lymphatic vascular cells: The blood and lymphatic networks provide oxygen and nutrients as well as removing carbon dioxide and metabolic wastes to sustain the necessary for the survival of the tumor. The complexity of the blood and lymphatic network increases via the process of angiogenesis: the growth of new blood vessels from pre-existing vessels.

- Adipose cells: White adipose tissue and adipocytes are found to be attracting proinflammatory elements, which are more prone for carcinogenesis. They secret more than 50 different cytokines, which facilitate the initiation of a tumor.

All of these cells (and others in minority) create the *tumor microenvironment*. They create a complex network of interactions in constant evolution. Overall, the components of the tumor environment affect directly to the tumor initiation, progression and metastasis.

Taking all this into account, *Hanahan et al* proposed 10 distinctive and complementary capabilities that enable the tumor to grow and derive metastasis; the 10 hallmarks of cancer[11, 12]:

1. Sustaining proliferative signaling: the ability to sustain chronic proliferation.

2. Evading growth suppressors: cancer cells must avoid the tumor-suppressor effect of many genes.

3. Resisting cell death: the ability to avoid natural cell death (apoptosis).

4. Enabling replicative immortality: cancer cells require unlimited replicative potential in order to generate macroscopic tumors.

5. Inducing angiogenesis: tumors require sustenance in the form of nutrients and oxygen as well as an ability to evacuate metabolic wastes and carbon dioxide.

6. Activating invasion and metastasis: carcinomas arising from epithelial tissues progress to higher pathological grades of malignancy, reflected in local invasion and distant metastasis.

7. Deregulating cellular energetics: uncontrolled cancer cell proliferation needs the corresponding readjustments in energy metabolism in order to provide the necessary for cell growth and division.

8. Avoiding immune destruction: the immune system is able to recognize and eliminate the great majority of initiating cancer cells but eventually some cancer cells develop the ability to avoid immune detection and therefore its eradication.

9. Genome instability and mutation: rates of mutation are often increased in cancer cells in order to acquire enough mutant genes for the evolutionary process of tumorigenesis.

10. Tumor promoting inflammation: immune cells, mainly from the innate immune system, secrete pro-inflammatory factors contributing to proliferative signaling, cell death limitation, angiogenesis, invasion and metastasis.

A tumor tends to progress and invade adjacent tissues and colonize as well distant locations. There is a sequence of events leading to the development of tumor invasion and metastasis. At certain point the tumor cells acquire the ability to penetrate the surrounding tissues. This tumor invasion occurs when the tumoral cells acquire the ability to pass through the basal membrane and the ECM. Eventually, tumoral cells penetrate the lymphatic or vascular circulation. These metastatic cells then start travelling through the circulatory system invading the vascular basement membrane and extracellular matrix in the process of extravasation. Eventually, these cells will attach to a new location and proliferate to produce the secondary tumor[13].

1.2.3. Cancer-originating tissues in breast

There are several types of tumors that may develop within different areas in the breast. Most tumors are the result of benign (non-cancerous) changes within the breast. The majority of breast cancers initiate from the cells that form the ducts (ductal cancers) and in the cells forming the lobules (lobular cancers), while a small number start in the other tissues[14].

There are two main subtypes of carcinoma depending on the site and the level of malignancy (**Figure 3**):

- Non-invasive Breast Cancer / Carcinoma *In Situ*:

The term "carcinoma *in situ*" refers to patterns of abnormal epithelial cell proliferation confined in the ductal and/or lobular structures of the breast. In Non-Invasive Breast cancer cells are confined to ducts/lobules and do not invade surrounding tissues of the breast. Depending on the localization of the lesion, we differentiate two categories[14, 15]:

- *Lobular Carcinoma In Situ (LCIS):* An increase in the number of cells within the milk glands (lobules) of the breast. The cells are confined inside the lobular structures of the breast. LCIS is less common and considered a marker for increased breast cancer risk.

- *Ductal carcinoma In Situ (DCIS):* The cells are confined inside the ductal structures of the breast. DCIS is the most common type of non-invasive breast cancer (90%).

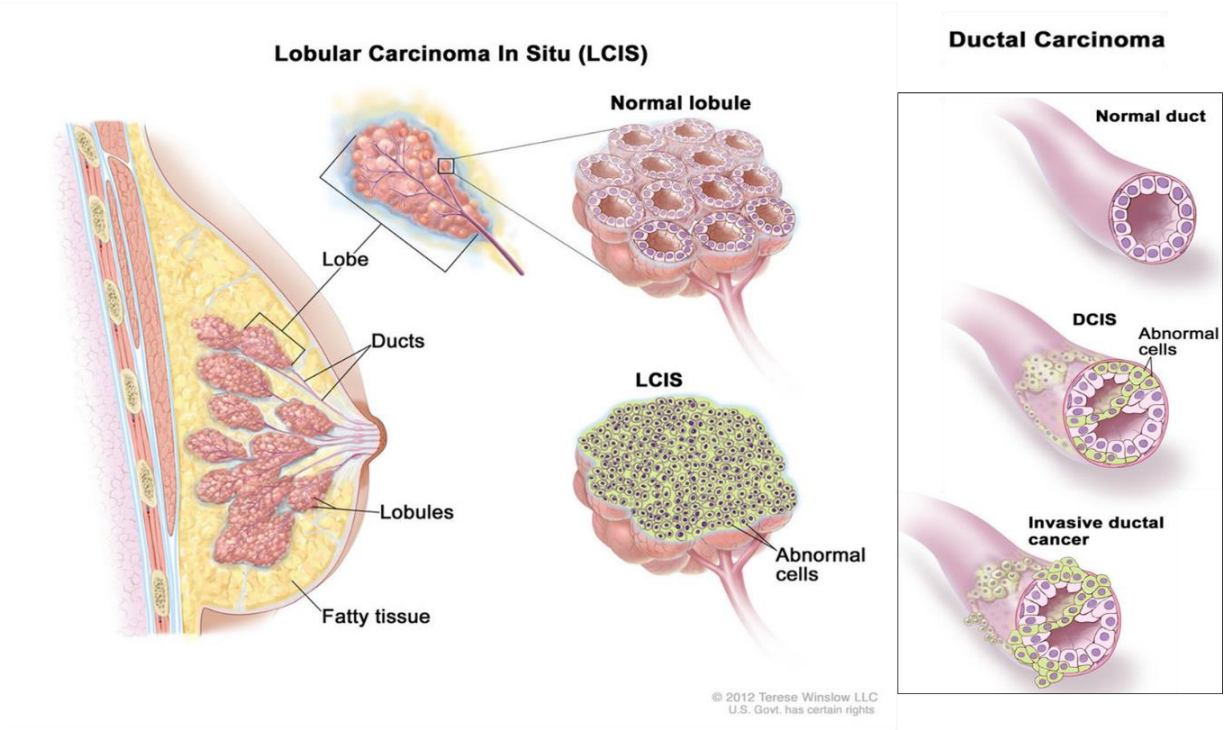

Figure 3. Types of breast carcinomas. Lobular carcinomas originate in the milk glands (lobes), while ductal carcinomas initiate in the ducts that transport the milk to the nipple. *In situ* refers to uncontrolled cell proliferation confined inside the lobes or ducts, while invasive carcinomas break the basal membrane of the epithelium and invade adjacent tissues. *Image modified from the National Cancer Institute © 2012 Terese Winslow LLC, U.S*

- Invasive Breast Cancer / Infiltrating carcinomas

The carcinoma is defined as infiltrating or invasive when it breaks through the basal membrane of the duct and lobular wall and invade the surrounding tissues of the breast. Cancer can be invasive without being metastatic to the lymph nodes or other organs[2, 15].

  - *Invasive / Infiltrating Lobular Carcinoma (ILC):* ILC initiates from the milk glands (lobules) of the breast, but have invaded adjacent tissues and often spreads (metastases) to other regions of the body. Approximately 5% to 15 % of invasive carcinomas are classified as invasive lobular (ILC).

  - *Invasive /Infiltrating Ductal Carcinoma (IDC):* IDC begins in the milk ducts of the breast and penetrates the wall of the duct, invading the adjacent tissues of the breast and possibly other regions of the body. This cancer subtype is the most common type of breast cancer, accounting for 80% of the breast cancer diagnoses.

Other less common types of breast cancer comprehend the 5% or less of breast cancer cases, such as Medullary Carcinoma (a type of invasive breast cancer), Mucinous Carcinoma (rare carcinoma formed by mucus-producing cancer cells) and Tubular Carcinoma (a special type of infiltrating / invasive breast carcinoma).

Male Breast cancer (MBC) is a rare disease worldwide. As a result of its rarity, it is treated similarly to female breast cancer, but important differences exist. The worldwide female-to-male incidence rate ratio of breast cancer is 122:1, although it can be significantly increased in patients with a genetic predisposition containing genes such as *BRCA1* and *BRCA2*[16]. MBC compared with female breast cancer occur later in life with higher stage, higher grade, and more estrogen receptor (ER)-positive tumors. The median age of onset in MBC is 72 years of age, compared with the 61 years in women[17].

1.3. Breast cancer molecular subtypes

Traditionally breast cancer has been classified according to the morphologic features. Despite the emerging era of personalized medicine and the availability of molecular testing, the traditional pathologic classification of infiltrating breast carcinoma remains valuable for

determining the treatment strategy. Molecular classifications have contributed to the paradigm that human breast cancer is not one disease. Breast cancer shows different molecular subtypes, each characterized by distinct gene expression profiles. This is very important because the patients with varying subtypes have different clinical outcomes, and each respond differently to certain treatments[2, 18].

1.3.1. Traditional Histopathological classification

The histopathological classification has been routinely used by the pathologists for the last 20 years. Still nowadays it is of enormous importance to identify the breast cancer subtype through the presence of different receptors in order to find the best treatment option: Estrogen Receptor (ER), Progesterone Receptor (PR) and Human Epidermal Growth Factor 2 (HER2) (**Figure 4**)[18-20].

- Luminal A: The luminal subtype comprises those cancers which express ER in at least 10% of the cells and PR in at least 20% of the cells. The subclass Luminal A is as well marked by low levels of proliferation markers (<14% Ki-67), and absence of HER2 amplification. This subtype comprehends the 40% of breast cancer cases.

- Luminal B: This group expresses ER (>10%), and may, or may not, co-express PR (<20%) and HER2. Luminal B tumors have higher level of expression of proliferation markers (>14% Ki-67) compared with luminal A. This subtype is among the 20% of breast cancers.

- HER2+: This group is characterized by the HER2 gene amplification (>2.2 ratio or >6 gene copies)/protein overexpression (3+ of IHC score). This subtype occurs in approximately 10% to 20% of breast cancers.

- Triple Negative Breast Cancer (TNBC): This group comprise those cancers which are negative for ER, PR and HER2. This group represents 10-15% of all invasive cancers.

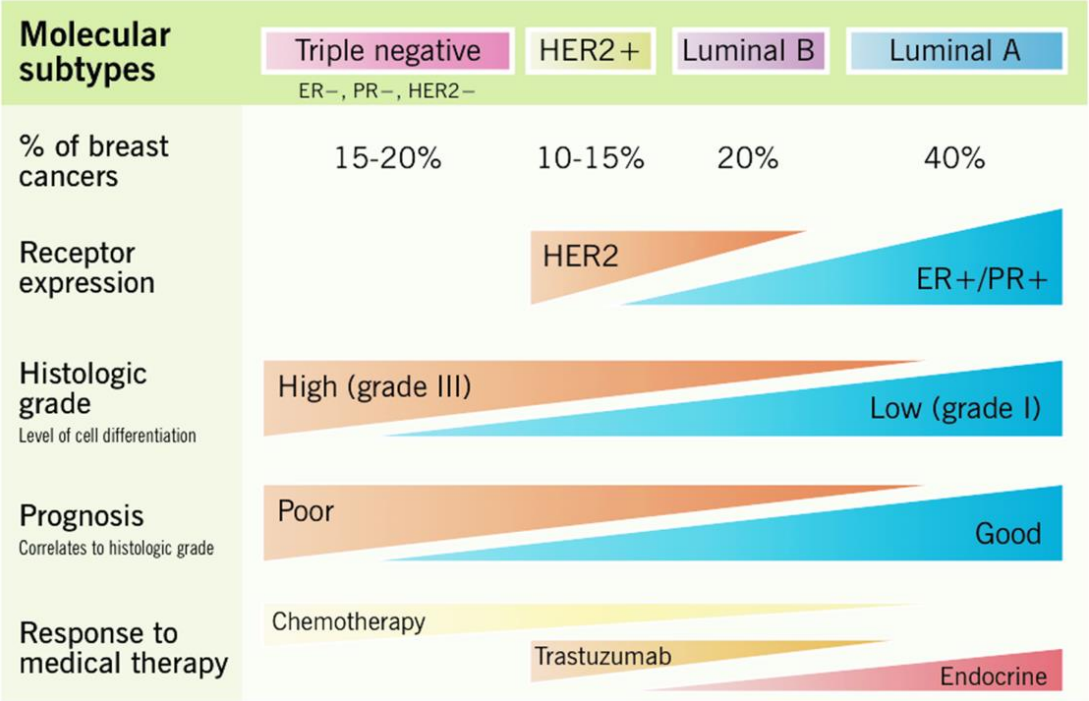

Figure 4. Molecular classification of breast cancer. Traditional histopathological classification distributes breast cancer in 4 groups: Luminal A, positive for hormonal receptors, with the best prognosis and sensitive to endocrine therapy; Luminal B, ER+ and PR+ but with high proliferation index, also responding to endocrine therapy; HER2+, expressing HER2 receptor and responding to HER2-targeted therapy; and Triple Negative (TNBC), expressing none of 3 biomarkers, with the worst prognosis and chemotherapy as the best treatment strategy. Figure taken from[21].

1.3.2. Intrinsic subtype classification

A key event in breast cancer research over the last two decades was the description of the so-called intrinsic breast cancer subtypes (luminal, basal-like, HER2-positive enriched and normal-like) employing microarray-based gene expression profiling[22], including subdivision of luminal tumors into A and B categories. The intrinsic subtypes differ in their genomic complexity, relevant genetic alterations and prognosis[18, 19]:

- Luminal: Luminal tumors harbor similarity to the expression profile of normal luminal breast epithelium. While luminal A overexpress ER-regulated genes and underexpress HER2 gene cluster and proliferation-related genes, luminal B have much lower expression of ER-related genes, a variable expression of HER2 cluster and relatively high expression of proliferation related genes.

- HER2-enriched: HER2 group is defined by high expression of HER2 and related genes.

- Basal-like: This subtype is generally characterized by expression of the high -molecular-weight cytokeratins CK 5/6 and CK14 together with EGFR, c-kit, FOXC1, frequent TP53 mutations and a high proliferation index. They show aggressive clinical behavior. This group shows the greatest diversity with respect to histopathological features, mutation profiles, response to chemotherapy, metastatic behavior and survival rates. Subtyping within this diverse basal-like category is important to delineate the biological characteristics of tumors and to identify targeted therapies. For instance, Lehmann et al[23] identified 6 TNBC subtypes: basal-like 1, basal-like 2, immunomodulatory, mesenchymal, mesenchymal stem-like and luminal androgen receptor.

- Normal-like: The normal-like subtype is characterized by expression of genes associated with adipose tissue and other stromal cell types. This is a controversial group and is thought by some authors to represent normal cell contamination of samples rather than a real intrinsic subtype.

Gene expression profiling to classify breast cancer has been of increased utility in daily clinical practice. In the last two decades, these gene expression profiles have been optimized to fewer genes in clinically applicable gene expression panel tests such as MammaPrint[24] (which can distinguish between good and poor prognosis using 70 genes), Oncoprint DX[25] (using 21 genes, patients are divided into 3 risk groups: low, intermediate and high), PAM50[26, 27](determines the intrinsic subtype and the risk of recurrence with 50 genes) and EndoPredict[28] (uses 11 genes to determine the molecular fingerprint of a tumor)[29].

2. Breast Cancer therapy

Breast cancer therapy depends on the molecular subtypes (Hormone –estrogen and progesterone– Receptor (HR) and/or HER2 positive or negative) and the level of malignancy (early or advanced/metastatic). For early breast cancer, the main goals of therapy are eradicating tumor from the breast and regional lymph nodes and preventing metastatic relapse. For metastatic breast cancer, the therapeutic goals are prolonging life and symptom palliation. Currently, metastatic breast cancer is considered incurable among all patients[30].

2.1. Local therapy

Local therapy is important for early disease, and it is only considered in metastatic cases for palliation approaches. There are two types of local therapy for nonmetastatic breast cancer: the surgical resection of breast tissue and/or axillary lymph nodes, and radiation, which is given after the surgery. Depending on the size of the tumor, localization or invasion of the cancerous tissue, and results from the sentinel lymph node biopsy (the closest lymph node to the breast) there will be different levels of tissue removal[30, 31]:

- Lumpectomy: Extraction of the tumor and some adjacent tissue, conserving most of the breast anatomy. This intervention is performed generally when the tumor is delimited in a specific area, and the sentinel lymph node biopsy resulted negative for cancer cells. After lumpectomy, radiation is given to the site where the tumor has been removed.
- Mastectomy: Extraction of the whole breast tissue. This intervention is performed when there is an extended invasion of the tumor tissue to adjacent areas, or if the sentinel lymph node biopsy resulted positive. In this case, axillary lymph nodes are removed and analyzed to determine the extension of the cancer invasion.

Radiation therapy in breast cancer may be delivered to the whole breast or a portion of the breast (after lumpectomy), the chest wall (after mastectomy), and the regional lymph nodes.

2.2. Systemic therapy

Systemic therapy follows the same treatment categories in both metastatic and nonmetastatic. In early breast cancer, treatment can be either adjuvant (treatment after surgery) or neoadjuvant (treatment before surgery). Depending on the breast cancer subtype, there will be different therapeutic strategies followed. Endocrine therapy is given for all HR+ tumors (with some patients requiring chemotherapy as well), trastuzumab-based HER2+ tumors (with endocrine therapy given in addition, if concurrent HR positivity), and chemotherapy alone for triple-negative breast cancer[30, 32].

2.2.1. HR+/HER2-

Endocrine therapy, which counteracts estrogen-promoted tumor growth, is the primary systemic therapy for HR+/HER2- breast cancer (**Figure 5**). Standard adjuvant endocrine therapy consists of oral antiestrogen medication taken daily for 5 years, and options differ according to menopausal status:

- *Tamoxifen* is a selective estrogen receptor modulator (SERM) that competitively inhibits estrogen's binding to ER and is effective in both pre- and postmenopausal women.
- *Aromatase Inhibitors* (AI) (anastrozole, exemestane and letrozole) decrease circulating estrogen levels by inhibiting conversion of androgens to estrogen and are effective only in postmenopausal women (including those who are postmenopausal because of medical ovarian suppression or oophorectomy).
- *Fulvestrant* is a selective ER degrader (SERD), which is given for breast cancer patients not responding to the previous endocrine therapies. This inhibitor binds to ER inducing its ubiquitination and degradation. Currently, new generation SERDs are being developed with higher affinity for ER.

Metastatic HR+/HER2- breast cancer (HR+ mBC) may develop resistance to endocrine therapy. Therefore, new agents have been developed to counteract the appearance of resistance to hormonal therapy. Inhibitors targeting mTOR Complex 1 (mTORC1), which promotes cell proliferation and growth; cyclin-dependent kinases (CDK) 4/6, which control the first checkpoint of the cell cycle; and, most recently, Phosphoinositide 3-Kinase (PI3K), which activates pathways for proliferation, have been approved by the Food and Drug Administration (FDA) for the treatment of metastatic breast cancer, in combination with endocrine therapy[33-37].

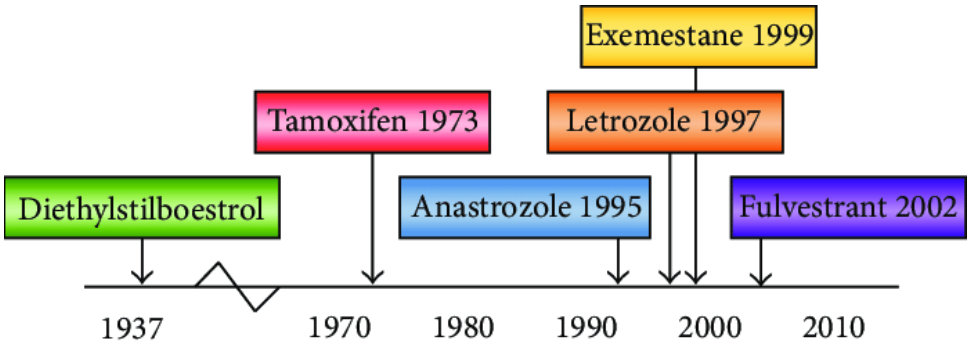

Figure 5. Timeline of the approvals in endocrine therapy. Diethylstilbestrol was the first antiestrogen molecule synthesized, but had severe side effects; Tamoxifen was approved in 1973 and still nowadays is of clinical value; Aromatase Inhibitors, anastrozole, letrozole and exemestane, were later approved, showing better outcomes in adjuvant setting; Fulvestrant was approved in 2002, the first selective estrogen receptor degrader (SERD). Figure taken from[38].

2.2.2. HER2+

The development of HER2-targeted therapy has been one of the greatest advances in breast cancer treatment. Trastuzumab, a monoclonal antibody targeting the extracellular domain of HER2, first entered clinical trials in the 1990s. Given the excellent long-term outcomes and reduced toxicity of single-agent accompanying chemotherapy, paclitaxel/trastuzumab is now the standard of care for patients with small, early HER2+ tumors. Recently, it has been approved by the FDA the antibody-drug conjugate trastuzumab emtansine for adjuvant treatment in early HER2+ BC patients with residual invasive disease after neoadjuvant taxane and trastuzumab neadjuvant treatment[39].

In HER2+ metastatic breast cancer, standard first-line therapy consists of taxane plus trastuzumab and pertuzumab, and emtansine is frequently used as second line therapy. Subsequent treatment generally combines a new chemotherapy agent (or endocrine therapy, if HR+) with an HER2-targeted agent.

2.2.3. TNBC

Given the relatively unfavorable prognosis of TNBC and lack of targeted therapies, chemotherapy is generally administered to all patients with triple-negative breast tumors, even with negative axillary nodes. Chemotherapeutic agents are the only agents approved by the FDA for treating early triple-negative disease.

For metastatic triple-negative breast cancer cytotoxic chemotherapy is the only therapeutic option available in patients except for cancers harboring germline *BRCA1/2* mutations, where targeted inhibitors of poly(adenosine diphosphate-ribose) polymerase (PARP) enzymes are approved; and PD-L1 positive cancers, where atezolizumab (anti-PD-L1) is approved in combination with placlitaxel. AKT inhibitors, such as Ipatasertib, are being evaluated in clinical trials in combination with paclitaxel[40, 41].

3. Resistance to endocrine therapy

Resistance to hormonal therapy is often associated with disease recurrence and progression. Over the last decade, several genetic and epigenetic alterations have been identified to bypass endocrine therapy and activate cell proliferation independently of estrogen binding to ER. These include activating mutations in ERα (*ESR1*); activation of the cell cycle through CDK4/6; activation of growth factor receptors such as HER family and/or Fibroblasts Growth Factor Receptor (FGFR); activation of growth and proliferation pathway members from the PI3K/AKT/mTOR axis; epigenetic modifications by histone deacetylase (HDAC) and interactions with tumor microenvironment and host immune response. To improve efficacy to hormonal therapy, inhibitors targeting elements of these pathways have been developed, in both metastatic and early-stage disease. Many agents are approved by the FDA, primarily in combination with hormone therapy but as well novel combinations are under investigation[42].

- *ESR1* mutations

ESR1 mutations, although very rarely seen in primary tumors, have been reported to be in 11% to 55% of the recurrent metastatic cancers that progressed to a long-term treatment with endocrine therapy, typically after AI treatment[43-46]. The hot-spot mutations are located in the ligand-binding-domain of ER, inducing a constitutive activated conformation, independently of the presence of estrogen. Therefore, mutant ER is resistant to Aromatase Inhibitors (AI), as well as to tamoxifen. Fulvestrant is still active in *ESR1* mutants except for Y537S mutation[47]. The development of newer generation SERMs, SERDs and other strategies is required in order to improve the targeting of ER and its mutated forms.

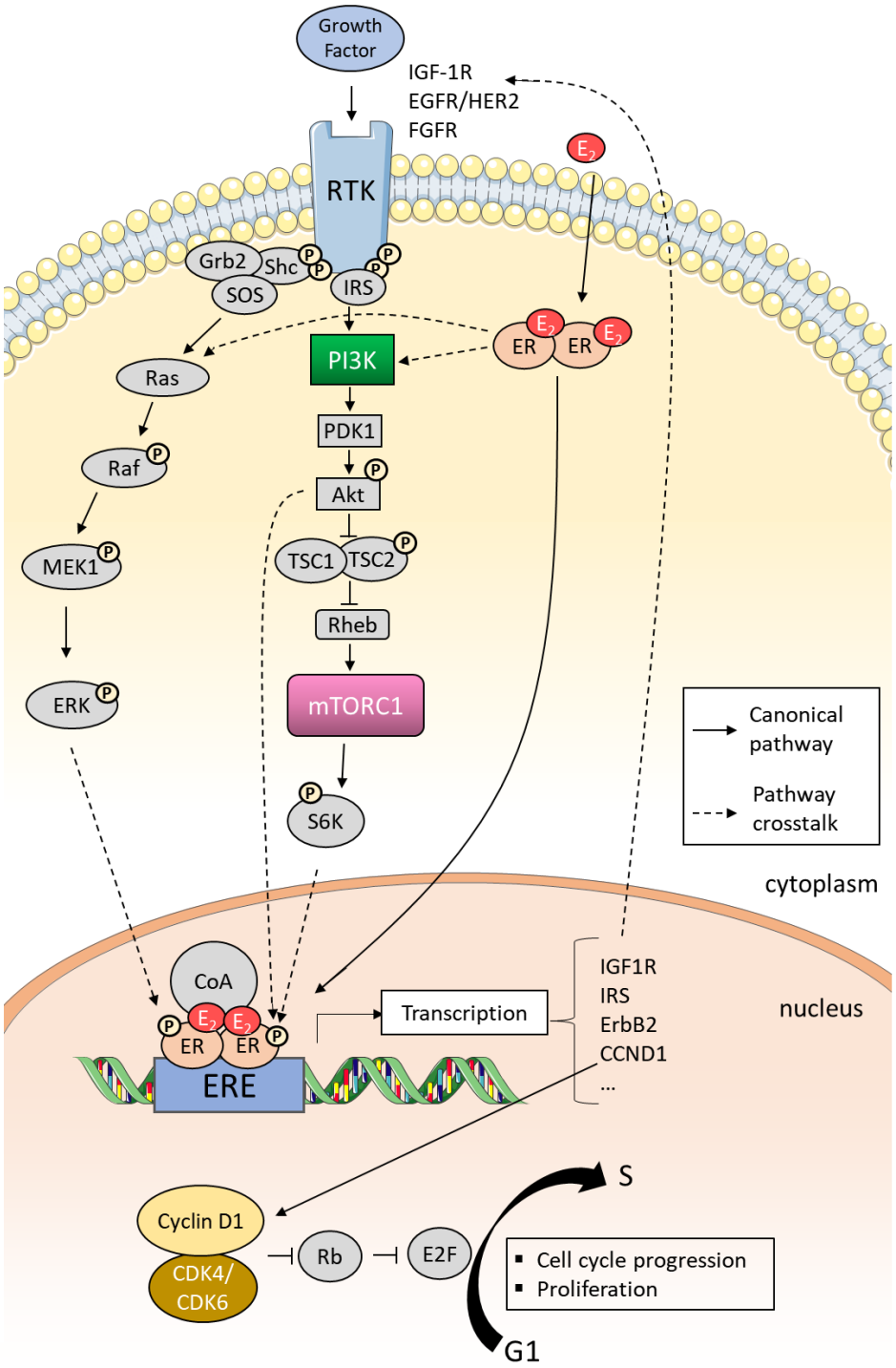

Figure 6. Estrogen Receptor pathway and cross-talk with Growth Factor Receptors, PI3K/AKT/mTOR and CDK4/6 pathways[42, 48, 49]. Estrogen (E_2) binds to Estrogen Receptor (ER) leading to dimerization and activation of the receptor. Activated ER promotes proliferation through translocation to the nucleus, where it will bind to the Estrogen Receptor Elements (ERE) in the genome. In complex with other Co-Activators (CoA), ER regulates target gene expression, such as Insulin Growth Factor Receptor 1 (IGF1R), Insulin Responsive Element (IRS), *ErbB2* (HER2) and *CCND1* (Cyclin D1) among others. Importantly, cyclin D1 binds to CDK4/6 to overpass the G1 to S cell cycle restriction point and proceed with cell division. Alternatively, proliferation can be promoted through the non-genomic pathway: estrogen binds to the membrane associated ER which activates the Ras/Raf/Mek/Erk mitogenic pathway[50] and the PI3K/AKT/mTOR pathway[51]. ER can be further phosphorylated in the nucleus by ERK[52], AKT[53] and S6K[42, 48, 54].

- HER2 Gene amplification and mutations

HER2 amplification comprises around 10% of ER+ breast cancers and it is well recognized as a mechanism of resistance to endocrine therapy[55]. In such cases, trastuzumab is the standard of care as well as for the metastatic setting, where it is given in combination with hormonal therapy.

Another way to activate HER pathway signaling is with somatic mutations in HER2. The mutation rate is approximately 2% in primary breast cancers but can reach up to 20% on invasive lobular cancers[56]. These mutations can be located in two domains of the receptor: the tyrosine kinase domain and the extracellular domain, both leading to a constitutively activated pathway. The treatment options for these HER2 mutated cancers are irreversible HER2 Tyrosine Kinase Inhibitors (TKI), such as neratinib. Given that most of the HER2-mutated cases are ER+, the combination of neratinib with fulvestrant is being studied[57].

- Fibroblast Growth Factor Receptors amplification

The fibroblast growth factor (FGF) signaling pathway is composed of four transmembrane tyrosine kinase receptors (FGFR1, FGFR2, FGFR3, and FGFR4) and 18 ligands. They are expressed in many different cell types and control a wide range of biological functions, such as cellular proliferation, survival, migration, and differentiation[58]. *FGFR1* gene locates in the 8p11 amplicon, which is found amplified in 10% of ER+ breast cancer and associated with increased Ki-67, early relapse, and poor survival[59]. Several studies have demonstrated that high FGFR1 signaling is associated with endocrine resistance[60-62]. Very recently, it has also been shown that *FGFR1* amplification is a mechanism of resistance to CDK4/6inh[63]. Less frequently, breast cancer could harbor amplification of *FGFR2*[64] or *FGF3/4* ligands, which are located in the 11q13 amplicon[65]. Inhibitors targeting FGF Receptors have been developed, and will be further described in a later chapter.

- PI3K/AKT/mTOR Pathway

The PI3K/AKT/mTOR pathway is a pivotal signaling axis for cell proliferation and growth. Upregulation of the PI3K pathway through increased activity of PI3K, AKT and mTOR kinases is a common resistance mechanism to endocrine therapy[66-68] (**Figure 6**). The most frequent genetic alteration in ER+ breast cancers are activating mutations in *PIK3CA* (30% to 40%),

the gene coding for the α isoform of the catalytic subunit of PI3K[7]. Common mutations are E242K, E525K and H1047R, which bring PI3K in a constitutively activated state[69]. Novel inhibitors targeting kinases of this pathway have been developed, such as mTOR, AKT and PI3K inhibitors.

- Cyclin D, CDK4/6 and Rb pathway

CDK4/6 control the transition of the G1/S restriction point[70]. They are activated upon binding with cyclin D, which phosphorylate the retinoblastoma protein (Rb) leading to the release of E2F, a transcription factor that activates the transcription of several genes involved in cell cycle progression (**Figure 6**). Cell cycle progression is a downstream effector of the estrogen receptor activation, being cyclin D, c-Myc and cyclin E, rapidly upregulated upon estrogen stimuli[71, 72]. High levels of cyclin D1 and Rb phosphorylation have been linked to endocrine therapy resistance[73]. Cell cycle related alterations are found enriched in the poorer prognosis group of the ER+ breast cancers, the luminal B subtype. *CCND1* and *CDK4* amplification is present in 58% and 25% of Luminal B, while in luminal A they are at 29% and 14%, respectively[7].

Several inhibitors targeting CDK4/6 have been developed showing very promising data on ER+ breast cancer in combination with endocrine therapy[74]. To date, three CDK4/6 inhibitors have been approved by the FDA in combination with hormonal therapy: palbociclib[75], abemaciclib[36] and ribociclib[35].

Of note, *CCND1* gene co-localizes with FGF3/4/19 genes in the 11q13 amplicon, as well as with other genes implicated in pathway proliferation: P21 Activated Kinase 1 (*PAK1*) and Ribosomal Protein S6 Kinase B2 (*RPS6KB2*) genes. This chromosomic region is frequently amplified in breast cancer[7] (**Figure 7**). PAK1 protein is a serine/threonine kinase that regulates cell proliferation and cell cycle progression. PAK1 interacts with both MAPK pathway by phosphorylating Rac and MEK, and PI3K pathway by interacting with AKT[76]. *PAK1* also has shown to function as an oncogene in breast cancer[77]. *RPS6KB2* codes for the Beta isoform of P70/S6K (S6K2), and it has been related with endocrine resistance in breast cancer[65, 78].

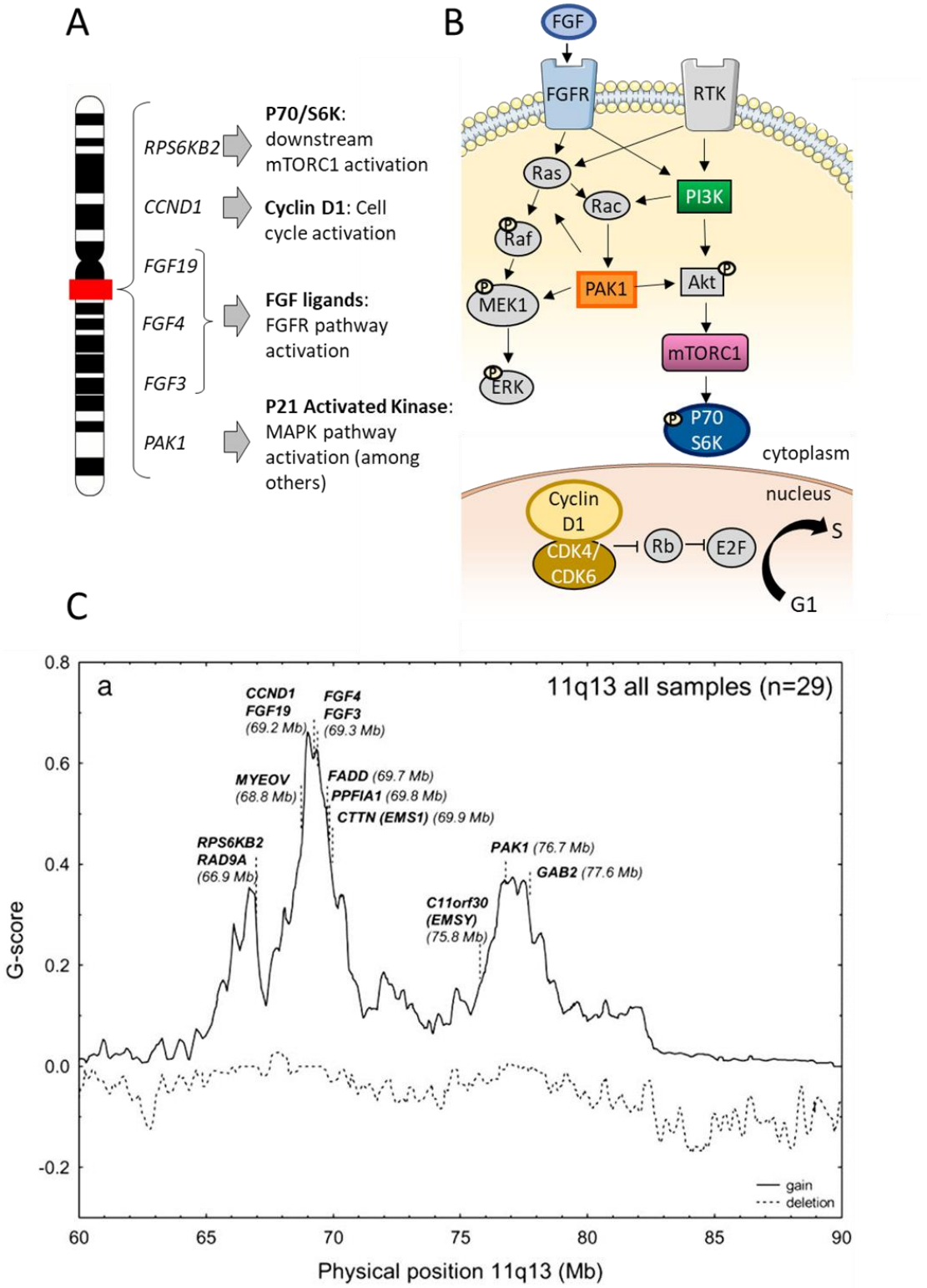

Figure 7. 11q13 amplicon in breast cancer. A) 11q13 region contains four genes related to cell growth and proliferation: *RPS6KB2* (S6K2*), CCND1* (Cyclin D1), *FGF3/4/19* and *PAK1* (P21 Activated Kinase 1) B) FGF ligands can activate FGFR and MAPK pathway; PAK1 is involved in the crosstalk between MAPK and AKT signaling; S6K2, a downstream effector of mTORC1, further activating protein synthesis and cell growth; cyclin D1 overexpression can lead to PI3Kinh resistance through cell cycle progression C) Physical genomic distance between 11q13 genes (X-axe) and relative copy number variations (Y-axe) in 29 breast cancer samples. Graph taken from[65].

- Epigenetic pathways

Epigenetic regulatory mechanisms of *ESR1* and growth factor receptor gene promoters have been linked to endocrine resistance[79]. Several mutations have been found in genes that regulate histone and DNA modifications, such as Myeloid/Lymphoid Or Mixed-Lineage Leukemia Protein 3 (MLL3) which occurs in 14% of luminal BC[7]. Histone deacetylase (HDAC) inhibitors have been tested in the clinics with promising data. In 2017, entinostat received «breakthrough designation» status from the FDA in combination with exemestane in the advanced setting of breast cancer due to an improvement of the overall survival (OS) in a phase III clinical trial[80, 81].

- Insulin Growth Factor Receptor Signaling

The Type-1 Insulin Growth Factor Receptor (IGF1R) signaling regulates cell growth, survival, motility and is linked to mammary gland development[82]. IGF ligands stimulate cell growth via binding to IGF1R and the subsequent activation of the PI3K/AKT and Ras/Raf/Mek/Erk mitogenic (MAPK) pathways (**Figure 6**). Alterations in this pathway are linked to endocrine therapy resistance[83, 84]. Estrogen receptor is a major regulator of IGF1R and the insulin Receptor substrates (IRS), mainly by activating the transcription of these genes and other components of the pathway[85]. There are multiple mechanisms of cross-talk between ER and IGFR1R. Preclinical data shows that IGFR1R activation amplifies the biological effects of ER activation, independently of estradiol[86]. Similarly, the IGF pathway signaling regulates ERα through S6K1-dependent mechanism in breast cancer cells[87]. Therefore, it is not rare that IGF signaling is linked to endocrine resistance[83, 84]. Several IGFR inhibitors have been developed in the clinics but with disappointing results[88].

- Vascular Endothelial Growth Factor

Vascular Endothelial Growth Factor (VEGF), besides its contribution to angiogenesis, has shown to induce breast cancer cell proliferation and resistance to endocrine therapy through paracrine and autocrine signalling[89]. Elevated levels of VEGF have been linked to disease recurrence and resistance to hormonal therapy[90]. VEGF inhibitors have been tested in combination with hormonal therapy with relative improvement in the response[91]. In 2008,

FDA approved bevacizumab (an antibody targeting VEGF) for mBC but later in 2011 the approval was withdrawn due to lack of safety and effectiveness[92].

- Microenvironment and Immune Checkpoint Pathway

Programmed cell Death protein 1 (PD1) and PD1 ligand (PD-L1) confer one of the major immune check points of the immune system[93]. PD-1, present in the T cells, binds to PD-L1, expressed by tumoral cells, to abolish the capacity of the immune system to attack cancer cells. In ER+ breast cancer, up to 20% of the patients have been reported to express PD-L1[94]. Antibodies targeting both receptor and ligand are being tested in the clinics[95].

4. Targeted therapy beyond endocrine resistance

The increasing knowledge on the mechanisms of endocrine resistance have reported new potential targets, which have emerged as potential treatment options in combination with hormone therapy. In this sense, several agents have been developed and tested in the clinics, such as mTOR inhibitors (everolimus), PI3K inhibitors (buparlisib, alpelisib, and taselisib), CDK4/6 inhibitors (palbociclib, ribociclib, and abemaciclib), HDAC inhibitors (entinostat), FGFR inhibitors (dovitinib and lucitanib), and IGFR inhibitors[42].

This study will focus on two therapeutic strategies: PI3K/mTOR targeted therapy and FGFR targeted therapy.

4.1. Targeting PI3K/AKT/mTOR pathway

The PI3K/AKT/mTOR pathway is a canonical axis for cell proliferation. As previously mentioned, it interacts with the ER pathway, and its activation is considered a mechanism of resistance to endocrine therapy.

Activating mutations in the *PIK3CA* gene are the most common alterations in luminal breast cancer, being 45% in luminal A and 29% in luminal B BC subtypes[7]. Therefore, it is reasonable to consider this pathway a target for cancer treatment.

4.1.1. The PI3K pathway

The PI3K pathway has the function of translating a proliferative signal from the outer part of the cell through a receptor (**Figure 8**). PI3K is a kinase that phosphorylates phosphatidylinositol (PtdIns) lipid substrates: it adds the phosphorylation at the 3rd position of the inositol ring of PtdIns(4)P and PtdIns(4,5)P_2 (PIP_2) forming PtdIns(3,4,5)P_3 (PIP_3). There are three classes of PI3K isoforms, but class I is the most relevant in cancer. Class I isoforms are formed by two subunits: p110, the catalytic subunit, and p85, the regulatory subunit. There are 4 isoforms of p110 subunits: p110α, p110β, p110γ and p110δ. *PIK3CA* encodes for the p110α subunit isoform[7, 96].

There are 3 *PIK3CA* hotspot or recurring mutations: H1047R, E542K and E545K, accounting for 70-80% of the mutation spectrum[97, 98]. These mutations are located in exon 9 (E542K, E545K), within the p85 regulatory domain and in exon 20 (H1047R), in the kinase domain[99, 100].

PI3K is activated upstream through the binding of a growth factor signal with its cognate growth factor receptor (RTKs). PIP_3 acts as a docking site for AKT, a serine/threonine kinase, inducing its activation through phosphorylation in the T308 position by the phosphoinositide-dependent kinase 1 (PDK1). AKT is also phosphorylated at the S473 position by mTOR Complex 2 (mTORC2), which is formed by mTOR, Deptor, mLST8, mSin1, Protor and Rictor, and as well activated by PIP_3 in the cell membrane via Sin1[101, 102]. A canonical function of AKT is to activate protein synthesis and cell growth by activating mTOR Complex 1 (mTORC1) through inhibition of the TSC1/2 complex (composed by the two proteins TSC1 and TSC2/Tuberin). The mTORC1 complex is composed by several elements: mTOR, Deptor, Raptor, Pras40 and mLST8 proteins. This complex phosphorylates S6 kinase (S6K) to finally activate protein, lipid and nucleotide synthesis in the cell[103].

Phosphatase and tensin homologue deleted on chromosome 10 (PTEN) is a phosphatase that has the opposite function to PI3K: it dephosphorylates PIP_3 to PIP_2. Another phosphatase, inositol polyphosphate 4-phosphatase type II (INPP4B), is also involved in PIP_3 to PIP_2 dephosphorylation. They both act as tumor suppressors, and its loss can lead to a constitutive activation of the PI3K pathway[103].

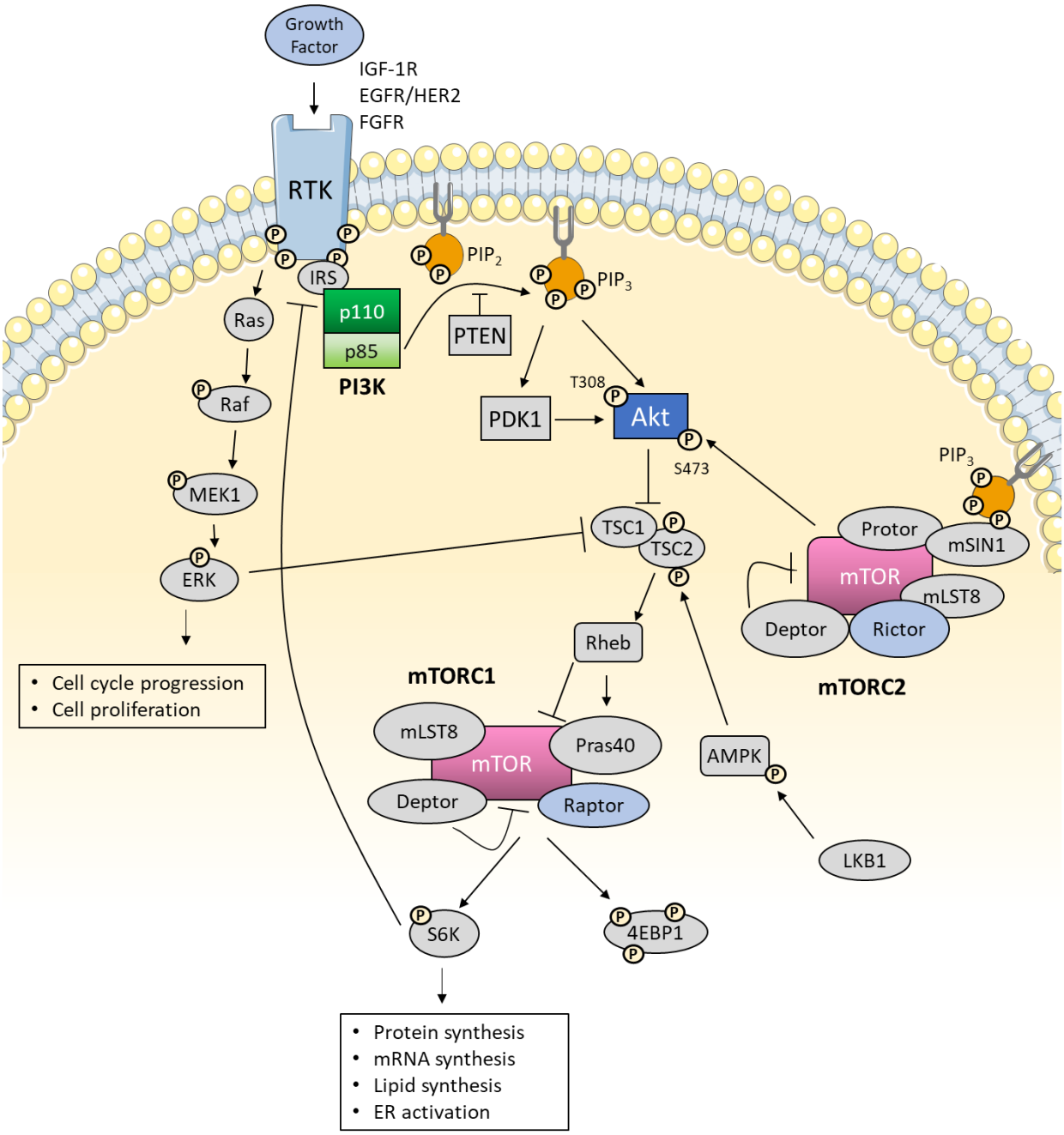

Figure 8. The PI3K/AKT/mTOR pathway. This canonical pathway for proliferation is composed by multiple interconnected elements. A tyrosine kinase receptor is activated upon binding with a growth factor. PI3K is then activated through IRS and will therefore phosphorylate PIP_2 into PIP_3. PIP_3 serves as a docking site for AKT, which is activated via PDK1. AKT regulates many biological processes in the cell, but importantly it inhibits the negative regulator of mTORC1, the TSC1/2 complex. Activated mTORC1 will activate several pathways in the cell related to protein, mRNA, lipid and nucleotide synthesis, as well as it serves as a negative feedback for RTK signaling. Production of PIP_3 also results from mTORC2 activation, which will phosphorylate AKT at the S473 site. The MAPK pathway is also able to activate mTORC1 pathway through inhibition of TSC1/2 complex.

AMP-activated protein kinase (AMPK) is a sensor for low nutrients and high AMP/ATP ratio[104] that inhibits cell growth in adverse situations. In the presence of AMP, Liver Kinase B1 (LKB1) phosphorylates AMPK, which activates the TSC1/2 complex, thus inhibiting mTORC1 function. Loss if *STK11* gene (LKB1 protein) can lead to constitutive activation of mTORC1 and it has been associated with non-small cell lung cancer[105] and hematologic malignanices[103, 106].

4.1.2. PI3K/mTOR inhibitors

Several inhibitors have been developed in the PI3K-AKT-mTOR axis. In fact, everolimus was the first targeted therapy approved in combination with an AI (exemestane) for the treatment of HR+ breast cancer[33]. Kinase inhibitors against both mTORC1/2, as well as inhibitors against AKT or PI3K, have been tested in the clinic[42]. The efficacy of pan-PI3K inhibitors is limited by dose-limiting toxicities that include rash, diarrhea and elevated transaminases. PI3Kα-specific inhibitors are advantageous in improving the therapeutic window, but resistance mechanisms have been recurrent. Preclinical models also indicated that effective inhibition of mTOR remains important for upstream inhibitors[107], but combined PI3K and mTOR inhibition may not be feasible due to overlapping toxicities. Importantly, *PIK3CA* mutation status has been thoroughly validated as a response biomarker in several clinical trials[108].

- Inhibition of mTOR

The first mTORC inhibitors introduced in the clinic are the rapalogues. These molecules are derived from rapamycin, a metabolite produced by *Streptomyces hygroscopicus*[109]. Rapalogues bind to the 12 KDa FK506-binding protein (FKBP12), and this complex acts as an allosteric inhibitor of mTORC1. However, resistance mechanisms have been limiting their efficacy, such as AKT activation via mTORC2[110]. To better block mTORC complexes, dual mTORC1/2 inhibitors were developed. These inhibitors competitively bind to the ATP site (mTORC1/2inh). Due to targeting directly the catalytic domain, some negative feedback loops are prevented, giving a much efficient mTOR activity blockade[42, 103, 109].

- *Sirolimus* (Rapamycin): This inhibitor is the direct product extracted from *Streptomyces hygroscopicus*. This is the first mTORC1 inhibitor developed.

- *Temsirolimus:* This rapalogue was evaluated in a trial in combination with the AI letrozole as first line therapy for HR+ breast cancer. However, no difference in progression-free survival (PFS) between the two arms were found[111].

- *Everolimus:* This rapalogue was the first agent approved in combination with exemestane for postmenopausal women HR+/HER2- metastatic breast cancer progressing to AIs in 2012. The BOLERO-2 trial showed a 10.6 months difference in the PFS, compared to AI monotherapy[112].

- *Vistusertib* (AZD2014): This dual mTORC1/2inh showed promising results in cellular models[113-115]. However, results from the MANTA study in 2018 did not succeed to offer better response on vistusertib plus fulvestrant in comparison with everolimus with fulvestrant treatment[116].

- Inhibition of PI3K

Two classes of PI3K inhibitors are being studied in HR+ breast cancer, the pan-class I inhibitors (buparlisib and pictilisib) and the isoform-specific inhibitors (alpelisib and taselisib)[42]. Results with the pan-PI3K inhibitors have been complicated due to toxicity and disappointing efficacy. Nowadays, the use of ctDNA to detect *PIK3CA* mutations is routinely being used as a predictive biomarker for response to α-specific PI3K inhibitors[117].

- *Buparlisib* (BKM120): The phase III BELLE-2 trial showed that PI3K inhibition combined with endocrine therapy is effective in postmenopausal women with endocrine-resistant, HR+ HER2- advanced breast cancer[118]. Overall, the toxicities observed in the buparlisib treated patients and the development of more specific inhibitors have precluded further clinical development of this inhibitor.

- *Pictilisib* (GDC-0941): The FERGI trial, a phase II trial with HR+ postmenopausal metastatic breast cancer, tested fulvestrant with pictilisib or placebo. Results were disappointing: besides increasing toxicity in the pictilisib arm, PFS was similar between

the two treatment arms –even among patients with *PIK3CA*-mutant tumors. No further investigation is ongoing with Pictilisib[119].

- *Taselisib* (GDC-0032): This β-sparing inhibitor (specific for all isoforms except PI3Kβ) has demonstrated encouraging efficacy in early-phase trials, with certain degree of toxicity. The SANDPIPER phase III trial tested this inhibitor in *PIK3CA*-mutant HR+ metastatic breast cancer in combination with fulvestrant and the PFS increased in Taselisib + fulvestrant arm from 5.4 to 7.4 months compared to placebo + fulvestrant arm. Toxicities were manageable, although some patients had to quit the trial due to Taselisib-related toxicities[120].

- *Alpelisib* (BYL719): Early phase trials showed promising data for this α-specific inhibitor. Recently, results from the SOLAR-1 clinical trial have shown a significantly prolonged PFS with the addition of alpelisib to fulvestrant arm, with a median PFS of 11 months *vs.* 5.7 months in *PIK3CA*-mutant patients. Toxicities in this case were more manageable[121, 122]. This encouraging data have led to the approval of alpelisib in combination with fulvestrant early 2019 by the FDA for the HR+ metastatic breast cancer setting, being the first PI3K inhibitor approved for a solid tumor disease[37].

4.1.3. Resistance mechanisms to PI3K inhibitors

Intrinsic and acquired resistance to PI3Kinh is a problem in the clinic. Several studies from the last decade have described mechanisms that overpass PI3K inhibition. These mechanisms can be intrinsic, where the tumor does not depend on the PI3K pathway for its growth so it will not respond to PI3Kinh; or acquired, where the tumor, after showing response, acquires a genetic or epigenetic change that leads to overpass PI3K inhibition. Below are described the most relevant mechanisms of resistance to PI3K inhibition described to date (**Figure 9**)[123].

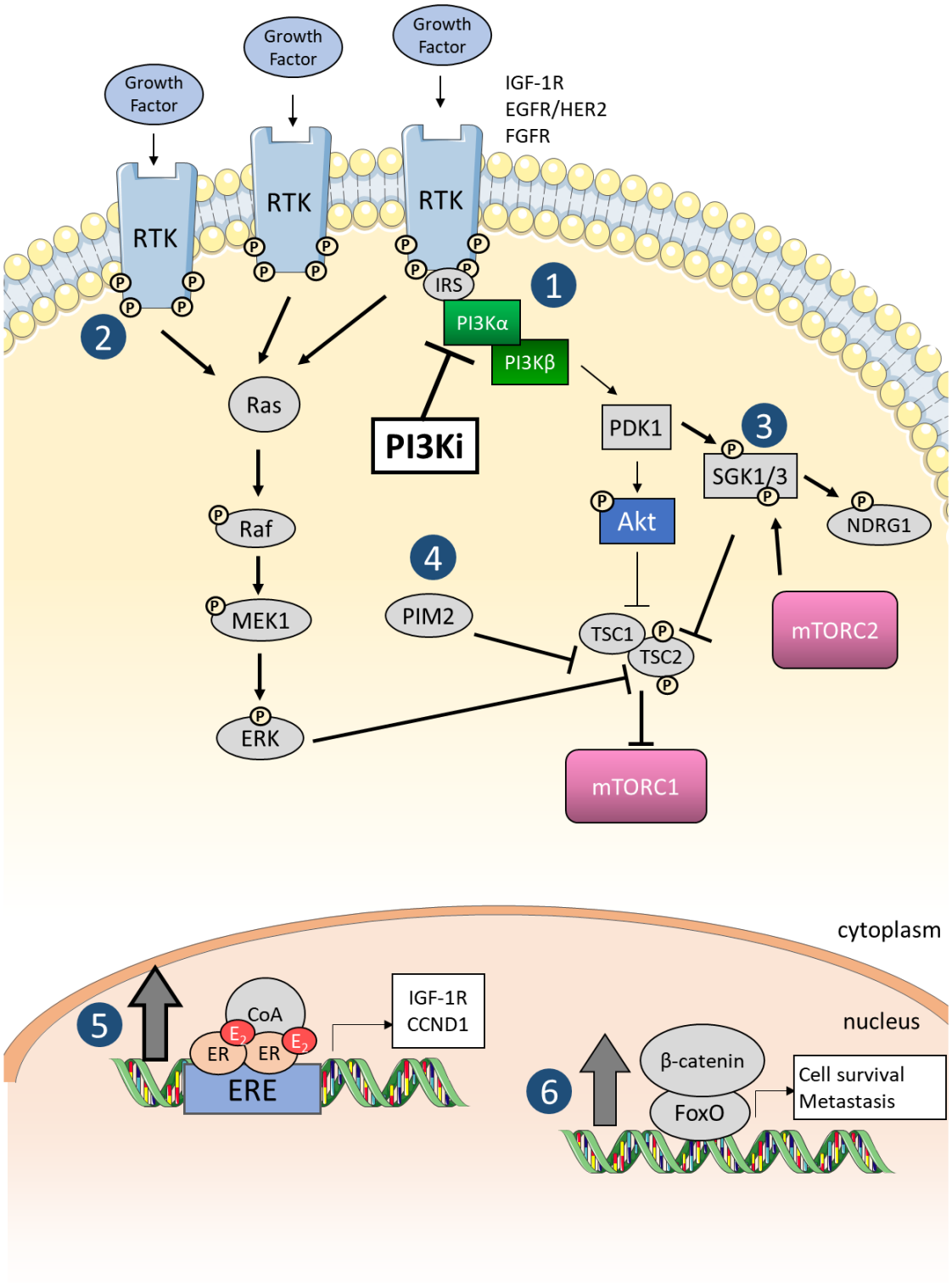

Figure 9. Resistance mechanisms to PI3K inhibitors. 1) Redundant PI3Kβ isoform takes over the role of the PI3Kα isoform, which is described for tumors that lack PTEN[124, 125]; 2) PI3K inhibition results in RTK overexpression and activation of compensatory MAPK signaling[126-128]; 3) SGK1/3 phosphorylation by PDK1 and AKT activates mTORC1 through TSC1/2 complex blockade and phosphorylates NDRG1 at the T346 position[129]; 4) PIM2 is another TSC1/2 inhibitor that can potentially activate mTORC1[130]; 5) ER is upregulated upon treatment with PI3Kinh and this results in drug resistance[131]; 6) β-catenin associates with FoxO in the nucleus to activate the transcription of cell survival and metastasis related genes[132].

- Use of redundant PI3K isoforms: The current pharmacological strategy has focused on targeting PI3Kα in *PIK3CA* mutant cancers, in an attempt to improve the therapeutic window of these drugs. Therefore, other PI3K isoforms could participate in the re-activation of the pathway, when PI3Kα is inhibited. The rewiring of PI3K signaling towards p110β isoform can occur either upon PI3Kα inhibition, where PI3Kβ produces and accumulates PIP_3 over time[133], and in the context of *PTEN* loss, where PIP_3 production appears to be more dependent on PI3Kβ isoform[125, 134].

- RTK activation: There is an upregulation of RTK expression and activation of HER3, HER2 and other RTK's upon PI3K blockade [126-128]. This increased RTK activity has been shown to activate the MAPK pathway.

- Hormone Receptor-dependent resistance: PI3K pathway activation leads to resistance to endocrine therapy, and inversely, an upregulation of ER leads to PI3Kinh resistance. In fact, ER-positive breast cancer cell lines and patient samples exhibit an increased luminal gene expression signature when exposed to PI3K inhibitors, due to an increased ER expression upon PI3K inhibition[131].

- Transcription factors: Activation of notch and c-MYC are markers of resistance to PI3K and mTORC1inh[135]. Besides, c-MYC amplification has proven to induce PI3Kinh resistance in *PIK3CA* mutant mice-derived tumor cells[136]. Additionally, it has been shown in colon cancer that β-catenin promotes PI3Kinh resistance by associating with the transcription factor FOXO in the nucleus and thus activating the transcription of genes related to cell survival and metastasis[132].

- Downstream PI3K Kinases and parallel pathways: PI3K activates several downstream Ser/Thr kinases, and their constitutive activation can compensate the inhibitory effects of targeting PI3K.

    - *RSK3/4:* It has been shown that RSK3/4 have the ability to drive resistance to PI3K and AKT inhibitors in preclinical models[137].

    - *PIM, PKC and AKT:* These kinases have been as well identified as putative resistant mechanisms to PI3Kinh[130].

- *PDK1/SGK1 axis:* It has been shown that upon PI3K blockade, SGK1 inhibits TSC2 via PDK1 thus activating mTORC1. However, PDK1 blockade restores sensitivity to PI3K inhibition[129].

4.2. Targeting FGFR and angiogenic pathways

FGFR signaling plays a crucial role in cancer cell proliferation, migration, angiogenesis, and survival. Studies from the last decade have demonstrated FGFRs as driving oncogenes in certain tumor types, such as bladder, gastric and breast cancer[58]. The most recurrent FGFR genetic alterations described in cancer are: *FGFR1*amp in breast cancer (10%)[138, 139], *FGFR2*amp in gastric cancer (10%)[140], *FGFR2* activating mutations in endometrial cancer (12%)[141], *FGFR3* activating mutations in bladder cancer (50-60%)[142] and *FGFR3* translocations in myeloma (15%)[143, 144]. Therefore, FGFRs have been proposed as putative therapeutic targets. Even though the initial results using MTKI were promising, the efficacy shown by specific FGFRinh inhibitors in ER+BC has been limited[145]. Therefore, biomarkers of FGFRinh sensitivity are needed to identify those tumors with FGFR-driving carcinogenesis. Of note, the FGFR1/2/3 inhibitor erdafitinib, has recently been approved for the treatment of metastatic bladder cancer with FGFR2/3 mutations or translocations[146].

4.2.1. FGFR pathway: proliferation, invasion and angiogenesis

The FGF family comprises 22 family members, from which 18 act as ligands. They bind to 4 cognate receptors: FGFR1, FGFR2, FGFR3 and FGFR4 (FGFR1-4). The FGF ligands are glycoproteins secreted by numerous cell types, such as endothelial cells, stem cells and epithelial cells[147]. FGF ligands get rapidly trapped in the ECM as well as the cell surfaces, by heparan sulphate proteoglycans (HPSGs). In order to activate the FGF Receptors, they are liberated from the ECM by heparinases, proteases and other FGF-binding proteins. HPSGs stabilize the binding between FGFs and FGFRs, forming a ternary complex. The specificity of each FGF ligand to the FGFRs is established partly by differing ligand-binding affinities of the receptor paralogues (FGFR1-4), but as well through different splicing isoforms (IIIb/IIIc) which alter the specificity for certain FGF ligands[58]. This alternative splicing is located at the third extracellular immunoglobulin domain (Ig III). Thus, some FGF ligands have higher affinity for IIIb and others for IIIc receptor isoforms[58, 148].

FGF Receptors dimerize in a ligand-dependent manner forming a complex with the ligand[149], although it can occur in a ligand-independent manner in some cases[150]. These receptors contain an intracellular tyrosine Kinase (TK) domain, which changes conformation upon dimerization. This starts the cascades of activation in several proliferation pathways. The tyrosine kinase domain is transphosphorylated by the intermolecular contacts within the two receptors. This serves as docking sites for adaptor proteins, which can be as well phosphorylated by the TK domain. FGFR Substrate 2 (FRS2) is a key adaptor protein very specific for FGFRs. FRS2 is phosphorylated on several sites, allowing the recruitment of the adaptor proteins son of sevenless (SOS) and growth factor receptor-bound-2 (GRB-2) to activate Ras and the downstream Raf and MAPK pathways. Another complex involving the GRB2-associated binding protein 1 (GAB1) recruits a complex, which includes PI3K, activating the PI3K/AKT/mTOR pathway[58].

FGF signaling can affect multiple biological processes across cell types, tissues and organs. It regulates from fundamental developmental pathways, such as mesoderm patterning in the early embryo, to many physiological roles in the adult organism, including the regulation of angiogenesis and wound healing. In cancer, FGF signaling participates in numerous oncogenic aspects. Here are presented some of the oncogenic behaviors promoted by FGF signaling[58]:

- FGF in angiogenesis: FGF signaling has been extensively involved in angiogenesis[151, 152], where FGF2 is important for the growth of new blood vessels[153]. Furthermore, a crosstalk between FGFR and VEGFR pathway can mediate resistance to VEGF targeted therapy[154, 155].

- FGF and proliferation: FGF signaling participates in the activation of typical proliferation pathways such as MAPK, PI3K and PLCγ pathways[58]. To date, two studies have demonstrated that FGF ligand signaling activate tumor cell proliferation in transgenic mice: both enhanced paracrine FGF10 expression and FGF8b overexpression (in a haploinsufficient PTEN background)[156] led to the formation of prostate adenocarcinoma.

- FGF and survival: Besides promoting cell proliferation, FGF signaling is able to activate anti-apoptotic pathways through PI3K-AKT or STAT signaling. FGF2 expression has been as well related to increased proliferation and decreased apoptosis in bladder cancer[157].

- FGF and migration and invasion: Several studies have confirmed the relation between FGF signaling and cell migration; for instance, it has been proven that FGF10/FGFR2 signaling promotes migration and invasion in pancreatic cancer cells *in vitro*[158] and that FGFR1 pathway activation leads to the generation of invasive mammary lesions in transgenic mice[159]. Furthermore, it has been shown that FGF signaling promotes epithelial-mesenchymal transition (EMT), which leads to cell-to-cell contacts disruption and cancer cell metastasis[160, 161].

4.2.2. Genetic alterations in the FGFR pathway

FGFR amplifications (*FGFR*amp) are among the most recurrent genomic alterations in breast cancer patients[7], but several other genetic alterations occur in cancer. Next are described the main oncogenic alterations that drive FGFR-related cancer growth (**Figure 10**).

- *FGFR1-4* gene amplifications: *FGFR1* and *FGFR2* gene amplifications have been commonly described. While *FGFR1* amplifications are more common in breast cancer, *FGFR2* amplifications are more common in gastric cancer. *FGFR1* is located at the 8p11-12 chromosomal region, which is amplified in 10% of luminal breast cancers[58, 138].

- *FGFR1-4* mutations: Activating mutations in the *FGFR* genes are rare in breast cancer. Bladder cancer has the highest frequency of *FGFR* mutations, especially in *FGFR3*[162]. *FGFR* activating mutations occur in hotspot regions. For instance, *FGFR3* mutations are located in the extracellular domain (S249C, which leads to constitutive dimerization and activation of the receptor), in the transmembrane domain (Y373C) and in the kinase domain (K652E)[163, 164].

- *FGFR1-4* translocations: Several translocations implicating the *FGFR* genes have been identified in cancer, either involving the N-terminus of a transcription factor and the kinase domain of the FGFR[165, 166], or fusions at the FGFR C-terminus leaving the extracellular, transmembrane and kinase domain intact[167]. While in breast cancer *FGFR*

translocations are uncommon, in other diseases constitute up to 15% of the cases. For instance, in multiple myeloma, the fusion between *FGFR3* at 4p16.3 to the *immunoglobulin heavy chain* (*IGH*) locus 14q32, results in *FGFR3* gene expression under the control of the *IGH* promoter[168, 169].

- 11q13 amplification (*FGF3*, *FGF4* and *FGF19*): Amplification of the 11q13 locus is frequent in many cancers, such as breast cancer (15-20%)[7, 65] and head and neck cancer (39%)[145, 170]. This locus includes, as previously mentioned, *CCND1*, *FGF3/4/19*, *PAK1* and *RPS6KB2*. Not all cancers that harbor an 11q13 amplification overexpress the FGF3/4/19 ligands[65, 171, 172]: as much as 15% of the hepatocellular carcinomas (HCC) with amplification in the 11q13, express high levels of FGF19[173].

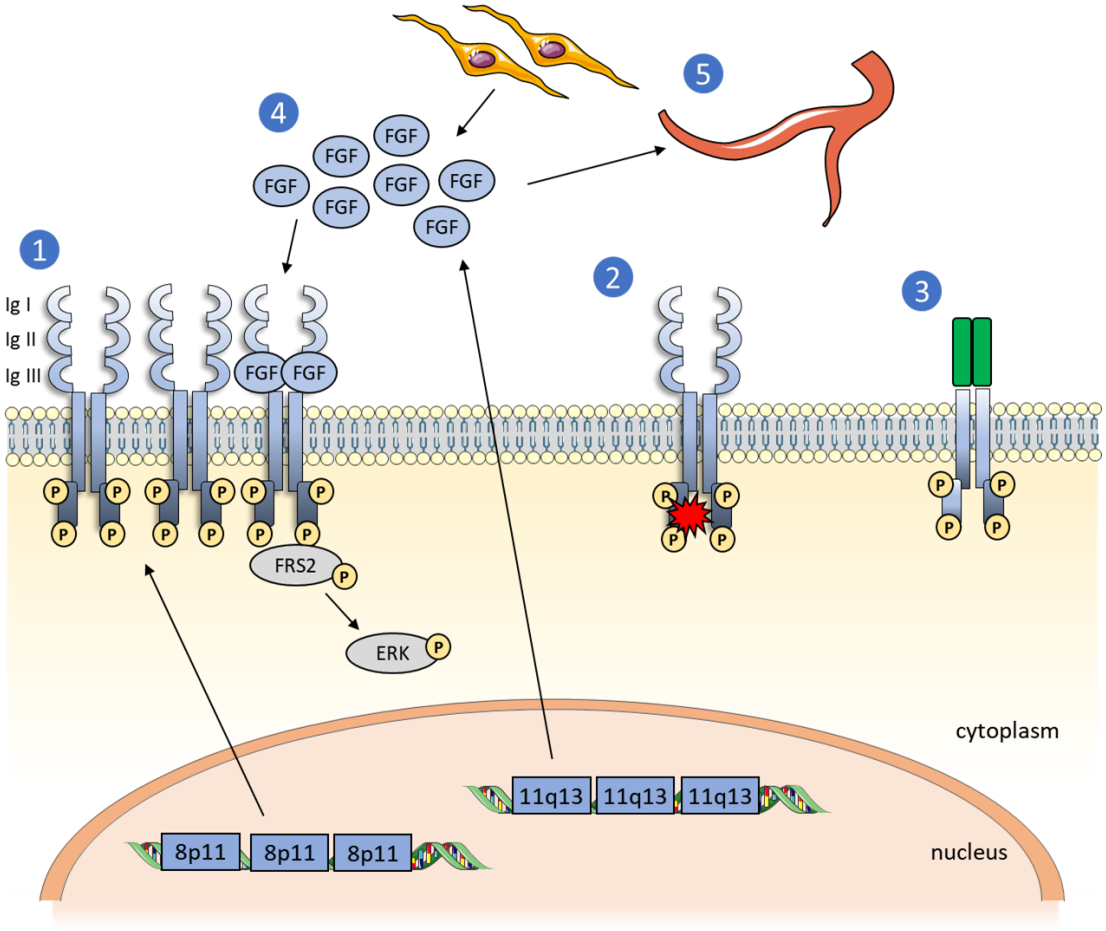

Figure 10. FGFR pathway activation in cancer. The FGFR pathway is activated by 1) receptor gene amplification, e.g. *FGFR1*, which is located in the 8p11 amplicon, is a very common genetic alteration in breast cancer[7]; 2) activating mutations in hotspot locations of the receptors; 3) Gene translocations; and 4) FGF ligands, which can be expressed either from the amplification of the 11q13 region (autocrine signaling) or secreted by CAFs and other stromal cells (paracrine signaling). 5) FGF ligand overexpression can lead to increased angiogenesis.

- FRS2 amplification: Although not yet seen in breast cancer, it has been described that FRS2 amplification could as well activate FGFR signaling in liposarcoma[174], in high-grade serous ovarian cancer[175] and in low grade osteosarcoma[176].

4.2.3. MTKI and FGFR-specific inhibitors

Given the high frequency of *FGFR1-4* genetic aberrations in cancer, several FGFR-targeted therapies have emerged in the clinic. To date, there is still no FGFR therapy approved for the treatment of breast cancer, and early clinical studies suggested that: the response rate of MTKI was higher than the one of pan-FGFRinh, and the need to identify better response biomarkers.

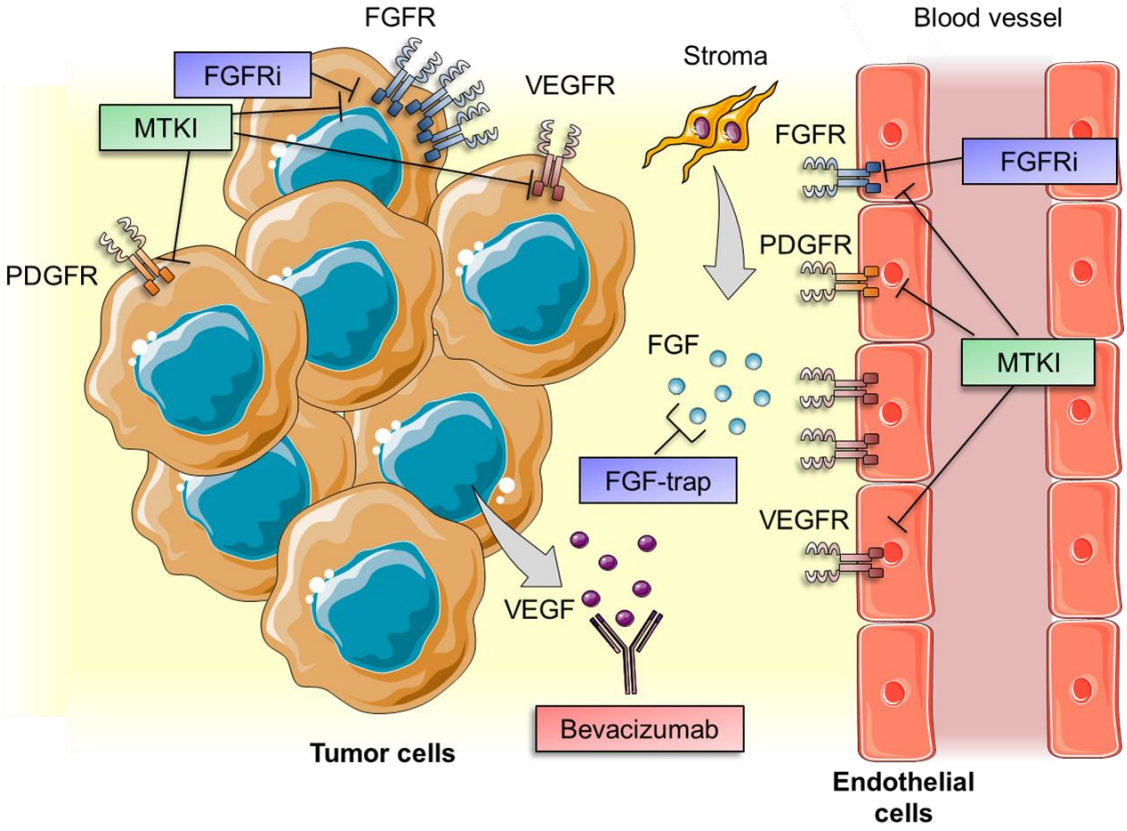

Figure 11. FGFR-targeted therapy. Specific FGFR inhibitors (FGFRi) block mainly FGF Receptors from both the tumor and blood vessels endothelial cells. Multi Tyrosine Kinase Inhibitors (MTKI) block FGFRs, VEGFRs and PDGFRs. Bevacizumab, an antibody targeting VEGF, is used to block VEGF signaling. FGF-traps serve as a mechanism to block FGF signaling from the extracellular space.

There are two main types of FGFR inhibitors: the first-generation Multi-Tyrosine Kinase Inhibitors (MTKI) that target RTK with structural similarities in the TK domain, namely FGFRs, VEGFRs, PDGFRs and c-kit; and the second-generation specific pan-FGFR inhibitors (FGFRinh), which target the TK domain of the FGFR1/2/3 receptors with high specificity and limited off-targets (**Figure 11**).

- Multitarget Tyrosine Kinase Inhibitors (MTKI)

Several MTKI have been under investigation in advanced HR+ breast cancer to overcome endocrine resistance:

- *Dovitinib* (TKI258): This is a first-generation oral tyrosine kinase inhibitor of FGFR1-3, VEGFR and PDGFR at nanomolar concentrations[177]. Phase I and Phase II trials in renal cell carcinoma showed limited efficacy[178, 179]. When compared with sorafenib, a VEGFR inhibitor (VEGFRinh), it failed to show significant differences in the outcome, and neither FGF2 levels where predictive for dovitinib responses; therefore, the effectivity of dovitinib was suspected to be only through VEGFR inhibition. In the case of breast cancer, a phase II trial showed some limited responses on *FGFR* or 11q13-amplified ER+ tumors but not on non-amplified, indicating that the inhibitor is effective when *FGFR1* acts as a driver oncogene[177, 180].

- *Lucitanib* (E3810): This is a potent FGFR1-2/VEGFR1-3/PDGFR tyrosine kinase inhibitor. A phase I/IIa trial showed encouraging response data for FGF-aberrant tumors[181] and very recently the results from phase II trial (FINESSE) on HR+/HER2- mBC showed responses among *FGFR1*amp population. The trial prematurely stopped due to severe side effects[182]. Importantly, this trial has offered the possibility to examine FGFR expression in addition to *FGFR1-4*amp as biomarker of response.

- *ODM-203*: This is an inhibitor targeting dually FGFR1-4 and VEGFR1-3. The phase I/II trial KIDES has recently showed promising results on FGFR-aberrant or VEGFR sensitive tumors from different types of malignancies (breast cancer, cholangio, endometrial, colorectal, ovarian and thyroid carcinoma)[183].

- FGFR specific inhibitors

Specific FGFR inhibitors were developed to avoid the off-FGFR target toxicities of the MTKI. Unexpectedly, these inhibitors have shown very limited responses. Therefore, efforts must be made in order to find better treatment strategies and response biomarkers for FGFR-altered tumors.

  - *AZD4547*: This inhibitor targets the catalytic domain of FGFR1-3. A phase Ib in 2017 showed modest antitumor activity in *FGFR1*amp squamous cell lung cancer (SCLC)[184]. These results indicate a high variability in gene expression of the 8p11 amplicon. In relation to breast cancer, a phase II trial showed that only 12% of *FGFR1*amp breast cancers, responded to the inhibitor[185]. In *FGFR2*amp gastric cancer, a phase II trial failed to show significantly improved PFS versus paclitaxel; tumor heterogeneity of FGFR2 expression indicated the need for alternative predictive biomarker testing[186].

  - *NVP-BGJ398*: This is another FGFR1-3 specific inhibitor. Phase I studies showed modest antitumor response in NSCL harboring *FGFR1*amp and *FGFR3*-mutant bladder/urothelial cancers[187] and in advanced gastrointestinal cancer[188]. A phase II study in advanced cholangiocarcinoma exhibit promising clinical activity with manageable toxicities in *FGFR* fusions[189].

  - *Erdafitinib (JNJ-42756493)*: This is a pan FGFR inhibitor, which targets FGFR1-4 at similar doses. A phase I in advanced solid tumors showed response in tumors with *FGFR2/3* translocations[190]. Recently, a phase I study showed encouraging responses in cholangiocarcinoma and urothelial carcinoma, carrying *FGFR* mutations or translocations[191]. After these results, the FDA approved erdafitinib for the treatment of advanced or metastatic urothelial carcinoma with FGFR mutations and translocations, being the first FGFRinh to be approved for cancer treatment[146].

  - *LY2874455:* This is an FGFR1-4 pan inhibitor. A phase I trial in 2017 showed mild responses in *FGFR*-altered patients[192], although the study indicates the need to perform further studies on FGFR inhibition.

- *TAS120:* This is an FGFR1-4 inhibitor. A phase I study showed promising results in cholangiocarcinoma harboring *FGFR2* rearrangements, and the phase II is currently ongoing[193].

- *Debio-1347:* This is an FGFR1-3 inhibitor. A phase I study in *FGFR*-altered cancer patients (*FGFR1-4*amp, mutated and translocated), including breast cancer, showed RECIST responses across tumor types and alteration nature[194]. A phase II trial is ongoing.

- *Rogaratinib (BAY1163877):* This is an FGFR1-3 inhibitor. A phase I study in urothelial carcinoma showed responses on high mRNA expressing tumors. Later on, a patient selection based on mRNA level, showed an increment on the number of responses, even in those with no reported genetic alteration in the FGFR pathway[195], indicating the possibility to screen for mRNA expression to select patients for future clinical trials.

- Antibodies and ligand traps

FGF-traps and monoclonal antibodies (mAb) target the FGFR pathway in the extracellular part, by avoiding the binding between the ligand and the receptor. Limited data and efficacy have been reported with these drugs. Nevertheless, some clinical data presented some cases where responses were achieved.

- *Bemarituzumab (FPA114)*: This mAb blocks the FGFR2-IIIb isoform. It has recently entered in a phase I trial with gastric cancer patients overexpressing FGFR2-IIIb and it seems to be very well tolerated with very mild side effects and no major toxicities[196].

- *MFGR1877S:* This mAb targets FGFR3. A phase I showed disease stabilization as the best response with manageable side effects[197].

- *FP-1039:* This FGF-trap is an engineered soluble fusion protein which consists on the extracellular domain of an FGFR1-IIIc splice form, acting as a competitive inhibitor. It has shown antiproliferative and antiangiogenic properties in cancer cell lines[198]. A phase I study in unselected advanced-solid tumors showed stable disease as best response in 41.7% of patients with measurable disease[199].

- Inhibition of angiogenesis

Antiangiogenic therapy has long been studied for the treatment of breast cancer to improve the outcomes of endocrine therapy and chemotherapy. The first drug tested was bevacizumab in combination with taxanes and later on, sorafenib in an attempt to overcome bevacizumab-related toxicities[200].

  - *Bevacizumab:* This is a mAb targeting VEGF-A. Bevacizumab has been approved by the FDA for ovarian cancer in combination with chemotherapy in 2018[201]. In breast cancer, two phase III trials evaluated the potential efficacy from adding bevacizumab to first line hormone therapy with letrozole or fulvestrant[91, 202], and a limited improvement was observed with some 3 to 4 degree toxicities. Of note, bevacizumab was granted FDA/EMA-approval on 2008 for the treatment of advanced TNBC and later on withdrawn due to lack of efficacy in follow up studies[92].

  - *Sunitinib:* This is an MTKI targeting VEGFR1-3, PGFR, KIT, RET FLT-3 and CSF-1R, with very low specificity for FGFR. Although this inhibitor has been approved by the FDA in 2018 for renal cell carcinoma[203], a phase III trial in mBC in combination with capecitabine did not improve the patient outcomes[204].

  - *Sorafenib:* This MTKI targets Raf-1, b-Raf and VEGFR-2. The FDA approved this inhibitor for advanced renal cell carcinoma in 2005 and for inoperable liver cancer in 2008. In breast cancer, its efficacy has been limited, including combinations with other drugs such chemotherapy[205]. The combination of paclitaxel with sorafenib did not show improved responses[206].

Working hypothesis and aims

This PhD thesis is focused on refining the response biomarkers to two therapeutic strategies for luminal mBC resistant to endocrine therapy: PI3K/mTORC1-targeted therapy (PART1) and FGFR-targeted therapy (PART2).

PART 1: Targeting the PI3K/mTORC1 pathway

PI3Kinh have shown limited clinical benefit in HR+ mBC. Several mechanisms of resistance have been identified, although further studies remain to be performed in order to stablish the efficacy window for PI3Kinh. The 11q13 amplicon contains several genes crucial for proliferation and cell growth and it is remarkably amplified in breast cancer[65]. Additionally, among mBC, there is an enrichment of PI3K downstream alterations (e.g. *TSC1/2* 0.7% in eBC to 6.3% in mBC)[44]. It is intriguing whether some of these genetic alterations could sensitize to mTORC1/2 inhibition. Given that, we generate the next hypothesis:

Hypothesis 1: mTORC1-activating genetic alterations confer resistance to PI3Kinh but sensitize to mTORC1/2 dual blockade

Specific aims:

a) Identify mTORC1 activating mutations in a cohort of mBC patient-derived tumor xenografts (PDX) treated with alpelisib
b) Compare the antitumor response of a PI3Kinh with an mTORC1/2inh (single treatment or in combination with endocrine therapy) in models containing mTORC1 activating mutations

Hypothesis 2: 11q13 amplification, which contains important genes for proliferation, such as *FGF3*, *FGF4*, *FGF19*, *CCND1*, *PAK1* and *RPS6KB2*, confer resistance to PI3Kinh.

Specific aims:

a) Identify 11q13 amplified models among the alpelisib treated PDXs
b) Validate the anti-tumor activity of PI3Kinh (single treatment or in combination with endocrine therapy) in genetically modified cell lines with the 11q13 genes.

PART 2: Targeting the FGFR pathway

Both MTKI and FGFRinh have shown anti-proliferative and anti-angiogenic activity *in vivo* and *in vitro*. While treatment with MTKI has resulted into remarkable disease control rates among *FGFR*-aberrant breast cancer patients, specific FGFRinh have translated into limited clinical responses, and increasing data indicates that mRNA and protein expression better predict for specific FGFR sensitivity rather than *FGFR* gene copy amplification[207]. Furthermore, there is need to understand the mode of action of agents targeting the FGF Receptor and to decipher the mechanism by which MTKI have higher effectivity than specific pan FGFRinh. Given that, we generate the next hypothesis:

Hypothesis 3: FGFR mRNA/protein expression levels and/or ligand co-amplification are better biomarkers for specific pan-FGFRinh efficacy than *FGFR* Copy Number Alterations

Specific aims:

a) Evaluate the FGFRinh response in an *FGFR1-4* and/or 11q13-amp mBC-PDX cohort
b) Determine the potential molecular determinants of sensitivity to FGFR inhibition:
    i. CN alterations
    ii. mRNA expression
    iii. protein expression
    iv. Ligand co-amplification
    v. Ligand mRNA expression
c) Stablish correlations between the potential biomarkers and the response to FGFRinh

Hypothesis 4: MTKI have higher effectivity than specific pan-FGFRinh due to dual blockade of FGFR and VEGFR

Specific aims:

1. Evaluate the response to MTKI *vs.* FGFRinh in *FGFR1*amp PDX models
2. Analyze and compare the blockade of proliferation *vs.* angiogenesis in PDX tumors treated with MTKI or FGFRinh
3. Study the combination of an FGFRinh and VEGF-targeted therapy to replace MTKI

Material and methods

1. Generation of the PDX collection

Fresh tumor samples from breast cancer patients were collected prospectively for implantation into nude mice at VHIO under an institutional review board (IRB)-approved protocol and the associated informed consent. The experiments conformed to the principles of the WMA Declaration of Helsinki and the Department of Health and Human Services Belmont Report were conducted following the European Union's animal care directive (2010/63/EU) and were approved by the Ethical Committee of Animal Experimentation of the Vall d'Hebron Research Institute. Metastatic human breast tumors were obtained from patients at time of surgery or biopsy and immediately implanted into the lower flank of 6-week-old female athymic HsdCpb:NMRI-Foxn1nu (Harlan Laboratories) or NOD.Cg-Prkdc scid Il2rg tm1Wjl /SzJ (Charles River) mice. Animals were continuously supplemented with 1μM 17β-estradiol (Sigma-Aldrich) in their drinking water. Upon growth of the engrafted tumors, the model was perpetuated by serial transplantation onto the lower flank. In each passage, flash-frozen and formalin-fixed paraffin-embedded (FFPE) samples were taken for genotyping and histological studies.

Mònica Sánchez (MS) and Cinta Hierro (CH) from *Unidad de Investigación de Terapia Molecular del caner* (UITM) at *Hospital Universitari Vall d'Hebron* (HUVH) participated in the tumor biopsy collection. Marta Guzman (MG), Olga Rodriguez (OR) and Judit Grueso (JG) from the Experimental Therapeutic Group (ETG) implanted the tumor biopsies, and maintained and expanded the PDX models.

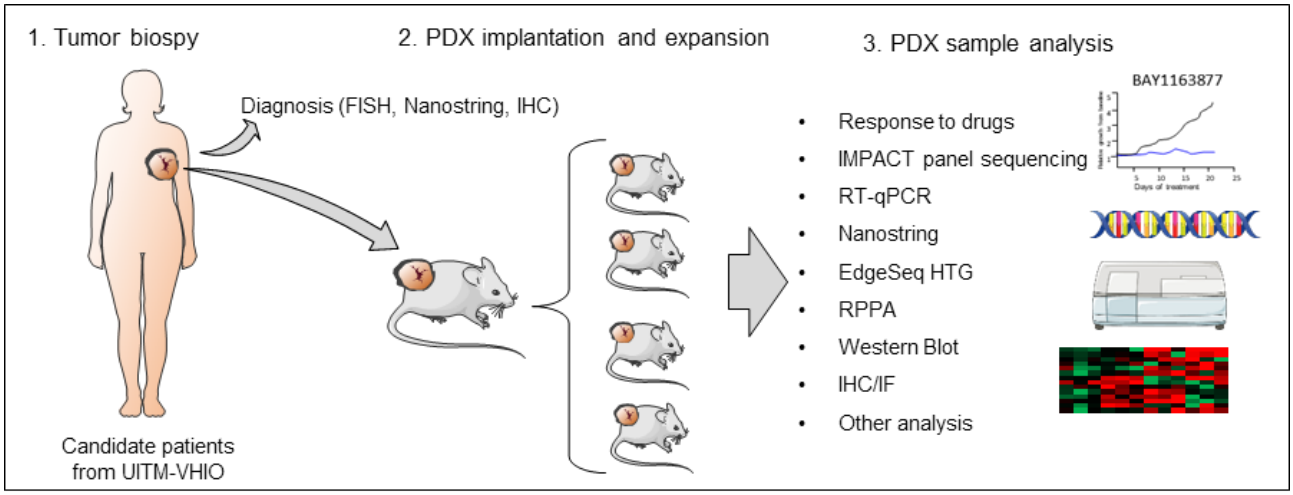

Figure 12. Tumor biopsies from patients were used for the generation of the PDX collection. Tumor biopsies were collected from patients in clinical trials from UITM-VHIO and tested for diagnostic purposes or taken for PDX implantation. Tissue fractions are implanted subcutaneously in both lower flanks of the mice. Once established the PDX line, several analyses are performed: drug efficacy assays, gene sequencing and expression, protein quantification, among others.

2. *In vivo* treatment assays

The following inhibitors were used for *in vivo* assays:

- Alpelisib, a PI3Kinh specific for the α isoform with an IC_{50} of 4.6 nM[208], was administered at 35 mg/kg/day p.o. SID 6 times per week in 0.5% carboxymethyl.
- AZD8835, a PI3Kinh specific for the α and δ isoform of PI3K with an IC_{50} of 6.2 and 5.7 nM respectively[209], was administered at 50 mg/kg p.o. BID 2 times per week in 5% Hydroxy prolyl methyl cellulose (HPMC) 1% polysorbate (Tween80).
- Vistusertib, a dual mTORC1/2inh which targets mTOR with an IC_{50} of 2.81 nM[113], was administered at 20mg/kg p.o. BID 2 times per week in 1% polysorbate (Tween80).
- AZD9496, a SERD specific for ERα with a binding affinity IC_{50} of 0.82 nM[210], was administered at 5mg/kg/day p.o. SID 6 times per week in 40% PEG 7.8% captisol.
- Rogaratinib, an FGFRinh which targets FGFR1, 2, 3 and 4 with IC_{50} of 1.8, <1, 9.2 and 1.2 nM respectively[207], was administered at 108 mg/kg/day p.o. BID 6 times per week (in 10 % ETOH/ 40 % solutol/ 50 % H_2O at pH=4).
- Lucitanib, a MTKI targeting VEGFR1/2/3, FGFR1/2/3, c-KIT, PDGFRα/β and CSF-1R, with IC_{50} of 7/25/10, 17.5/82.5/237.5, 456, 175/525 and 5 nM respectively[211], was administered at 20mg/kg/day p.o. 6 times per week in 0.5 % Methocel-methyl cellulose.

- DC101, an antibody targeting murine VEGFR2 with a K_D binding affinity of 110 pM[212], was administered at 0.8 mg/mice twice a week (Mondays and Thursdays) 150 µl IP in PBS
- Bevacizumab, an antibody targeting human VEGF-A with a K_D binding affinity of 58 pM[213], was administrated at 0.125 mg/mice twice a week (Tuesdays and Fridays) 250 µl IP in PBS.

To evaluate the sensitivity to the drugs tested, 2 to 5 mice were implanted per treatment condition with tumor fragments (3mm x 3mm) from the same "mother" tumor. After tumor growth to 100-300 mm^3, tumor-bearing mice were equally distributed into treatment groups. Tumor growth was measured with caliper bi-weekly from first day of treatment until the end of the experiment. The tumor volume was calculated as $V = 4\pi/3/Lxl^2$, "L" being the largest diameter and "l" the smallest. Mice were euthanized when tumors reached 1500 mm^3 or in case of severe weight loss, in accordance with institutional guidelines.

The antitumor activity was determined by comparing tumor volume at N days (N=35 for alpelisib and N=21 or best response for rogaratinib and lucitanib) to its baseline: % tumor volume change = $(V_{Ndays} - V_{initial})/V_{initial}$ x100. The best response was defined as the minimum value of % tumor volume change sustained for at least 10 days. To classify the response of the subcutaneous implants we modified the RECIST criteria, to be based on the % tumor volume change[214, 215]: CR (complete response), best response<-95%; PR (partial response), -95%<best response<-30%; SD (stable disease), -30%<best response<+20% (maintained at least during 35 days); PD (progressive disease), best response>+20%. Snap-frozen and FFPE tumor samples were collected 2h after dosage in all treatment arms.

For proliferation (Ki-67) and vascularization (CD31) analysis in immunofluorescence, tumors were treated during 15 days with rogaratinib or lucitanib with an initial tumor volume of 300-500 mm^3.

Drug preparation was performed by MG, OR, JG and Mireia Parés Guerrero (MPG) from ETG, with occasional help from MS. Implanted tumors were randomly distributed and measured throughout the experiments by MS (except the alpelisib-treated PDX which were performed by Marta Palafox Sánchez (MPS) from ETG) with occasional help from MG, OR, JG and MPG. MG, OR, JG and MPG dosed the mice with occasional help from MS and MPS. Tumor sample

collection was performed by MS or MPS with occasional help from MG, OR, JG and MPG. Posterior measurement analysis was performed by MS.

3. Genetic alterations identification

- MSK-IMPACT panel sequencing

Snap-frozen samples from PDX were prepared at VHIO and sent to Memorial Sloan Kettering Cancer Center (MSKCC) and processed for sequencing through MSK-IMPACT™, a hybridization capture-based next-generation sequencing which analyzes all protein-coding exons of 410 cancer-associated genes, as previously described[216, 217]. Data shown in this study are either Log2 ratios and fold-changes (PART1: PI3K/mTORC1 targeted therapy) or absolute gene copy numbers (PART2: FGFR targeted therapy).

Samples were prepared and shipped to MSKCC by MG, OR and JG. Obtained data from MSKCC was processed and analyzed by MS.

- Fluorescent In Situ Hybridization (FISH):

Formalin-Fixed Paraffin Embedded (FFPE) sample tumors were cut at 4-6 µm thick. Tissue sections were deparaffinized with xylene and hydrated with decreasing concentrations of ethanol. Samples were submerged in DAKO Pre-Treatment Solution 1X (DAKO Omnis) and put into the microwave (Whirlpool Jet Chef 6th sense) at *6th sense steam* mode –to rapidly reach the boiling temperature and avoid overheating of samples– during 15 minutes. Samples were cooled down during 15 minutes at room temperature (RT) and washed in Wash Buffer 1X (DAKO Omnis) 3 minutes two times. Samples were then digested with 5 drops of cold pepsin at 37ºC during 8 minutes in a pre-heated Hybridizer (S2450, DAKO). Samples were dehydrated with increasing concentrations of ethanol and air-dried. 1 µl of FGFR1 (G101100R-8) or FGFR4 (G101226R-8) probes were mixed with 1 µl of centromere probe (CEP8, G101034G-8; CEP5, G101067G-85501) in 9 µl of Agilent IQFISH Fast Hybridization Buffer (Agilent Technologies). The resulting 11 µl were added to each sample tissue. Samples were sealed with coverslips and Dako Coverslip Sealant and put at the Hybridizer at 90ºC 5 minutes and 45ºC 120 minutes. Coverslips were taken off and the slides were submerged in 59ºC pre-heated Dako Stringent Wash Buffer 1X (DAKO Omnis) during

10 minutes. Slides were washed during 3 minutes two times in wash buffer and dehydrated with increasing ethanol concentrations. Samples were air-dried, mounted with ProLong™ Gold Antifade Mountant with DAPI (P36931, Invitrogen) and covered with a glass cover-slip. Samples were stored in dark at -20ºC. FISH ratio was determined by dividing the number of gene copies (*FGFR1* or *FGFR4*) with the number of centromere copies, to avoid counting gene copies generated by polyploidy.

Assay performed and analyzed by the Molecular Oncology Group (MOG) at VHIO.

4. mRNA quantification

- HTG Edge Seq

2 cuts of 5 µm thick from each PDX FFPE sample were prepared in a slide. Percentage of tumor in sample was determined by Hematoxylin and Eosin (H&E) stained samples and tumoral areas were delimited in the tissue sections. Samples were sent to Firalis™ HTG EdgeSeq for posterior analysis. FFPE tissues were microdissected and lysed directly with HTG lysis buffer for 3 hours at 50ºC in the presence of proteinase K. Lysates were then run with the Oncology Biomarker Panel, which contains 2560 genes from 24 oncology related groups and pathways. Raw data were transformed to Count per millions (CPM) and Normalized using a standard HTG normalization method.

Samples were prepared and shipped to Firalis™ by MS, CH and the MOG. Obtained data was further analyzed by MS.

- nCounter

10 µm rolled cuts (≥5-10) were prepared in a safe-lock 2ml microcentrifuge tube to extract RNA. Samples were processed as previously described[218] through nCounter technology (NanoString), using an optimized VHIO-panel v.4.0 local pre-screening, which is able to detect the mRNA of 26 genes, including *FGFR1-4* and *FGF3*, *4* and *19*.

Samples were prepared by MS and MOG, and processed by the Cancer Genomics Group (CGG) at VHIO. Obtained data from the CGG was further analyzed by MS.

- RT-qPCR

mRNA from PDX biological triplicates was extracted (5 PRIME PerfectPure RNA Purification, Gentra Systems) and 0,5ug were used for PCR reaction (TaqMan™ Reverse Transcription Reagents, Invitrogen) following the methodology supplied by the company. For qRT-PCR reactions, the following predesigned assays were used: TaqMan (primers + probe FAM-MGB): Hs00915142_m1 (FGFR1), Hs01552918_m1 (FGFR2), Hs00179829_m1 (FGFR3), Hs01106908_m1 (FGFR4), Hs02800695_m1 (HPRT) and Hs01108265_m1 (POLR2A). Each reaction contained 1 µl of 1/10 diluted cDNA, 5 µl of Premix Ex Taq 2X (TAKARA), 0,4 µl of each assay mix, 0,1 µl of ROX Dye II 50x and 3,5 µl of water. Each sample had 2 assay replicates and were processed during 45 cycles on QuantStudio 5 Real-Time PCR System (Applied Biosystems).

Assay performed by MS at the Vascular Signaling Group (VSG) from IDIBELL, with occasional help from Erika Monelli (EM) from the VSG. Results were further analyzed by MS.

5. Protein quantification analysis

- Reverse phase protein array (RPPA) analysis

Snap-frozen samples from PDXs were prepared and sent to MD Anderson Cancer Center for RPPA analysis as previously described[219, 220]. PDX tumor proteins were denatured by 1% (w/v) SDS in the presence of β-mercaptoethanol and adjusted to a final concentration of 1mg/ml. Samples were diluted in five serial 2-fold dilutions in dilution buffer (lysis buffer containing 1% SDS) and arrayed on nitrocellulose-coated slides (Grace Biolab) using an Aushon 2470 Arrayer (Aushon BioSystems). Each slide was probed with a validated primary antibody plus a biotin-conjugated secondary antibody. The signal obtained was amplified using a DakoCytomation–catalyzed system (Dako) and visualized by DAB colorimetric reaction. Slides were scanned, analyzed and quantified using a customized-software Microvigene (VigeneTech Inc.) to generate spot intensity.

Samples were prepared and shipped to MD Anderson Cancer Center by MS, MPS, MG, OR and JG. Obtained data was analyzed by MS.

- Protein isolation and immunoblotting

Flash-frozen pieces of tumor and cell plates were lysed in ice-cold buffer containing Tris–HCl pH 7.8 20 mmol/L, NaCl 137 mmol/L, EDTA pH 8.0 2 mmol/L, NP40 1%, glycerol 10%, supplemented with 1X protease inhibitor cocktail (cOmplete, Roche) and Na_2VO_4 200 mmol/L. Homogenization was performed on ice with a POLYTRON® system PT 1200 E (Kinematica). Lysates were centrifuged at 15.000 xg 4ºC during 30 min and the supernatants were collected. Protein concentration was calculated using DC™ Protein Assay (Bio-Rad). A total of 30 µg of protein were separated on 12% SDS-PAGE at 100V and transferred to nitrocellulose membrane during 1.5h at 100V. Membranes were blocked for 1 hour in 5% milk in Tris-buffered saline (TBS)-0,1%Tween and then hybridized using the primary antibodies in 5% BSA TBS-0,1%Tween overnight at 1:1000 dilution, except were stated. Mouse and rabbit horseradish peroxidase (HRP)-conjugated secondary antibodies (1:5000; GE Healthcare) were diluted in 5% milk in TBS-Tween and incubated during 1 hour. Proteins were detected with Immobilon Western Chemiluminescent HRP substrate (Millipore). Blots were developed either with films (Fuji Medical X-Ray Film) or at a chemiluminescence imager (Amersham Imager 600). Films were digitalized and images were processed in Photoshop, Adobe Illustrator and PowerPoint. ImageJ (https://fiji.sc/) was used for immunoblot band quantification. The following primary antibodies were used:

LKB1 (Cell Signaling Technology (CST) #3047), Hamartin/TSC1 (CST #6935), Tuberin/TSC2 (CST #4308), phospho-AKT T308 (CST #4056), phospho-AKT S473 (CST #9271), AKT (CST #9272), phospho-S6 S235/236 (CST #2211, 1:2000), phospho-S6 S240/244 (CST #2215, 1:2000), phospho-4EBP1 T37/42 (CST #2855), phospho-4EBP1 T70 (CST #9455), phospho-NDRG1 T346 (CST #5482), NDRG1 (CST #9485), human-GAPDH (Abcam ab128915), tubulin (Sigma-Aldrich T5168, 1:5000), ERα (CST #8644), Cyclin D1 (Abcam, #ab40754), phospho-Rb S780 (CST #9307), phospho-Rb S807/811 (CST #9308), PAK1 (CST #2602), p70/ S6 kinase β2 (CST #14130), phospho-Erk1/2 T202/Y204 (CST #4376), Erk1/2 (CST #9102), FGFR1 (CST #9740), FGFR3 (CST #4574), phospho-FRS2α Y196 (CST #3864) and phospho-FRS2α Y436 (CST #3861).

Assays performed by MS except western blots from Figure 22, which have been performed by Laia Monserrat (LM) from ETG.

- Immunofluorescence (IF) and immunohistochemistry (IHC) assays

Immunofluorescence (IF) assays were performed in 3 µm thick FFPE tumor samples. Tissue sections were deparaffinized with xylene and hydrated with decreasing concentrations of ethanol. For target antigen retrieval, sections were heated for 20 min in a microwave (Whirlpool Jet Chef 6th sense) at *6th sense steam* mode (as stated before at FISH pre-treatment step) in DAKO Antigen Retrieval Buffer pH 6.0. Sections were cooled down in distilled water for 30 min, then permeabilized with DAKO Wash Buffer (containing 0.1% Tween 20) for 5 min, followed by incubation in blocking buffer (DAKO Wash Buffer with 1% bovine serum albumin) for 5 min. Primary antibodies were diluted in DAKO Antibody Diluent and incubated at RT for 1 hour. Sections were washed for 5 min in DAKO Wash Buffer followed by 5 min in blocking buffer. Secondary antibodies were diluted in blocking buffer and incubated for 30 min at RT. The 2-step washing was repeated followed by 5 min incubation in distilled water. Dehydration was performed with increasing concentrations of ethanol. Sections were mounted with DAPI ProLong Gold antifading reagent and stored at 4°C. CD31 antibody (Abcam ab28364) was diluted at 1/100 and Ki-67 antibody (Dako M7240) was incubated at 1/200. Goat anti-rabbit Alexa fluor 568 and goat anti-mouse Alexa fluor 488 (Invitrogen, 1:500) were used as secondary antibodies.

Immunohistochemistry (IHC) of FGFR2 (Novus Biologicals NB200-642) was additionally blocked in endogenous peroxidase block (3% H_2O_2 in dH_2O) for 10 min and antibody detection was performed with DAKO Envision HRP for 30 min with visualization using DAKO DAB solution for 10 min and counterstaining in Carazzi's hematoxylin. Samples were further quantified using QuPath (https://qupath.github.io/) and ImageJ (https://fiji.sc/).

Assays performed by MS. EM helped in the setting up for the CD31 IF.

6. Phospholipid quantification

Phospholipid extraction from frozen tissue and quantification was performed as previously described[221]. Frozen pieces of tumor from PDX models were grinded in liquid nitrogen into a fine powder. Small amounts of powder (approx. 0.5 mg) were net weighted in 2 ml Eppendorf tubes. Samples were diluted in 1 ml of solvent mixture containing chloroform, methanol and acidified aqueous solution at 1.25:2.5:1.0 (v/v). At this point, 10 µl of PI and

10 µl of PIP_3 are added as internal lipid standards (ISD, control for lipid extraction and posterior derivatization). To split the solution into 2 phases, additional chloroform, methanol and 0.1 HCl is added in order to reach final proportions of chloroform, methanol and acidified aqueous solution of 8:4:3 (v/v). An upper aqueous phase and a lower organic phase containing the phospholipids appear after the tubes are vortexed and centrifuged. After washing with more acidified aqueous solution, the organic phase is carefully removed for derivatization (methylation of the phosphoinositol free hydroxyl radicals). 50 µl of TMS-diazomethane are added to the samples during 10 min at RT for derivatization of the lipids. 6 µl of glacial acetic acid are added to remove any unreacted TMS diazomethane. The organic phase is then washed twice with a solution containing chloroform, methanol and water at 6:3:2.25 (v/v). 100 µl of 90% methanol are added to each sample and then carefully dried at RT. When almost dry, each sample was immediately dissolved in 100 µl of an 80% methanol solution. Samples were then vortexed, briefly sonicated and taken for the lipid quantification at the mass spectrometry core facility from Babraham Institute. The obtained phospholipid quantifications are normalized by the internal ISDs.

Assay performed by MS with assistance from David Barneda at Len Stephens and Phillip Hawkins lab in the Babraham Institute, Cambridge, UK.

7. Cell culture assays

MCF7, T47D, CAL120 and JIMT1 cell lines were purchased from ATCC. SUM44 cell line was a kind gift from N Turner lab. MCF7, T47D, CAL120 and JIMT-1 cell lines were cultured in DMEM (Gibco) + 10% FBS (LOT 42F8973K, Gibco) and SUM44 cell line was cultured in DMEM + 10% FBS + 1nM E_2. Cell lines were routinely tested for mycoplasma contamination.

- Generation of genetically modified cell lines

Plasmids were purchased from Origene: pLenti-*CCND1*-mGFP (RC204957L2), p.CMV-*PAK1*-tGFP (RG225947), p.CMV-*RPS6KB2*-tGFP (RG200525) and p.Lenti-C-mGFP (PS100071). p.CMV-*PAK1*-tGFP and p.CMV-*RPS6KB2*-tGFP were cloned at the p.Lenti-C-mGFP backbone: plasmids were digested with BamHI and NotI restriction enzymes during 1h at 37ºC; digestions were run in an agarose gel and inserts/vector bands were purified (NucleoSpin Gel and PCR Clean-up, Macherey-Nagel); 25 ng vector and 75 ng insert (ratio

1:3) were used for ligation with Rapid DNA ligation Kit (Roche) during 15 min at RT; ligations mix were transformed in OneShot Stbl3 bacterial strain (Invitrogen); 5 resulting colonies were selected for miniprep plasmid purification (Wizard® Plus Minipreps DNA Purification System, Promega) and purified plasmids were tested to check correct ligations through BamHI and NotI digestion and sequencing using VP.2 and LR50 probes; plasmids with correct sequences were selected for lentiviral infection (p.Lenti-*PAK1*-mGFP and p.Lenti-*RPS6KB2*-mGFP). Aliquots with high plasmid concentrations were generated using the Plasmid Purification Maxi Kit (Jetstar).

Lentiviral vectors (10 µg of p.Lenti-*CCND1*-mGFP, p.Lenti-*PAK1*-mGFP, p.Lenti-*RPS6KB2*-mGFP or pLenti-C-mGFP with 5 µg psPAX2 and 3 µg pMD.G2) were transfected using PEI (Polysciences) at ratio 1:3 (DNA:PEI) in an 80-90% confluent HEK293 cells (<20 passages) 150 mm plate in DMEM + 10% FBS (heat inactivated). Media was replaced 24h after transfection with DMEM + 5% FBS (inactivated) + 5mM Sodium Butyrate (Sigma-Aldrich). 48h after transfection, media was collected and filtered with 0.45 µm PVDF filters and stored at 4ºC. Media was replaced with new DMEM + 5% FBS + 5mM Na butyrate, and collected after another 24h. Collected and filtered media was used to infect MCF7 and T47D cell lines seeded in p6 plates at 50-60% confluency, at different ratios: 1:1, 1:2, 1:5 and 1:10 (supernatant with lentivirus : fresh media) with 8 µg/µl Polybrene (Sigma-Aldrich). MCF7 and T47D cells infection media was replaced after 24h with fresh DMEM +10% FBS. After 3 to 7 days cells were checked for GFP positivity in a fluorescence microscope. If GFP positive, cell plates for western blot were collected to check protein overexpression.

Vector cloning assays were performed by MS. *CCND1* lentiviral infection was performed by MPS and LM. *PAK1* and *RPS6KB2* lentiviral infections were performed by LM and MS.

- <u>Drug inhibition curves for cell assays</u>

AZD8835, AZD9496, rogaratinib and the following inhibitors have been used for *in vitro* assays:

- *FRAX-1036*: a PAKinh targeting PAK1, PAK2 and PAK4 at a Ki of 23.3 nM, 72.4 nM and 2.4 µM, respectively[222].

- *PF-4708671:* a P70/S6Kinh targeting the Alpha isoform of P70/S6K (S6K1) and S6K2 with an IC_{50} of 0.16 and 65 µM, respectively[223].
- *NSC12:* A small molecule derived from the soluble pattern recognition receptor long-pentraxin 3 (PTX3). It has been shown to limit proliferation by binding to multiple FGFs[224].

AZD8835, FRAX-1036 (S7989, Selleckchem), PF-4708671 (S2163, Selleckchem) and rogaratinib were used for drug-inhibition assays. 5 000 cells were seeded per well in a 96-well plate in DMEM + 10% FBS. To test resistance upon high FGF, cells were plated at DMEM + 1% FBS with or without 20 ng of basic FGF (bFGF/*FGF2*, 10018B, Preprotech, stock at 100µg/ml in PBS). Three replicates were used per experimental condition and 10 different drug concentrations (from 0,001 to 500 µM) were used to calculate IC_{50}. For FRAX-1036, 9 different drug concentrations were used (from 0.001 to 100 µM). For rogaratinib, cells were seeded in DMEM + 1% FBS, with 20 nM bFGF or 5 µM NSC12 (S7940 Selleckchem, stock at 5 mM in DMSO) depending on the experimental condition. For AZD8835 and AZD9496 combinations, 5 000 cells were seeded in 96-well plates in triplicates in DMEM + 1% FBS and 20 nM of bFGF was added according to the experimental condition. Cells were treated with 500 nM AZD8835, 1 µM AZD9496 or both inhibitors.

All plates were read after 4 days of treatment with CellTiter Glo® Luminiscent Cell Viability Assay (Promega) in an Infinite M200 PRO plate reader (TEKAN). Each experiment was repeated 3 times, except were stated.

All drug inhibition assays were performed by MS except AZD8835 curves of mock/*CCND1*/*PAK1*/*RPS6KB2* which were performed by LM with occasional help from MS.

8. Patient-derived organoids (PDO) *ex vivo* cultures

- Tumor tissue digestion

Tumors from PDX were extracted, minced and digested with dissociation media (collagenase (Sigma Aldrich) at 1mg/ml, hyaluronidase (Sigma Aldrich) at 0.1 mg/ml, 2% BSA, 5 µg/µl Insulin (Roche) and 50 µg/µl gentamycin (Gibco) in DMEM (Gibco)) for 1h at 37°C constantly shaking at 1500 rpm. Digested tumors were pelleted, washed with DMEM and centrifuged at 200xg during 3 minutes to enrich the pellet with epithelial cells. Further

digestions were performed with 2ml of trypsin-EDTA during 2-3 minutes and reaction was stopped using cold Hank's (HBSS) + Ca + Mg (L0612-500, Biowest) + 2% FBS + 2% Hepes (Gibco). 2ml of 1 mg/ml dispase (STEMCELL) and 200/500 µl of DNase I (Sigma) were added and reaction was stopped again with the supplemented cold Hank's buffer. Digestions were centrifuged at 450xg at 4°C. To eliminate erythrocytes from the samples, digestions were incubated with RBC digestion buffer (Invitrogen). Pellets were washed and resuspended in DMEM to count cells with Neubauer chamber.

Tumors were collected and processed by MG, OR and JG with occasional help from MPS and MS.

- Drug inhibition curves with PDOs

For drug inhibition curves of PDOs, isolated cells of each model were resuspended in RPMI media (Gibco) + 2% FBS, 1X B27 (Gibco), 20 ng/ml EGF (AF-100-15, Peprotech), 50 µg/µl gentamycin (Gibco) and 150 ng/ml Fungizone™ (Gibco). Depending on experimental conditions, 20 nM bFGF or 5 µM NSC12 were added in the media. 20 µl of Matrigel were seeded in each well of a 96-well plate. Two replicates per experimental condition were performed and 10 drug concentrations (from 0.001 to 500 µM) of rogaratinib were used. Cells were treated the day after seeding and plates were read 4 days after treatment. To eliminate Matrigel, wells were incubated with cold PBS+HEPES on ice during 1h, and then plate readings were performed using CellTiter Glo® Luminescent Cell Viability Assay (Promega). Each experiment was repeated 3 times except were stated.

Drug inhibition assays in PDOs were performed by MS.

9. Image analysis

Whole IF samples were scanned using NIS Elements Imaging Software with Nikon Eclipse Ti microscope and Nikon Intensilight C-HGFIE fluorescence source. Images were taken delimiting the top, bottom, left and right limits of the sample and creating a large image from individual 20X fields. The obtained large images were exported into TIFF and were analyzed in ImageJ (https://fiji.sc/). Tumoral, stromal and necrotic areas were delimited using DAPI channels and digitalized hematoxylin and eosin (H&E) stainings (NanoZoomer

2.0HT, Hamamatsu) from the same sample as references (**Figure 13**). CD31 in viable area was quantified setting a threshold for positive area in mCherry channel and excluding outside sample and necrotic areas. CD31 in tumoral and stromal area were quantified as positive mCherry area in respective areas. Ki-67 was quantified counting FITC positive nuclei per 100 DAPI nuclei in 5 different and representative tumoral areas. At least 3 biological replicates for each experimental condition were used.

IF image scanning and processing was performed by MS. H&E image scanning was performed by the MOG and processed by MS.

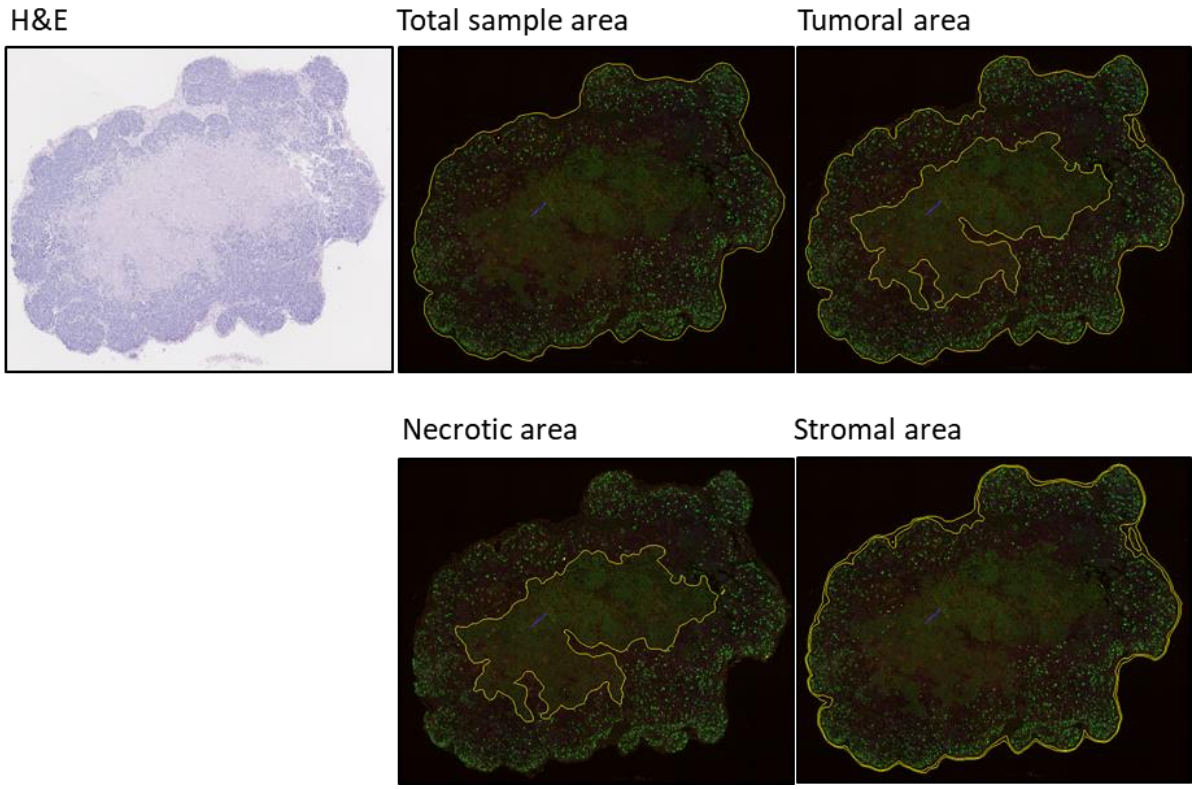

Figure13. Image processing for IF analysis. Two contiguous transversal cuts from FFPE tumor samples from PDXs were processed for hematoxylin and eosin (H&E) or for CD31 and Ki-67 IF. Whole dyed tissues were digitalized and analyzed in ImageJ for area delimitation: total sample area, tumoral area, necrotic area and stromal area. CD31 was measured in all viable area (total sample area minus necrotic area), or stromal and tumoral areas, separately.

10. Statistical analysis

All statistical tests were performed with GraphPad Prism version 6.01. Unpaired t test (two-tail), one-way or 2-way ANOVA were used to analyze differences among groups, except for **Figure 31 and 33**, where Mann-Whitney U test was performed due to a non-Gaussian distribution of the data. Fisher's exact test was used to determine associations with alpelisib response in **Table 1**. Individual t-tests of the RPPA data set (**Figure 15**) were performed after log2 transformation and Benjamini-Hockberg correction was used to correct for multiple comparisons, with a False Discovery Rate (FDR) set at 1%. Error bars in the *in vivo* assays represent ±SEM of at least two biological replicates, and error bars in the cell line assays represent ±SD of at least three biological replicates, unless otherwise stated. ROC curves (Receiver Operating Characteristics) were used to evaluate biomarkers of response in **Figure 28**, **31** and **33** comparing *sensitivity* (true positives in relation to true positives and false negatives) and *specificity* (true negatives in relation to true negatives and false positives). A ROC curve of a good biomarker of response will reach the upper left corner of the graph, tending for 100% sensitivity and 100% specificity. R square was used to determine the goodness of fit (0=no fit, 1=perfect fit) and F-test was used to determine the significance of the correlation in **Figure 21**, **29**, **30** and **32.**

Legend of the p-value symbols: ns, non-significant; *, $0.01 \leq p < 0.05$; **, $0.001 \leq p < 0.01$; ***, $0.0001 \leq p < 0.001$; ****: $p < 0.0001$

Results

1. PART 1: Targeting the PI3K/mTORC1 pathway

1.1. Identification of PI3Kα inhibitor response biomarkers in a BC PDX collection

We created a collection of 25 breast cancer PDXs and tested the antitumor activity of the PI3Kα inhibitor alpelisib, the specific α-isoform PI3Kinh (**Figure 14**). We established the molecular and the intrinsic subtypes of the PDX collection using immunohistochemistry and the so called "PAM50 nanostring panel". 17 models were ER+, 3 ER-/HER2+, 2 ER+/HER2+ and 3 TNBC. The majority of the intrinsic subtypes were concordant with the molecular subtype classification, except for 3 ER+ models that had basal-like expression profile (PDX313, STG201 and PDX098) and 1 ER+ showed a Her2-enriched profile (PDX225). 5 PDX (3 ER+ and 2 HER2+) showed a partial response (PR), 6 (3 ER+, 1 HER2+ and 2 ER+/HER2+) showed a stable disease (SD) and 14 (11 ER+ and 3 TNBC) showed a progressive disease (PD). All basal-like/TNBC PDXs were resistant to alpelisib (p-value=0.0161) and most of the Her2-enriched/HER2 models were sensitive (p-value=0.0109). No association was found for luminal B models (**Table 1**).

In order to identify response biomarkers and resistance mechanisms using a clinically relevant platform, we performed a capture-based cancer gene panel sequencing of the PDX models using the MSKCC panel of 410 genes frequently altered in cancer. For the analysis, we selected alterations in genes participating in the PI3K-AKT-MTOR pathway (*ERBB2*, *PIK3CA*, *ESR1*, *PTEN*, *AKT1-3*, *TSC1*, *TSC2*, *MTOR*, *RPTOR* and *STK11*), genes within the Ras/MAPK pathway (*FGFR1, KRAS, NF1, MAP3K1* and *MAPK3*) and cell cycle genes (*RB1, CDKN1B-p27, CDKN2A-p16, CDKN2A-p14, CDKN2B-p15, CCND1, CCND2* and *TP53*) including those located in the 11q13 amplicon, frequently altered in BC (*RPS6KB2*, *CCND1*, *FGF19*, *FGF4*, *FGF3* and *PAK1*) (**Annex Table S2**). *ERBB2* was amplified in all HER2+ models and it was associated with alpelisib response (p-value=0.0026). Seven models harbored a *PIK3CA* activating mutation and four of them were classified as sensitive, for which *PIK3CA* mutation was not significantly associated with alpelisib response. Similarly, *ESR1* and *TP53* mutations failed to show an association with response in this cohort (**Table 1**).

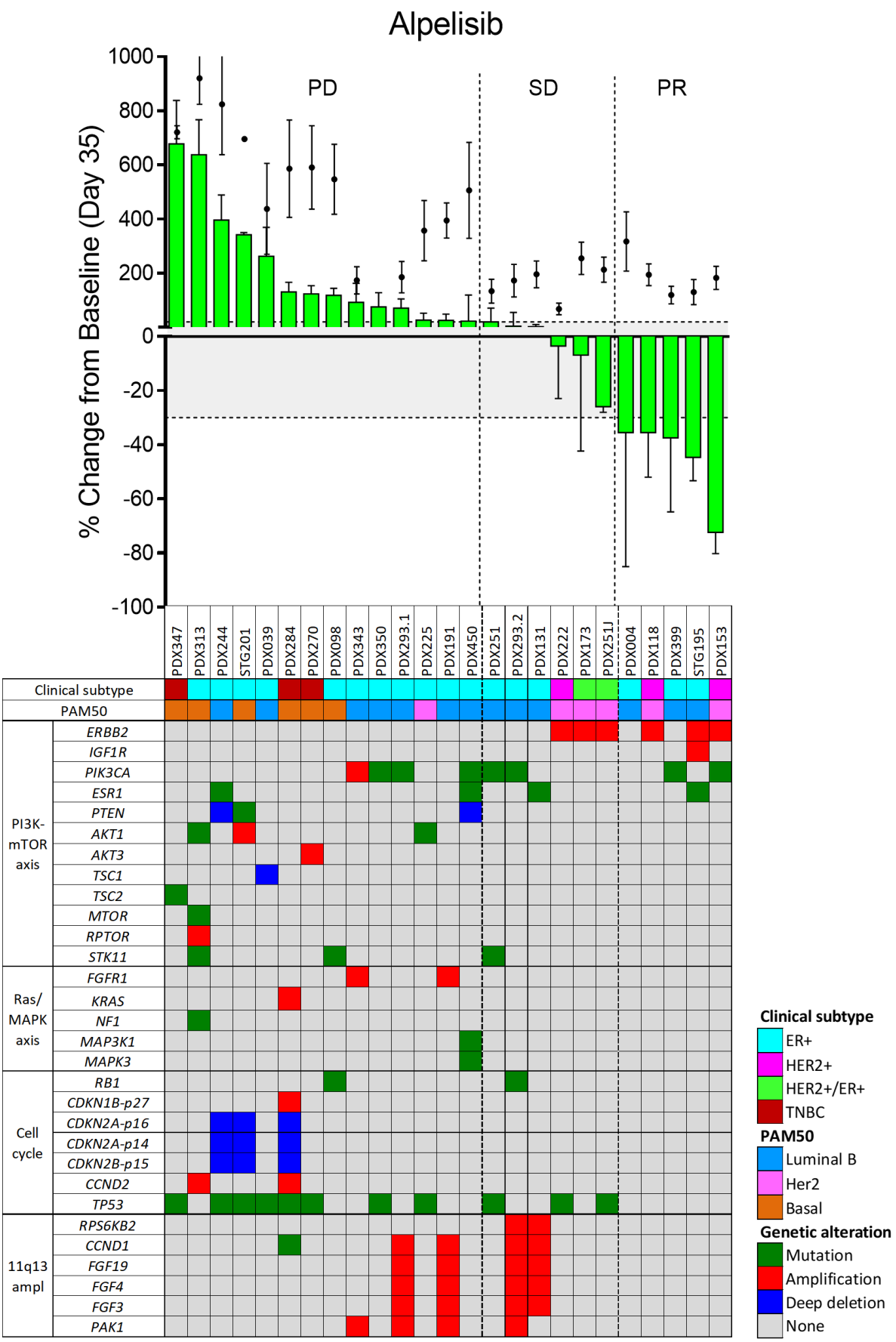
Alpelisib
PD
SD
PR
% Change from Baseline (Day 35)
1000
800
600
400
200
0
-20
-40
-60
-80
-100
PDX347
PDX313
PDX244
STG201
PDX039
PDX284
PDX270
PDX098
PDX343
PDX350
PDX293.1
PDX225
PDX191
PDX450
PDX251
PDX293.2
PDX131
PDX222
PDX173
PDX251J
PDX004
PDX118
PDX399
STG195
PDX153
Clinical subtype
PAM50
PI3K-mTOR axis
ERBB2
IGF1R
PIK3CA
ESR1
PTEN
AKT1
AKT3
TSC1
TSC2
MTOR
RPTOR
STK11
Ras/MAPK axis
FGFR1
KRAS
NF1
MAP3K1
MAPK3
Cell cycle
RB1
CDKN1B-p27
CDKN2A-p16
CDKN2A-p14
CDKN2B-p15
CCND2
TP53
11q13 ampl
RPS6KB2
CCND1
FGF19
FGF4
FGF3
PAK1
Clinical subtype
ER+
HER2+
HER2+/ER+
TNBC
PAM50
Luminal B
Her2
Basal
Genetic alteration
Mutation
Amplification
Deep deletion
None

Figure 14. Alpelisib showed antitumor activity in 11 models from a collection of 25 PDXs Waterfall plot of percentage change from baseline of alpelisib (green bars) at day 35 in 25 models of mBC PDX and their genetic profile. CNTL growth is represented in black dots. Measurements are denoted in **Annex Table S1**. Depicted in table below are the intrinsic subtypes, the genetic and overall pathway alterations obtained through IMPACT sequencing panel. VAF below 0.2 and Log2ratios below 1.58 (fold-change=3) are not considered.

We observed that genetic alterations downstream PI3K pathway were more frequent among the resistant models (PD) than among the sensitive models (SD+PR) (8 out of 14 *vs.* 1 out of 11, p value=0.0131): *PTEN* was altered in 3 models: PDX244 and PDX343, with a deep deletion, and STG201, with a frameshift mutation. *AKT1/3* were analyzed: we found 2 models with an activating mutation in *AKT1* p.E17K[225]: PDX313 and PDX225; one model with an amplification in *AKT1*, STG201, and an amplification in the *AKT3* gene, PDX270. The TSC1/2 complex was as well found to be altered: *TSC1* was deleted in PDX039 and TSC2 was mutated in PDX347, with an unknown effect on the protein. The PDX313 model, besides the *AKT1* mutation, contained other altered genes downstream PI3K: a mutation in *MTOR* gene (p.W1456G, VAF=0.46), located in a hotspot region of the gene previously described to harbor activating mutations[226] and a mutation with an unknown functional effect in *STK11* gene (p.K191E, VAF=0.99), coding for the LKB1 protein, among others. *STK11* was as well altered in 2 other models: PDX098, containing a nonsense mutation, and PDX251, with a missense mutation of unknown function.

We observed that alterations in the MAPK pathway were as well significantly associated with alpelisib response (p-value=0.0464). 5 models from the 14 PD contained an alteration in the pathway: PDX313 harbored a mutation with unknown effect in *NF1*, a Ras inhibitor; PDX284 had an amplification of *KRAS*; PDX343 and PDX191 contained an amplification of *FGFR1*, which would likely activate MAPK pathway; and PDX450, harbored a mutation in *MAP3K1* (MEKK1) and a mutation in *MAPK3* (ERK1), both with unknown functional effect.

We evaluated alterations in cell cycle-related genes and we did not find a significant association with alpelisib response. Nevertheless, important deletions in p16, p14 and p15 were found in PDX244, STG201 and PDX284 resistant models.

We observed that the four PDXs harboring an 11q13 amplification were located at the boundary between SD and PD responses, including two models derived from the same

patient that harbored a concomitant *PIK3CA* hotspot mutation PDX293.1/2. In detail, the PDX293.1 biopsy was taken on-treatment with taselisib + letrozole (with a confirmed response of -26% RECIST) and the PDX293.2 biopsy at progression. Intriguingly, PDX293.1 falls into PD category (+70.6% change from baseline) and PDX293.2 into SD category (+3.8% change from baseline). This suggests a subclonal selection at the time of the biopsy or during the passages of the PDX model in the mice. Of note, we observed the acquisition of a subclonal *RB1* missense mutation in PDX293.2. The other two models with an 11q13 amplification were PDX131 and PDX191, and PDX343 only showed *PAK1*amp.

		Progression Disease (PD)	**Stable Disease (SD)**	**Partial Response (PR)**	**P-value (Fishers exact test) PD *vs.* SD+PR**
Intrinsic subtype	**Luminal B**	7/14	3/6	3/5	1
	Her2-enriched	1/14	3/6	2/5	**0.0109 ***
	Basal-like	6/14	0/6	0/5	**0.0196 ***
Specific genetic alterations	***ERBB2* amplification**	0/14	3/6	3/5	**0.0026 ****
	***PIK3CA* mutations /amp**	4/14	2/6	2/5	1
	***ESR1* mutations**	3/14	1/6	1/5	1
	***TP53* mutations**	8/14	3/6	0/5	0.2272
	11q13 amplification	3/14	2/6	0/5	1
Pathway alterations	**PI3K downstream alterations**	8/14	1/6	0/5	**0.0330 ***
	MAPK pathway	5/14	0/6	0/5	**0.0464 ***
	Cell cycle	7/14	2/6	0/5	0.2077

Table 1. Biomarker analysis of PDX collection reveal a significant increase of genetic alterations downstream PI3K and in the MAPK pathway in the resistant setting. Count for PDX models intrinsic subtype, specific genetic alterations and pathway alterations. Statistical test: Fisher's exact test.

We further aimed to identify PI3Kinh biomarkers at the protein level. In collaboration with MD Anderson, we performed an RPPA analysis to study the differences in protein expression between the resistant and the sensitive models (**Figure 15**). Results from individual t-tests showed 19 proteins and phosphoproteins significantly different between the two groups, albeit below significance after False discovery rate (FDR) analysis was performed (Benjamini-Hockberg correction). Nevertheless, the proteins identified by the individual t-tests were consistent with our hypothesis that PI3Kinh-resistant tumors harbor activated downstream or parallel signaling, resulting in high mTORC1/MAPK activity: Tuberin (*TSC2*) was downregulated, and MEK and S6 phosphorylation, were higher in the resistant models. In addition, we also noted that INPP4b, the phosphatase converting $PI(3,4)P_2$ into PI(3)P was low in PI3Kinh-resistant tumors, suggesting a potential accumulation of $PI(3,4)P_2$, a lipid membrane also capable of recruiting AKT to the membrane[227]. In agreement with the previous data, we also observed that Her2 phosphorylation and the RTK/IRS signaling protein SHP-2 was higher in the sensitive models. Proteins related with other signaling pathways were found significantly different: PARP1 and caspase3 expression were high in resistant models suggesting that resistant tumors would have a more dependency on apoptosis pathways. Finally, PKM2 and glutaminase were high in PI3Kinh resistant tumors, suggesting an activated TCA cycle by both increased glycolysis and glutamate production.

In collaboration with the Babraham Institute in Camdridge, UK, we evaluated PIP_3 levels as biomarker of response to alpelisib (**Figure 16**). We quantified PI, PIP, PIP_2 and PIP_3 in 8 selected models –due to limited sample availability, we could not evaluate phosphoinositol levels in models with PR. Results showed a down-modulation of PIP_3/PI ratio in sensitive models upon alpelisib treatment. However, sensitive models failed to show higher PIP_3 ratios in untreated samples, pointing that PIP_3 could not function as a biomarker of response to alpelisib.

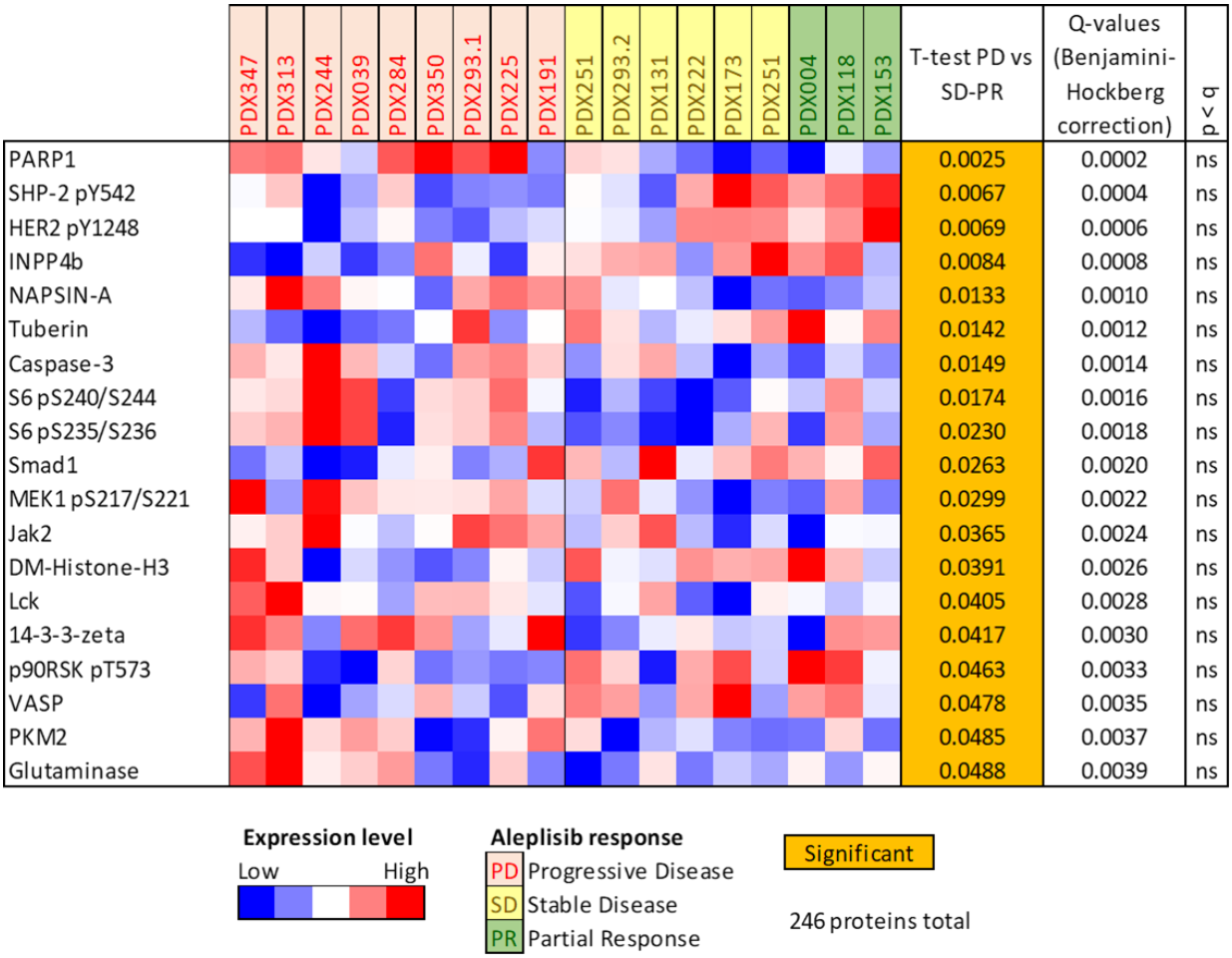

Figure 15. RPPA analysis shows high mTORC1 activity markers in the alpelisib resistant PDs. 18 samples from the total of 24 alpelisib-treated collection were analyzed with the RPPA protein expression assay. P-values for significant proteins from individual t-tests and generated q-values from the Benjamini-Hockberg multiple t-test correction are shown.

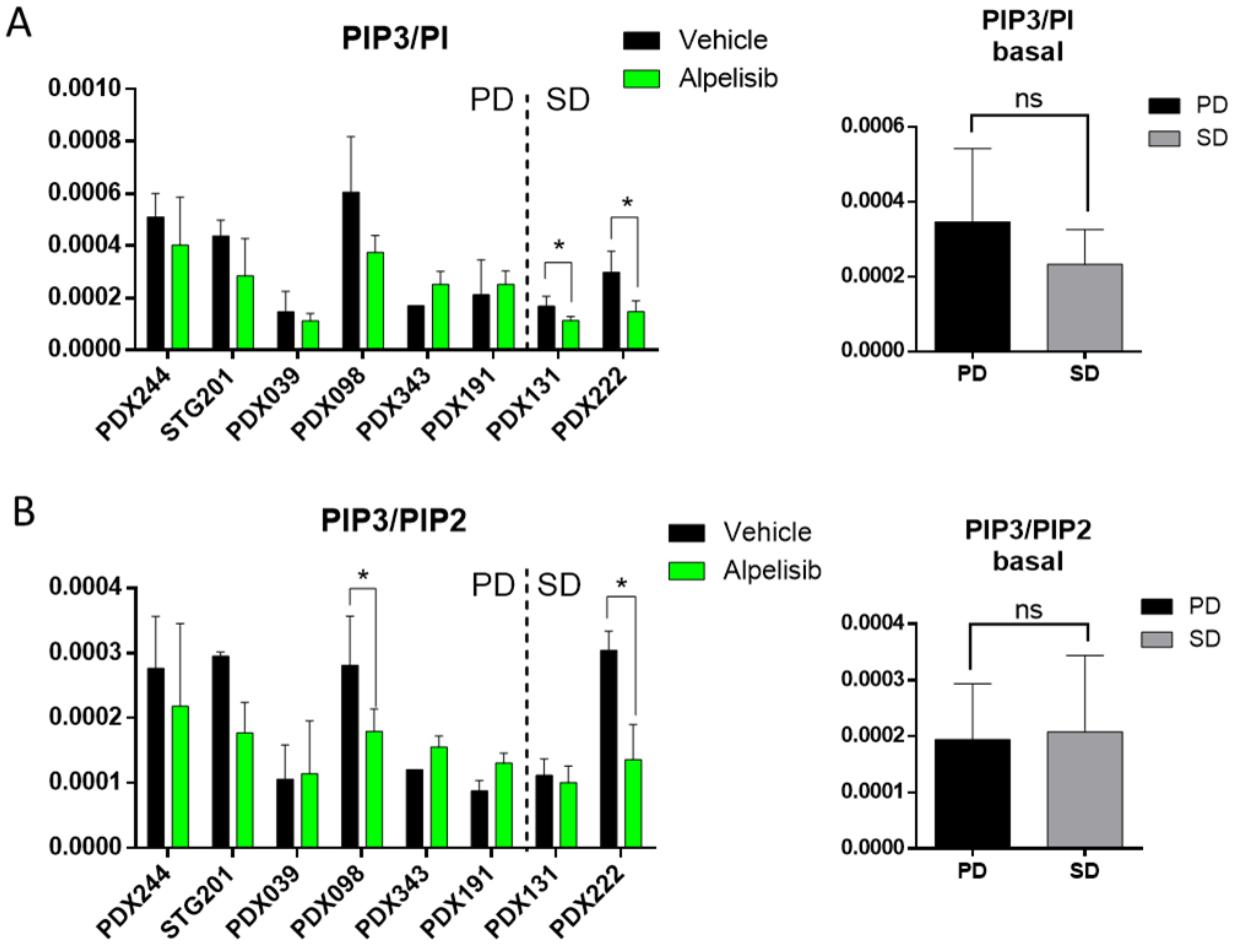

Figure 16. Relative quantification of PIP_3 show a modulation of PIP_3 in sensitive PDX models. A) PIP_3 levels are shown relative to PI levels in alpelisib-treated and untreated samples; B) PIP_3 levels are represented relative to PIP_2 levels. Error bars denote SD. At least 2 replicates per condition were analyzed except for untreated PDX343, where only 1 sample could be evaluated. Statistical test: unpaired t-test.

1.2. Models harboring mTORC1 activating alterations show resistance to PI3Kinh.

We noted that tumors harboring mTORC1 activations are resistant to PI3Kinh and argued that they might have intrinsic sensitivity to mTORC1 inhibitors. To this aim, we compared the activity of an mTORC1/2inh *vs.* a PI3Kinh in three models containing mTORC1-activating (or likely activating) mutations: PDX313 that contains several genetic alterations downstream PI3K; PDX039, with a *TSC1* deep deletion; and PDX251 that harbors a mutation in *STK11* in addition to a *PIK3CA* activating mutation (**Figure 17**).

Data from IMPACT panel sequencing showed 19 nonsynonymous alterations and 7 copy number alterations (CNA) in PDX313. Among all the alterations, *STK11* p.K191E, *AKT1* p.E17K and *MTOR* p.W1456G were selected to potentially activate mTORC1. The *MTOR* mutation is found in a hotspot for activating mutations in heterozygosity. The activating mutation *AKT1* p.E17K is in homozygosity, as it is *STK11* p.K191E, of unknown function. Other alterations found in this PDX could as well be determinant for tumor growth and resistance: an *NF1* mutation, a negative regulator of MAPK pathway, which could impair protein function, *RPTOR* amplification (a negative regulator of mTORC1 complex); and a *CCND2* amplification, coding for Cyclin D2, that could facilitate early entry in S-phase by activating CDK4/6.

PDX039 harbors 9 nonsynonymous alterations and 26 CNA, of which *TSC1* deletion is the most likely to be the oncogenic driver (log2 ratio below -6).

PDX251 harbors a *PIK3CA* p.E545K mutation, with other 11 nonsynonymous alterations and 26 CNA. The *STK11* p.R297S variant is of unknown function and identified at a variant allele frequency that is compatible with homozygosity.

Importantly, we performed western blot analysis to check protein expression and PI3K/mTORC1 pathway activation (**Figure 18**). In PDX313 and PDX251 LKB1 was not detected, compared to PDX039, suggesting that both mutations caused protein instability and degradation. TSC1 was not detected in PDX039, compared to PDX251. Intriguingly, PDX313 did not express TSC1 nor tuberin (*TSC2*), suggesting the presence of an additional component of mTORC1 activation in this model. As expected, mTORC1 pathway was activated in PDX313 and PDX039 (high phospho-S6 S235/236, S240/244, phospho-4EBP1-T37/46 and T70), but not in PDX251, suggesting that LKB1 alteration does not result in mTORC1 activation in this model. In turn, PI3K pathway activity, measured as phospho-AKT T308, was found lowest in PDX039 –compared to the other models by immunoblotting– and among the PDX with lower levels –according to RPPA data in cross-comparison with 18 total models (**Figure 18B**). mTORC2 pathway was activated in PDX313 (high phospho-AKT S473 and phospho-NDRG1 T346).

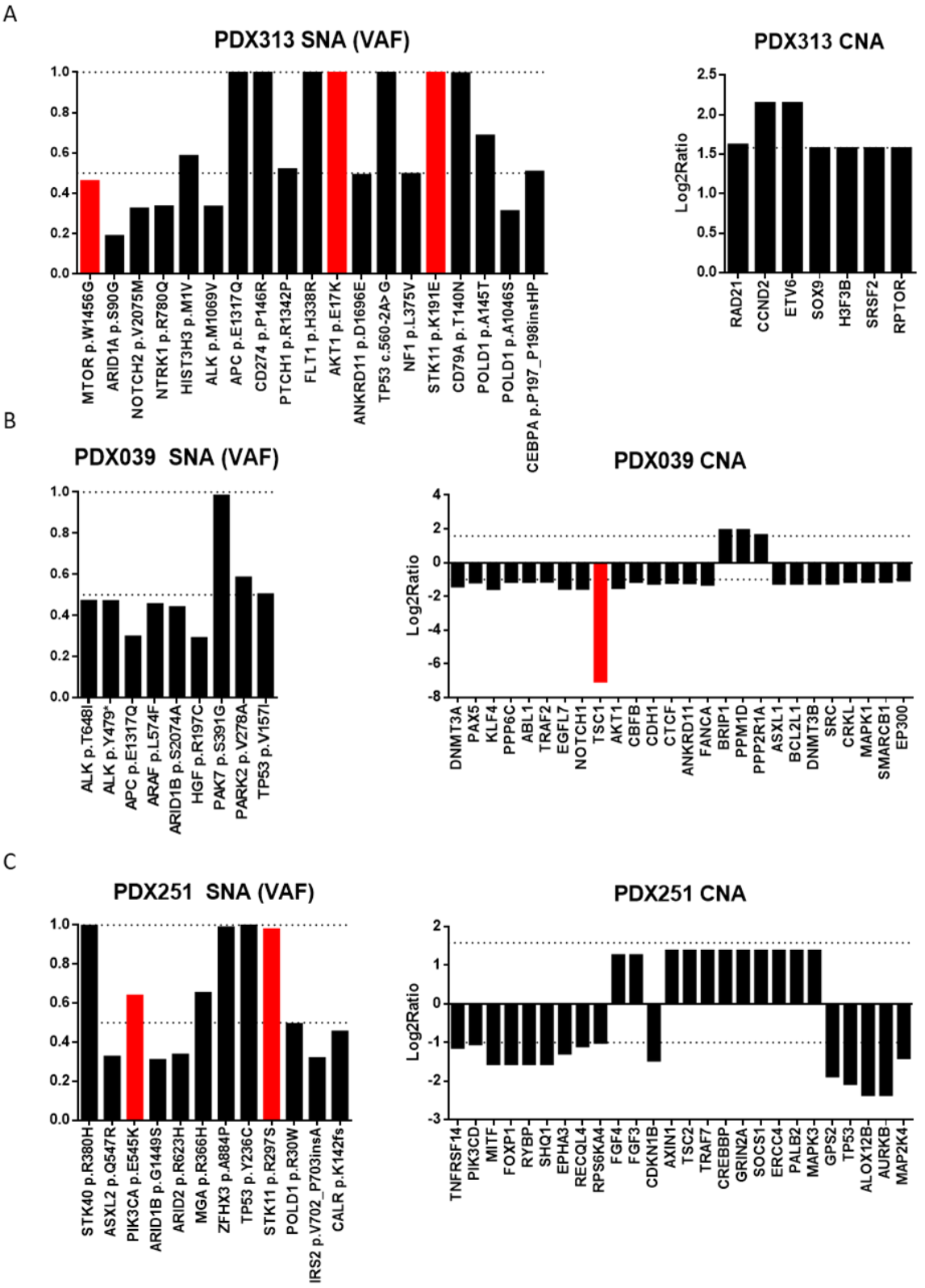

Figure 17. Three models with mTORC1 activating alterations were selected to test the efficacy of an mTORC1/2inh *vs.* PI3Kinh. Single nucleotide alteration (SNA) and copy number alteration (CNA) analysis was performed in PDX313 (A), PDX039 (B) and PDX251 (C). Variant allele frequency (VAF) are depicted for SNV analysis and Log2 ratio for CNA analysis.

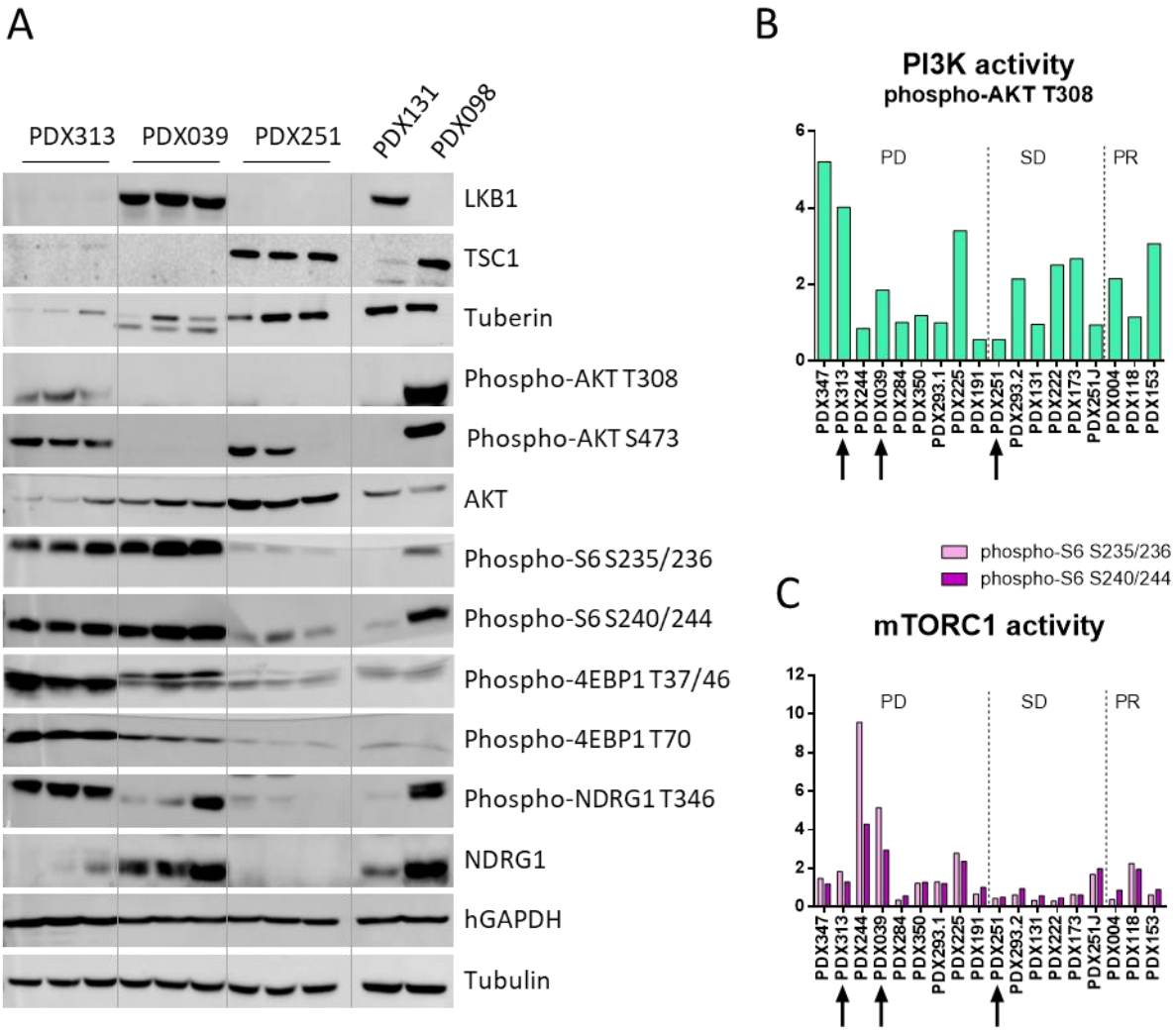

Figure 18. Protein expression analysis shows mTORC1 pathway activation in PDX313 and PDX039 models. A) Immunoblotting of PDX313, PDX039 and PDX251. PDX131 and PDX098 were used as control for LKB1 and TSC1 protein levels respectively. Human GAPDH (hGAPDH) was used for total human sample control and tubulin was used for total protein control. B) PI3K activity shown by phospho-AKT T308 levels relative to total AKT from RPPA data; C) mTORC1 activity shown by phospho-S6 S235/236 and S240/244 from RPPA data.

We further evaluated the antitumor activity of an α/δ-specific PI3Kinh (AZD8835) in comparison with the dual mTORC1/2inh vistusertib in the selected models, using doses and schedules that resemble the administration of these drugs in humans. Results showed a superior antitumor activity of vistusertib in PDX313 and PDX039 models (**Figure 19**), but not in PDX251.

Vistusertib elicited a potent decrease in the activity of mTORC1, seen as low phospho-S6 S235/236, phospho-S6 S240/244, phospho-4EBP1 T37/46 and phospho-4EBP1 T70 upon treatment. Similarly, mTORC2 activity was effectively blocked: phospho-AKT S473 and phospho-NDRG1 T346 were down-regulated in vistusertib-treated samples. Conversely, AZD8835-treated samples showed downmodulation of the PI3K phospho-site on AKT T308, of phospho-AKT S473 and phospho-4EBP1-70; and of phospho-S6 and phospho-NDRG1 exclusively in PDX251. This data shows that the limited antitumor activity of AZD8835 compared with vistusertib in PDX313 and PDX039 is associated with a lack of mTORC1 downmodulation (see phospho-S6 and phospho-4EBP1). In addition, the biochemical analysis, along with the antitumor activity shown in Figure 19, suggests that the *LKB1* mutation in PDX251 is not resulting in mTORC1 activation.

Even though vistusertib induced potent tumor growth inhibition in the three aforementioned models, it did not result in long-term tumor stabilization or tumor regression, which is clinically meaningful. Because these tumors express ER and given the crosstalks between this steroid nuclear receptor and the PI3K[131] we tested to combinate vistusertib/AZD8835 with a novel SERD (AZD9496) in PDX313 and PDX039 models (**Figure 20**). As expected, these experiments showed a significant improvement of tumor growth control in the vistusertib plus AZD9496 arm, albeit resulting in disease progression. We conclude that targeting mTORC1/2 with vistusertib at this dose and schedule does not result in tumor regression in models exhibiting an activation of the mTORC1 pathway, neither as single agent nor in combination with a novel SERD.

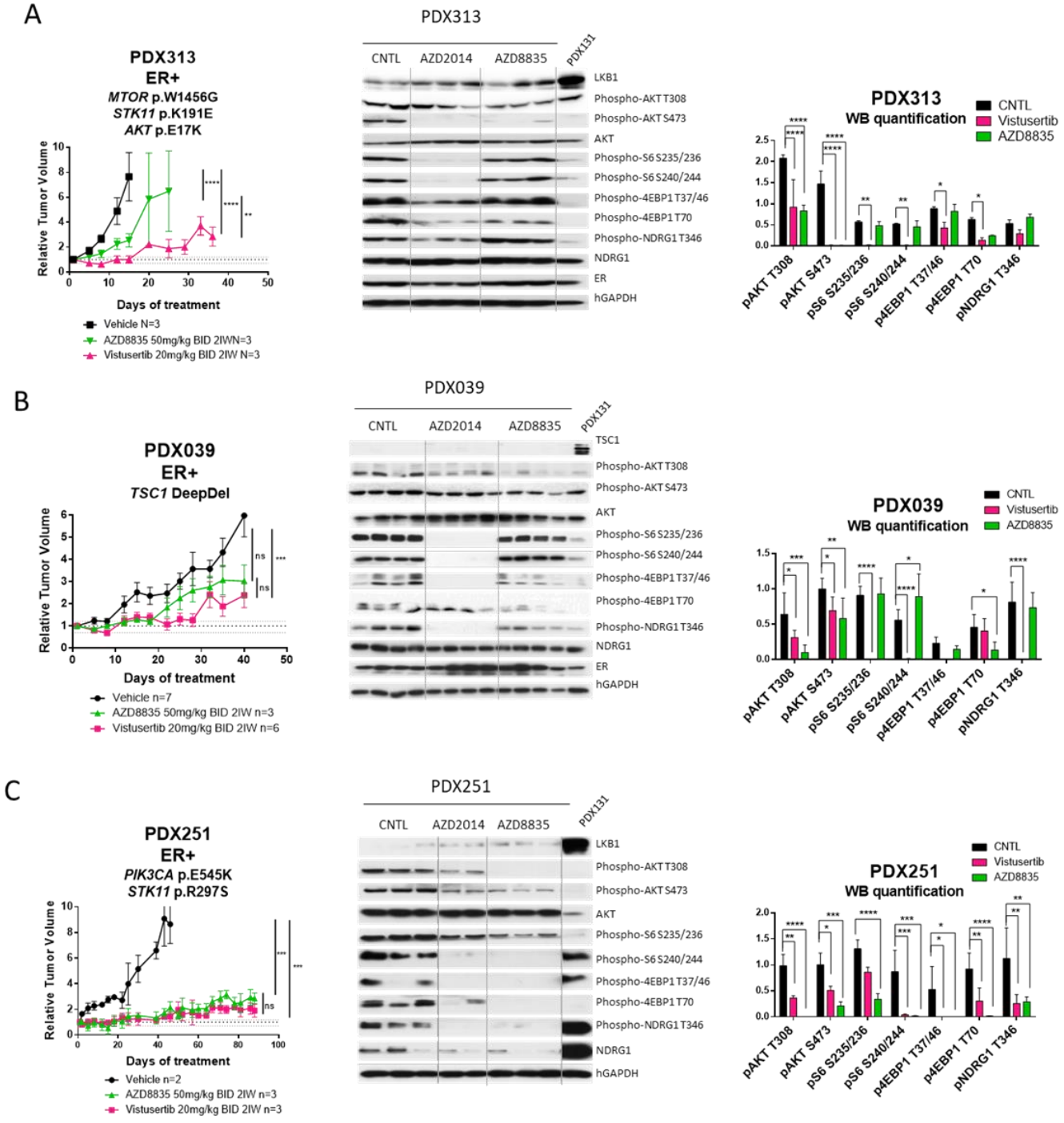

Figure 19. Dual mTORC1/2 inhibitor (vistusertib) showed superior antitumor activity than PI3Kinh (AZD8835). In vivo drug efficacy of AZD8835 and vistusertib and pathway modulation in PDX313 (A), PDX039 (B) and PDX251 (C); PDX131 lane is used as LKB1/TSC1 protein control. Statistical test: 2-way ANOVA, A) PDX313: vehicle *vs.* AZD8835 and vehicle *vs.* vistusertib at day 15; AZD8835 *vs.* vistusertib at day 25; B) PDX039: vehicle *vs*. AZD8835, vehicle *vs*. vistusertib and AZD8835 *vs.* vistusertib at day 28; C) PDX251: vehicle *vs.* AZD8835, vehicle *vs.* vistusertib and AZD8835 *vs.* vistusertib at day 46. WB quantifications: pAKT T308 and S473 are relative to total AKT; pS6 S235/236, S240/244, p4EBP1 T37/46 and T70 are relative to hGAPDH; and pNDRG1 T346 is relative to total NDRG1. Statistical test: 2-way ANOVA.

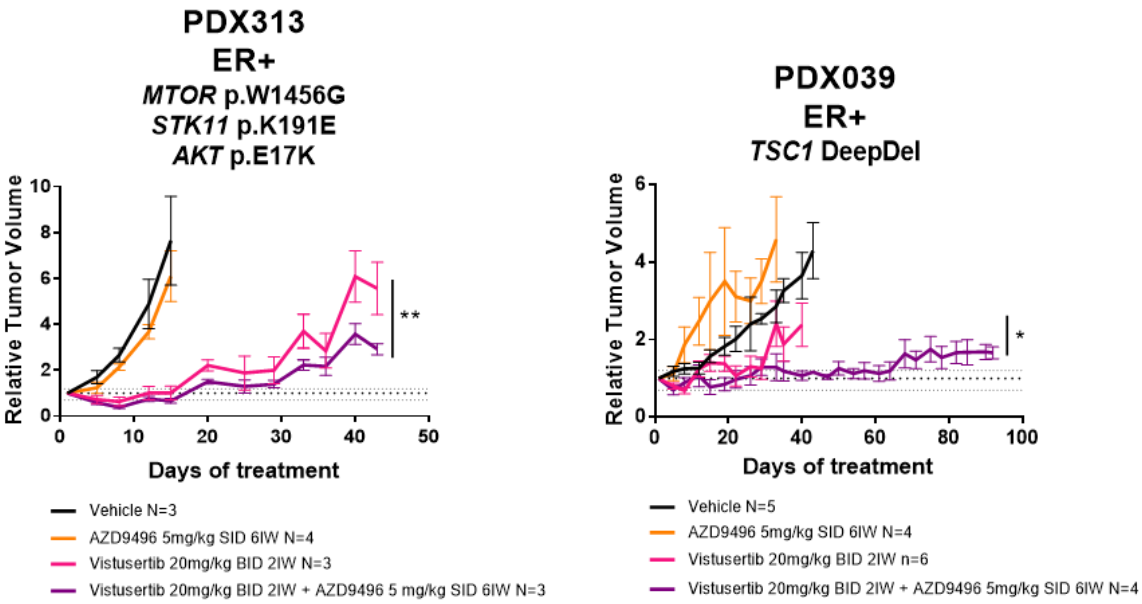

Figure 20. Combination of mTORC1/2 with a new generation SERD (AZD9496) improves response. PDX313 and PDX039 *in vivo* efficacies of AZD9496, vistusertib and the combination. Statistical test: Unpaired t-test.

1.3. Models harbouring an 11q13 amplification (11q13amp) are resistant to PI3Kinh

To dissect the potential effect of the amplification of the 11q13 chromosomic region as a mechanism of resistance to PI3Kinh, we firstly analyzed the relative expression of 11q13-contained genes and their downstream pathway activation in the selected 11q13amp models: PDX131, PDX191, PDX293.1/2. PDX251 was also included in this analysis albeit it contained a mild *FGF3/4* amplification (FC=2.40, below the threshold of fold-change=3 that was considered in the table from **Figure 14**) and PDX343 which harbors a *PAK1*amp (**Figure 21**). Western blot semi-quantitative analysis established that *CCND1*amp models (PDX131, PDX191 and PDX293.1/2) and *PAK1*amp models (PDX191, PDX293.1/2 and PDX343) contained high levels of the respective protein. *RPS6KB2*amp models (PDX131 and PDX293.1/2) did show only a minor increase of S6K2. However, correlation analysis between gene copy number and protein expression failed to show a significant correlation, although a tendency was observed in cyclin D1 and PAK1 expression (**Figure 21B**). PDX191 and PDX343 presented co-amplification of the 8p11 region (containing *FGFR1*), therefore PDX191 harbored both amplification in FGFR1 receptor and FGF3/4/19 ligands. Cell cycle

activation downstream of cyclin D1 was determined by phospho-Rb S780 and phospho-Rb S807/811. PDX191 and PDX293.1/2 showed high levels of phospho-Rb while PDX131 showed low levels. S6K pathway activity was determined by phospho-S6 S235/236 and S240/244, and it did not show higher levels in the *RPS6KB2*amp models. MAPK pathway activation downstream of FGFR1/FGF or PAK1 was determined by phospho-ERK1/2 T202/204, which was high in PDX293.1/2, containing *PAK1*amp and *FGF3/4/19*amp.

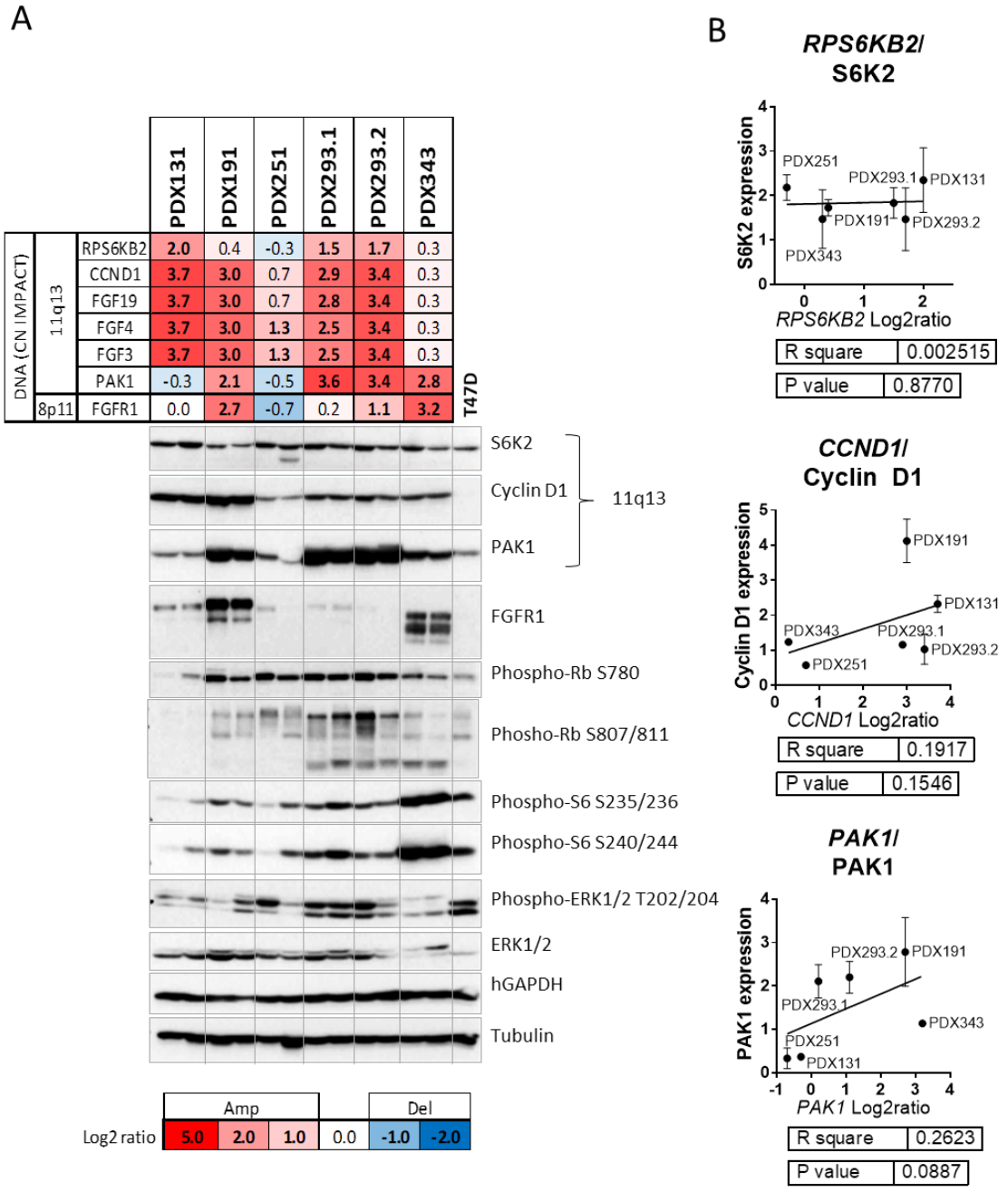

Figure 21. PAK1 and Cyclin D1 are highly expressed in the amplified models. A) Protein expression of 11q13 genes and pathway activation status in the 11q13amp PDX models. Co-amplification of the 8.11 chromosomic region is shown. hGAPDH control was used for human sample load and tubulin endogen to check total protein load; B) Gene log2ratio and protein expression correlations. Statistical test: F-test.

1.4. *In vitro* validation of cyclin D1 and FGF-ligands overexpression as resistance mechanisms against PI3Kinh in *PIK3CA* mutant cell lines MCF7 and T47D

In order to dissect the capacity of each individual gene within the 11q13 amplicon to generate resistance to PI3Kinh, we stably transfected T47D (containing a *PIK3CA* p.H1047R mutation) and MCF7 (containing a *PIK3CA* p.E545K mutation) cell lines with either *CCND1*, *PAK1* or *RPS6KB2* genes. However, in order to test FGF3/4/19 ligand expression for PI3Kinh resistance, we have used basic FGF (bFGF, coded by *FGF2* gene), an FGF ligand widely used for *in vitro* assays. This ligand binds to the IIIb isoform of FGFR1 and IIIc isoform of FGFR1/2/3, while FGF3 binds to the IIIb isoform of FGFR1/2, FGF4 binds to the IIIc isoform of FGFR1/2/3 and FGF19 binds to FGFR4[58, 148]. So, with this ligand we can closely mimic the effect of FGF3 and FGF4 but not FGF19.

We performed drug inhibition curves with AZD8835 in the generated cell lines and in non-transfected T47D and MCF7 cell lines with or without bFGF. These experiments showed that *CCND1*-transfected cells or addition of bFGF significantly increased the AZD8835 IC_{50} from 3.4 µM to 15.8 in T47D and from 0.18 µM to 0.96 µM in MCF7. *PAK1*- and *RPS6KB2*-transfected cells were equally sensitive to PI3Kinh (**Figure 22**).

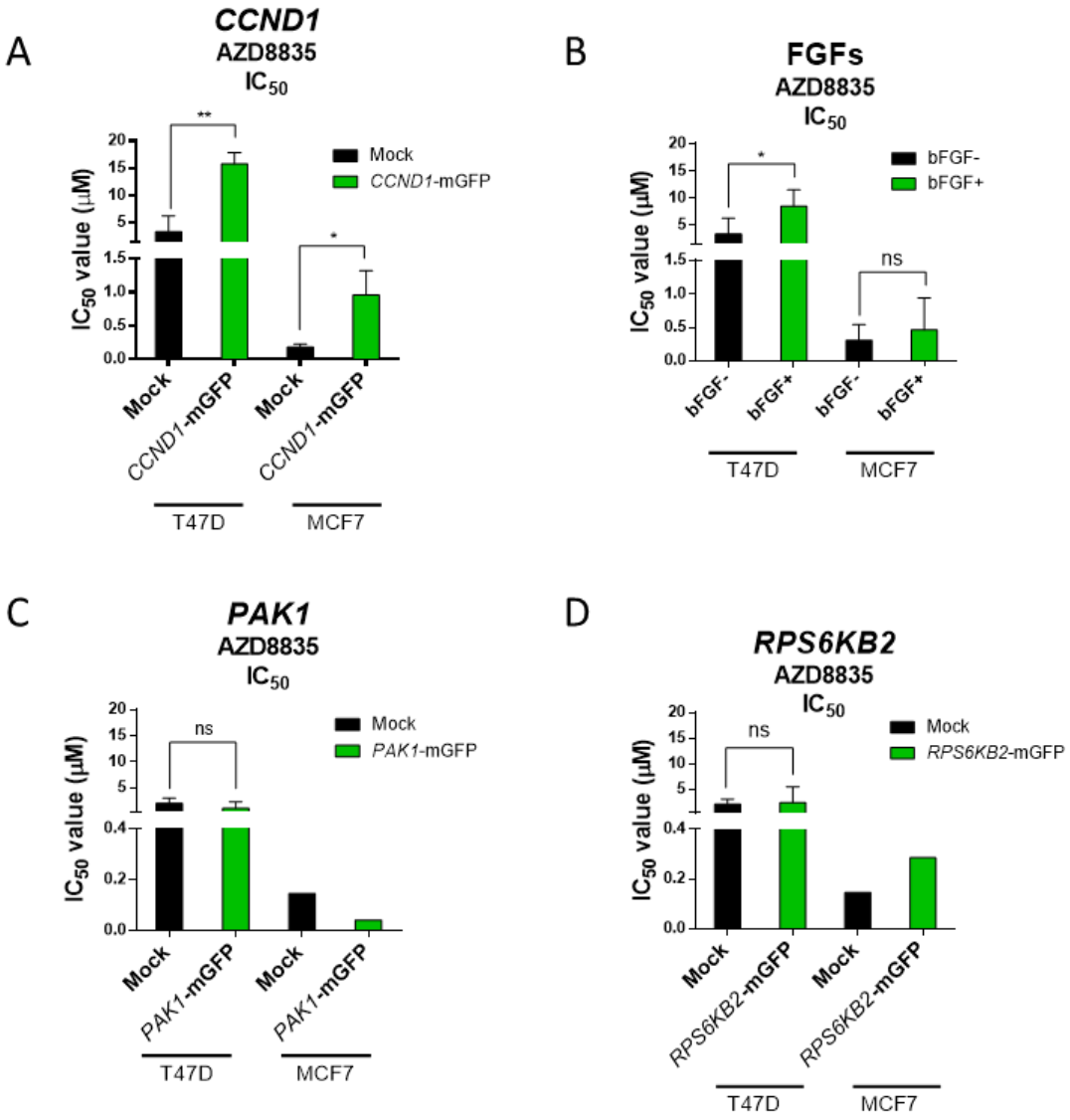

Figure 22. *CCND1*-transfected T47D and MCF7 cells and bFGF-stimulated T47D cells generate resistance to PI3Kinh. IC_{50} calculation from drug inhibition curves assays and in transfected MCF7 and T47D cells with *CCND1* gene (A), addition of bFGF (B), *PAK1* gene (C) and *RPS6KB*2 gene (D). Mock: *mGFP* gene transfection. Statistical test: unpaired t-test. IC_{50}s calculated from 3-indepnendent experiments for *CCND1*-transfected cells and FGF-stimulated cells, 2 independent experiments for *PAK1* and *RPS6KB2*-transfected T47D cells and 1 experiment was performed for *PAK1* and *RPS6KB2*-transfected MCF7 cells.

We further tested the relative protein expression and pathway activation of the transfected cell lines by western blot. Results showed an overexpression of cyclin D1 in *CCND1*-transfected cells and these cells presented increased phospho-Rb S780 and S807/811, indicating activation of CDK4/6 (**Figure 23**). Overexpression of S6K2 was detected in *RPS6KB2*-transfected cell lines but this did not result in higher levels of phospho-S6

S235/236 or S240/244. *PAK1*-transfected cells did not express higher levels of PAK1 protein, compared to the endogenous protein, and we did not observed increased phospho-ERK1/2.

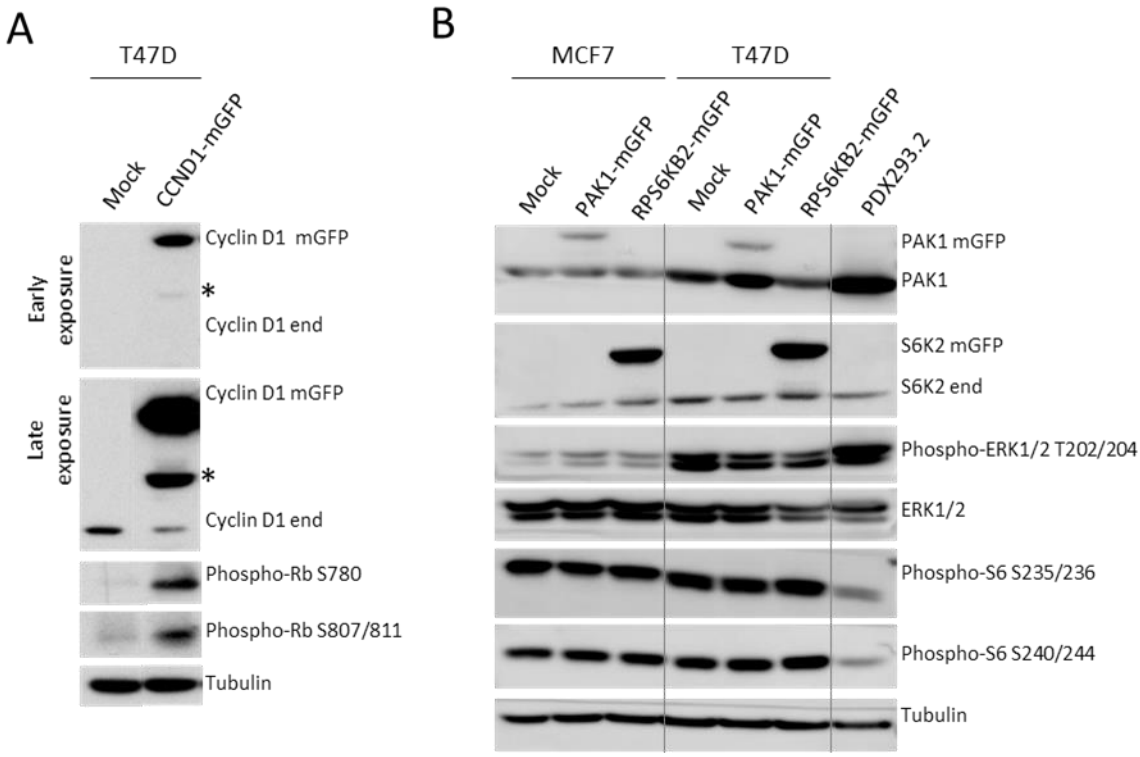

Figure 23. Genetically modified cell lines overexpress Cyclin D1 and S6K2 but low levels of PAK1. A) Cyclin D1 expression and cell cycle pathway activation in *CCND1*-transfected T47D cells B) PAK1 and S6K2 protein levels and MAPK/S6K pathway activation status in *PAK1*- and *RPS6KB2*-transfected MCF7 and T47D. PDX293.2 was used for PAK1 and S6K2 expression controls. *CCND1, PAK1* and *RPS6KB2* cDNAs were expressed as fusion proteins with mGFP, so bands appear 35 KDa upwards. "*end*" denotes for endogenous proteins. *A degraded/splice form of the overexpressed Cyclin D1.

To further study the implication of the 11q13 region in PI3Kinh resistance, and due to the proximity of *CCND1* with *FGF3/4/19* ligand genes in the amplicon, we tested whether both *CCND1*amp and FGFs together could increase the IC_{50}. We performed drug inhibition assays with mock or *CCND1*-transfected with or without bFGF, and results showed a higher IC_{50} in both cell lines, especially for MCF7, where the IC_{50} for AZD8835 increased from 0.18 µM to 5.3 µM, whereas in T47D the IC_{50} increased from 1.1 µM to 8.7 µM (**Figure 24**). Western blot analysis showed increased phospho-Rb in cyclin D1-overexpressing cell lines and activation of MAPK pathway (high phospho-ERK1/2 T202/204) under bFGF stimuli. PI3Kinh was able to block PI3K activity (lower phospho-AKT T308) but phospho-Rb S780 and phospho-ERK1/2 T202/204 was maintained in cyclin D1-overexpressing and bFGF stimulated cells.

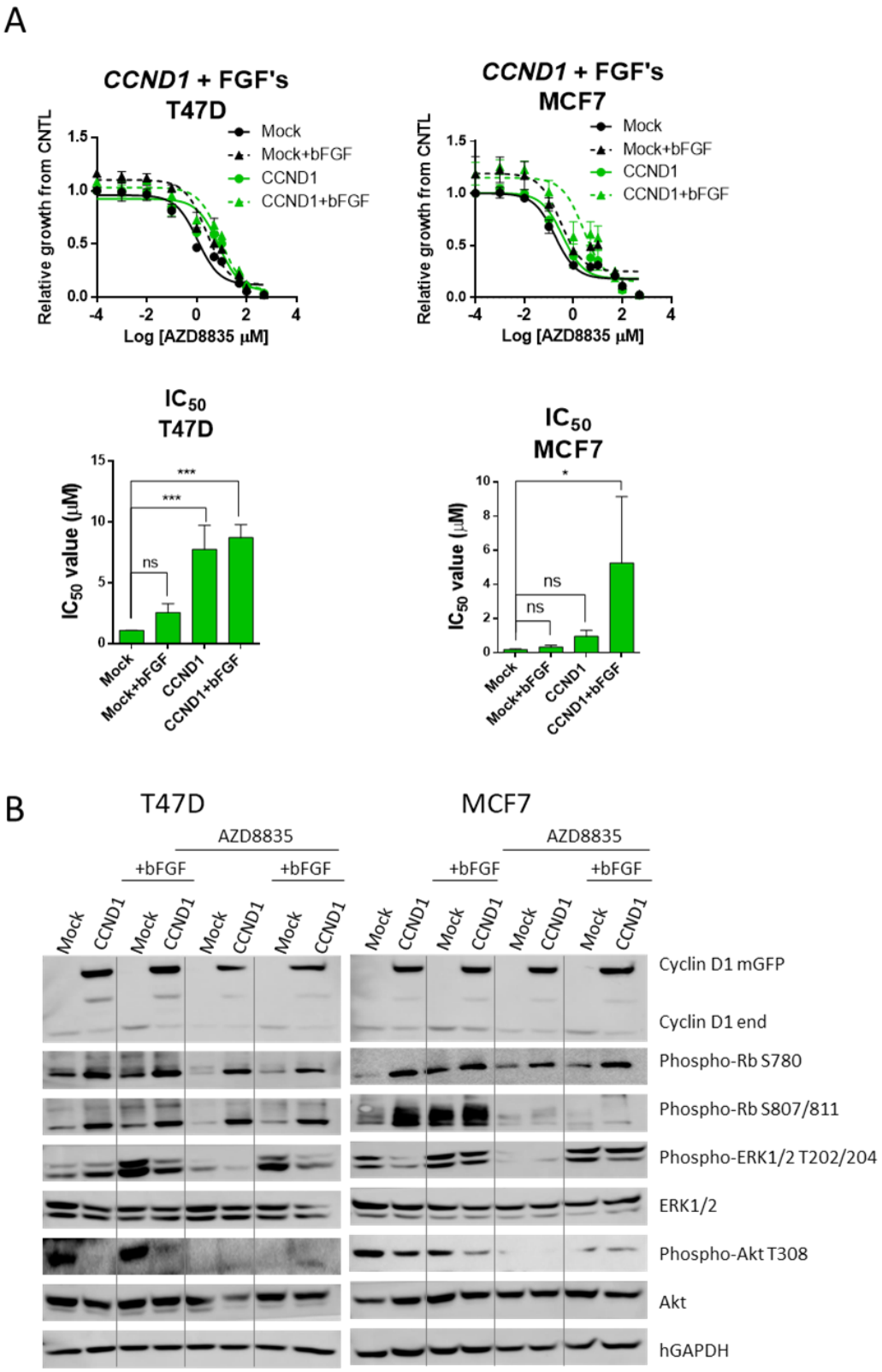

Figure 24. Cyclin D1 overexpression and FGF stimuli synergy and increase PI3Kinh resistance. A) Drug inhibition curves and IC_{50}s upon addition of bFGF to the *CCND1*-transfected T47D and MCF7 cells; IC_{50} values are calculated from 3 independent experiments; B) Western blot analysis of Mock or *CCND1*-transfected T47D and MCF7 cells with or without 20 nM of bFGF and/or 500 nM of AZD8835. Statistical test: One-way ANOVA.

To study the implications of *CCND1* and *FGF3/4/19* ligands co-amplification in the context of PI3Kinh in combination with hormonal therapy (the currently approved treatment combination), we tested the inhibitory effect of AZD8835, AZD9496 and their combination in the mock/*CCND1*amp cell lines with or without bFGF stimuli (**Figure 25**). Results showed that bFGF stimuli had a more profound effect in AZD9496 resistance than cyclin D1 overexpression in both T47D and MCF7 cell lines. In this specific experiment, *CCND1*-transfected cell lines failed to show significant resistance to AZD8835 or AZD9496. Upon AZD8835 and AZD9496 combination, only T47D cell line showed significant resistance in the bFGF stimulated mock and *CCND1*-trasnfected cells. MCF7 cell line exhibited an effective inhibition of cell growth under AZD8835 and AZD9496 combination treatment.

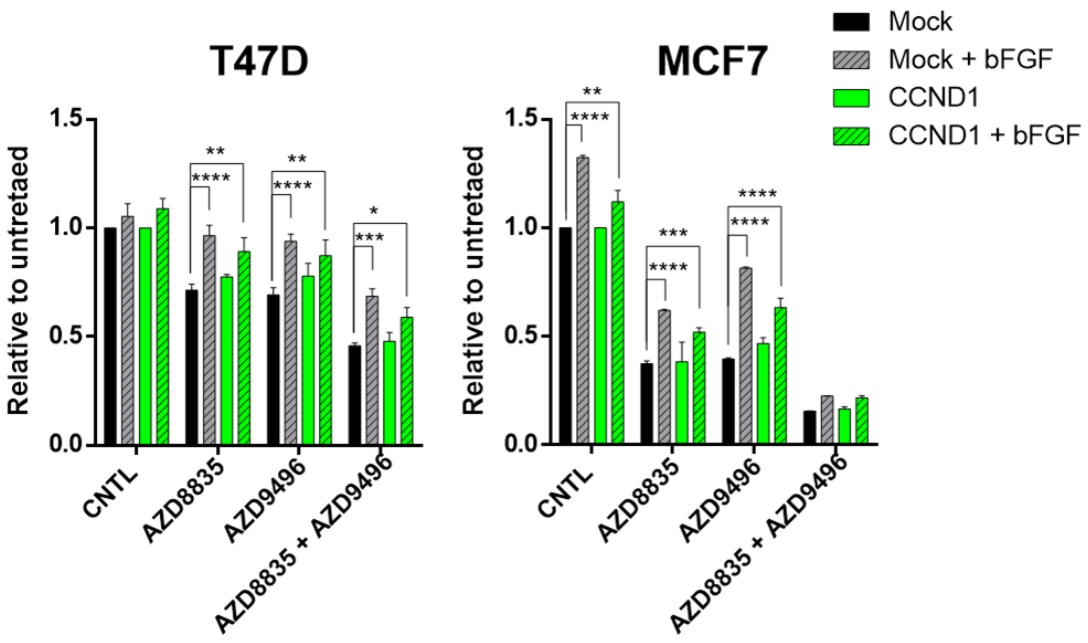

Figure 25. T47D cells stimulated with bFGF show resistance to the combination of PI3Kinh with hormonal therapy. Mock or *CCND1*amp T47D and MCF7 cells were treated with 500nM AZD8835, 1 μM AZD9496 or the combination, either with bFGF or without, during 4 days. Cell viability per experimental condition is normalized with the untreated CNTL samples, mock and *CCND1*-transfected, respectively. Data from 2 independent experiments. Statistical tests: 2-way ANOVA.

In order to further test the implication of *PAK1* and *RPS6KB2* amplification in cell growth and resistance, we performed drug inhibition assays in SUM44, an ER+ 11q13amp cell line, compared to MCF7 and T47D, that do not harbor this amplification. SUM44 express higher levels of PAK1 and S6K2 (**Figure 26A**). We tested 3 different inhibitors: AZD8835, the PI3Kinh; FRAX1036, a PAK1 inhibitor (PAK1inh); and PF-4708671, a P70/S6K inhibitor (P70inh) (**Figure 26B**). Results showed that SUM44 were resistant to (IC_{50}=51.6 µM) but equally sensitive to the PAK1inh (IC_{50}=4.8 µM, similar to MCF7 IC_{50}=1.3 µM and T47D IC_{50}=6.1 µM). Upon P70 inhibition, SUM44 presented high resistance (IC_{50}=45.1 µM); T47D as well presented resistance (IC_{50}=21.4 µM); only MCF7 could sensitize at relative low levels (IC_{50}= 6.8 µM).

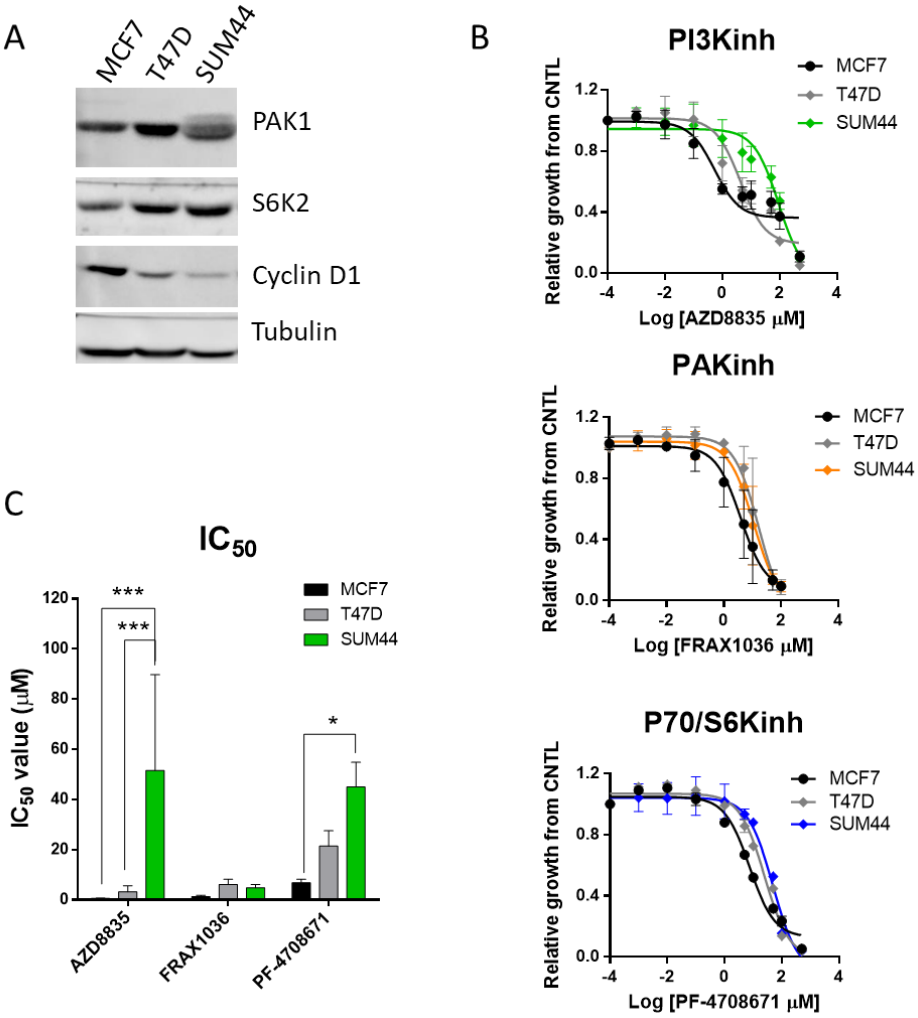

Figure 26. 11q13amp cell line SUM44 show resistance to PI3Kinh but sensitizes to PAK1inh. A) Western blot of PAK1, S6K2 and Cyclin D1 expression in MCF7, T47D and SUM44 cell line; B) Drug inhibition assays with three different drugs: AZD8835, a PI3Kinh; FRAX1036, a PAKinh; and PF-4708671, a P70inh. C) IC_{50} calculation of AZD8835, PAKinh and P70inh in MCF7, T47D and SUM44. Statistical test: 2-way ANOVA. Data from 3 independent experiments.

2. PART 2: Targeting the FGFR pathway

2.1. Antitumor activity of the FGFR1/2/3inh rogaratinib in FGFR-amp PDXs

We generated a PDX collection of 17 models based on the amplification of *FGFR1-4* and/or *FGF3/4/19* (11q13 amplicon) (**Figure 27A**). The majority of the tumors were derived from the metastatic setting. Using IMPACT, we identified 11 PDX models with *FGFR1*amp (PDX156, PDX302, PDX288.1/2, PDX343, PDX404, PDX153, PDX426, PDX291, PDX325 and PDX191), four of them with a co-amplification of 11q13 (PDX156, PDX426, PDX325 and PDX191); 3 PDX with *FGFR4*amp (PDX039, PDX225 and PDX222) and 3 PDX models with 11q13amp (PDX131, PDX251 and PDX293). PDX288.1 and PDX288.2 originated from the same patient at two different time-point biopsies: PDX288.1 is taken while the patient was on-treatment with debio-1347 (FGFR1/2/3inh) with no confirmed response and PDX288.2 short after disease progression.

We measured the anti-tumor activity of rogaratinib, a specific pan-FGFR1/2/3inh. Out of the 17 models tested, 2 models showed a PR response (PDX325 and PDX191), 7 models presented an SD response (PDX251, PDX404, PDX153, PDX222, PDX293, PDX426 and PDX291), and 8 progressed (PDX156, PDX302, PDX039, PDX288.1/2, PDX343, PDX225 and PDX131). Of the 9 PDXs responding (PR+SD), 6 were ER+, 2 HER2+ and 1 TNBC, and from the 8 progressing (PD), 4 PDXs were ER+, and 4 TNBC, showing a degree of enrichment for luminal subtype in the sensitive models. Intrinsic subtypes (PAM50) showed a similar distribution, albeit PDX325 and PDX225 exhibited a Her2-enriched while being ER+.

Rogaratinib pathway modulation downstream FGFR was evaluated through phospho-ERK1/2 T202/204 and ERK1/2 levels in western blot. Results showed that PDX291 and PDX191, which are sensitive to rogaratinib, show a down-modulation of phospho-ERK1/2 upon rogaratinib treatment, indicating a blockade of the MAPK pathway (**Figure 27B**).

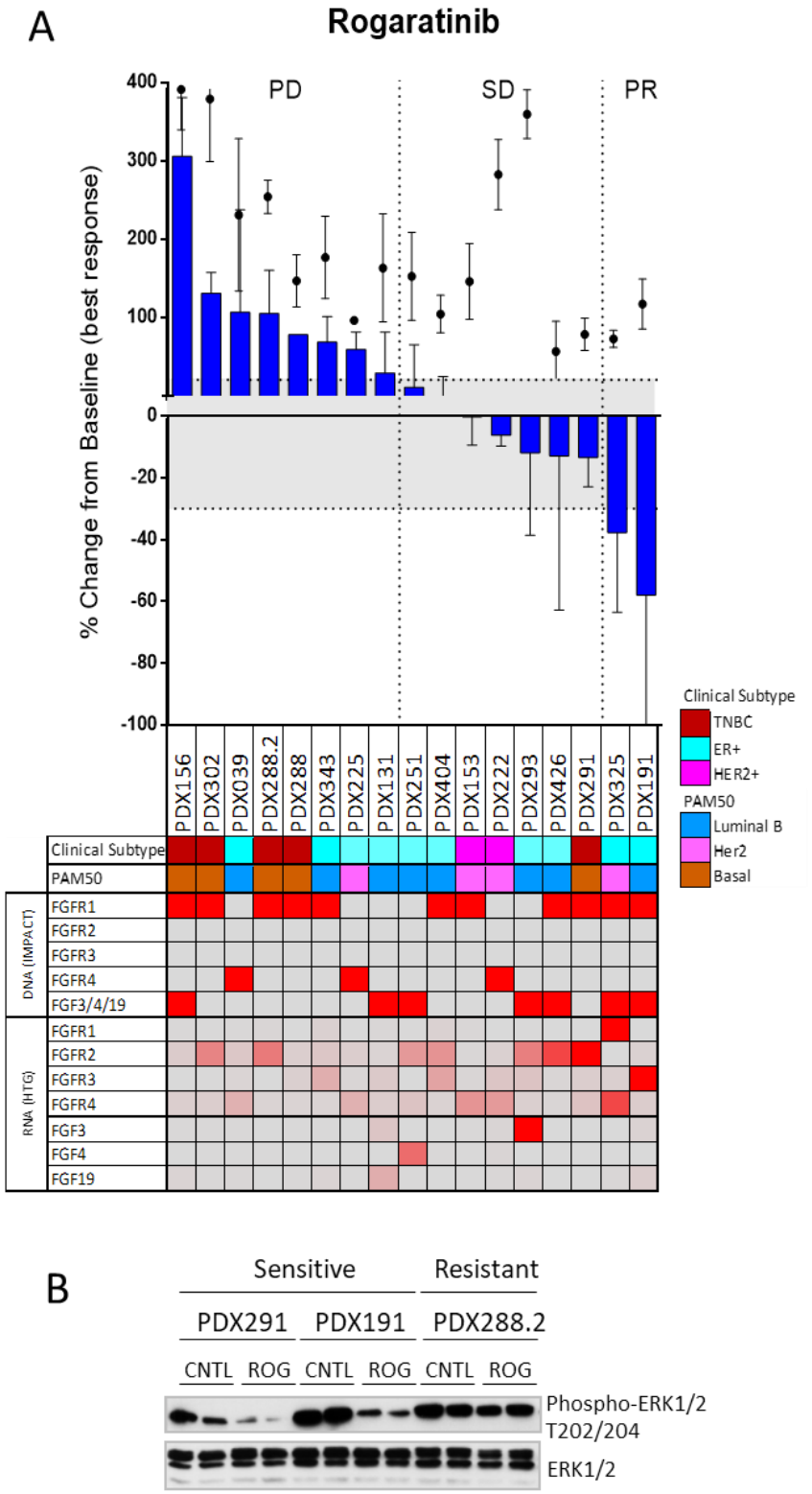

Figure 27. Rogaratinib shows antitumor activity in 9 PDX models from a 17 *FGFR/FGF*amp PDX collection. A) Waterfall plot of the percentage change from baseline of rogaratinib response in a collection of 17 *FGFR/FGF*amp PDX models. Tumor volume is measured as best response (**Annex Table S3**). Molecular subtype, PAM50 classification, FGFR/FGFamp status (IMPACT data, amplification=CN>4) and mRNA expression by HTG platform are denoted in the table below; B) MAPK pathway modulation in sensitive *vs.* resistant PDXs under rogaratinib (ROG) treatment.

2.2. FGFR1-4 mRNA levels predict for specific FGFRinh response in BC-PDX models

In order to set a biomarker of response to rogaratinib, we first analyzed the gene copy number of *FGFR1-4* in the 17 models (**Figure 28A**). Results from the IMPACT panel showed no association between copy number of FGFRamp with rogaratinib response. As previously described by Pearson et al[228], only a PDX with high copy number (>20 copies) exhibited PR as response (PDX325). We further analyzed CN variation considering: 1) CN>4 (based on the criteria for gene amplification from IMPACT panel; either *FGFR1* or *FGFR4*); 2) the sum of all the CN (in *FGFR1/2/3/4*); and 3) the ratio obtained by fluorescence in situ hybridization (FISH) (either *FGFR1* or *FGFR4*), where a CN/centromere superior or equal to 2.2 is considered amplified (**Figure 28B**). Using these parameters, there was no significant association between CN and rogaratinib response, neither analyzing the data as continuous variables nor dichotomized (**Figure 28C, D**).

We next analyzed *FGFR1-4* gene expression by quantifying the mRNA levels of each receptor (**Figure 29**). We measured mRNA levels using 3 different platforms: HTG EdgeSeq System, nCounter from Nanostring and RT-qPCR. We observed that the FGFR1 mRNA was significantly expressed at higher levels than the other 3 receptors and that the results from all 3 platforms were consistent with each other (**Figure 29A**). HTG and nCounter showed very similar measurements across the PDXs (r square=0.8485) and RT-qPCR showed values that were more divergent with the other two platforms (r square=0.4726 and 0.4721, respectively) (**Figure 29B**). This is consistent with the more error prone of individual gene RT-qPCR analysis, compared with HTG and nCounter.

FGFR1 mRNA was very high exclusively in PDX325, correlating with its *FGFR1* high CN (**Figure 29C**). FGFR2 mRNA was relatively high in PDX291 and PDX426, and PDX293 presented relative high levels of FGFR2 and FGFR3 mRNA. Intriguingly, we detected high levels of FGFR3 mRNA in PDX191, a PDX with *FGFR1*amp and no CN alteration in *FGFR3*. Individual FGFR1-4 mRNA levels did not associate with rogaratinib response. As expected, mRNA levels correlated with CN values for FGFR1 (p value<0.0001, **Figure 30**), and there was a tendency for FGFR4, but they did not correlate for FGFR2 and FGFR3.

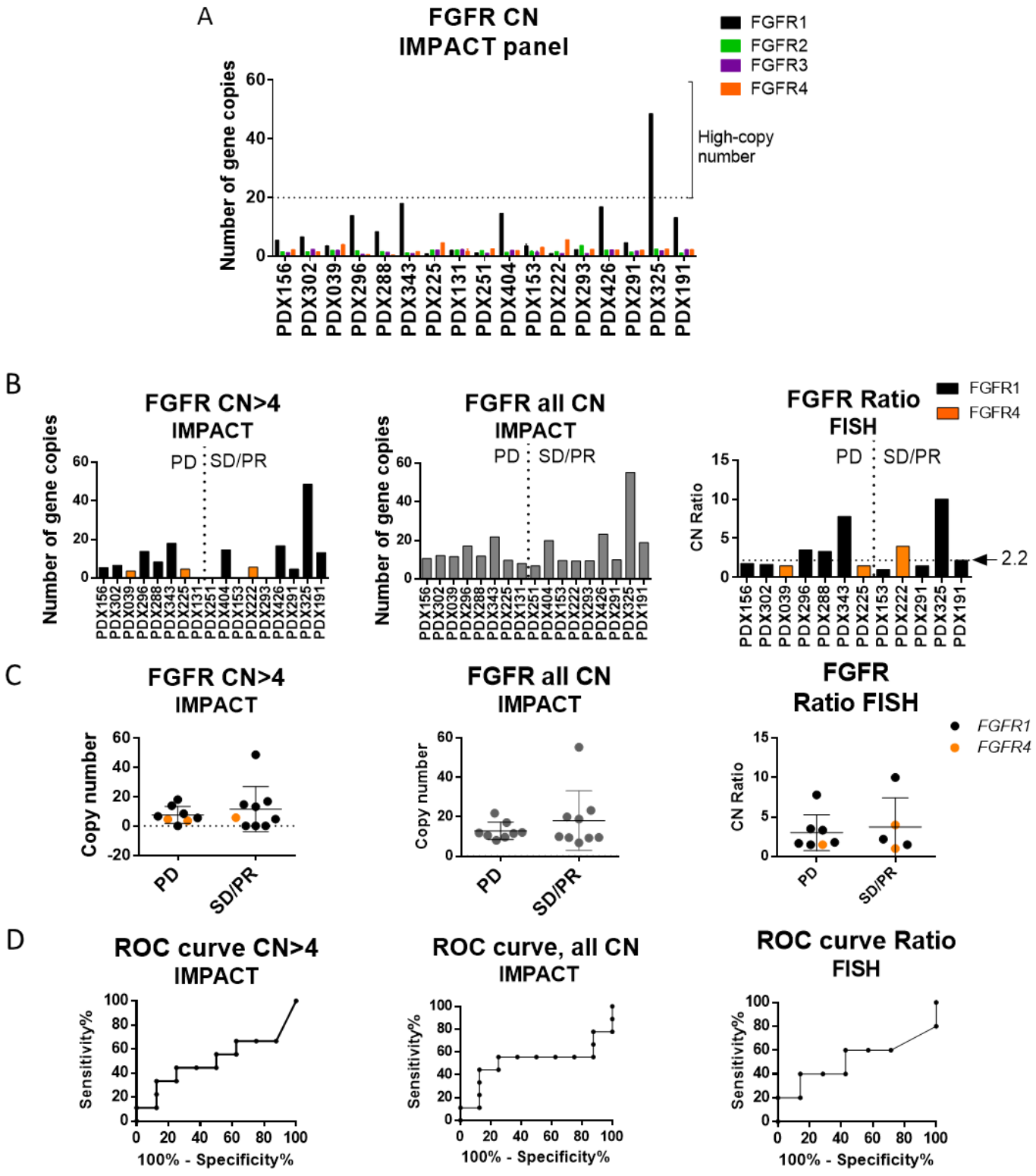

Figure 28. CN analysis of FGFR1-4 does not predict for rogaratinib response. A) Absolute copy number (CN) of *FGFR1-4* in the *FGFR/FGF*amp PDX collection B) Data was analyzed by amplified CN only (CN>4), all CN (FGFR1-4 sum) and FISH ratio (CN/centromere copies), where 2.2 is the threshold considered for amplification; C) PDXs CN values were distributed in PD and SD/PR groups; D) ROC analysis of the CN data as a biomarker of response to rogaratinib response. FISH was only performed in 12 out of the total 17 models.

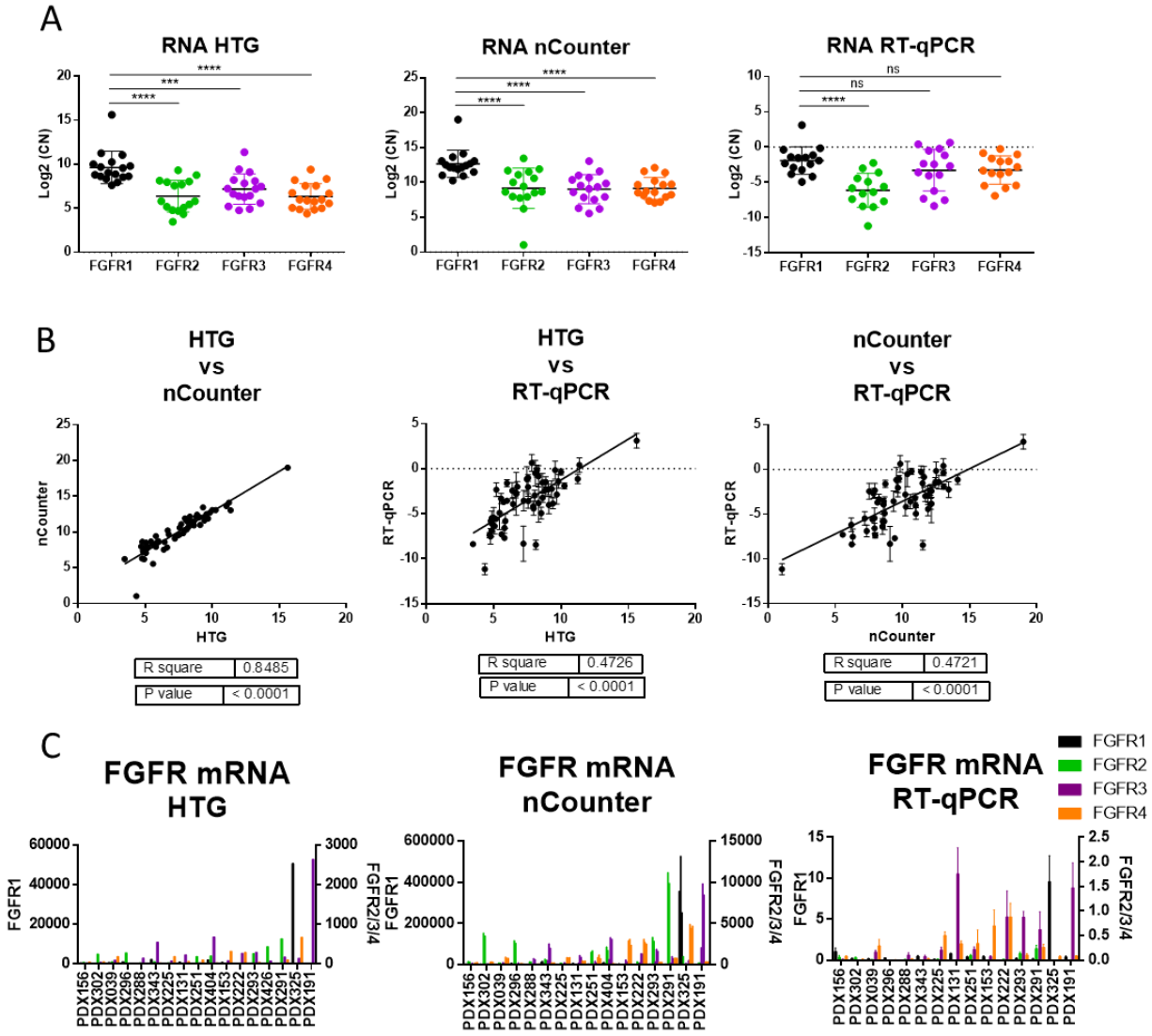

Figure 29. FGFR1 mRNA expression is higher than FGFR2/3/4 in HTG and nCounter platforms. A) FGFR1/2/3/4 mRNA expression in HTG, nCounter and RT-qPCR platforms; B) Correlation of expression levels of HTG *vs.* nCounter, HTG *vs.* RT-qPCR and nCounter *vs.* RT-qPCR. X-Y axis denote Log2 values. Statistical test: F-test; goodness of fit express by R square; C) FGFR1/2/3/4 mRNA expression levels depicted for each PDX model. Left Y-axis corresponds to FGFR1 expression levels and right Y-axis to FGFR2/3/4 expression levels.

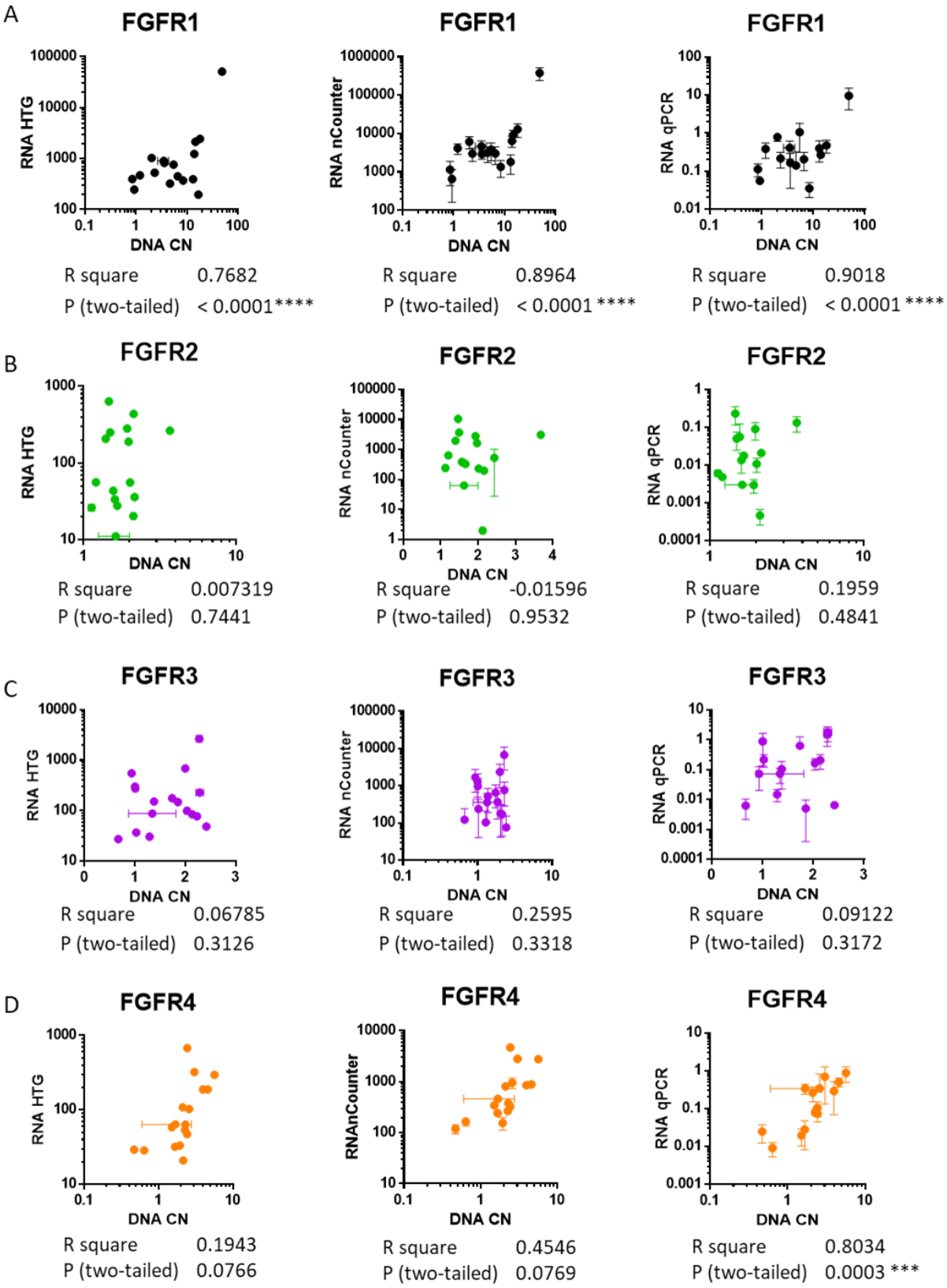

Figure 30. DNA CN-mRNA levels correlate only for FGFR1. Correlation between the CN (X-axis) and RNA levels (Y-axis) of *FGFR1* (A), *FGFR2* (B), *FGFR3* (C) and *FGFR4* (D) obtained from the respective RNA quantification platform (HTG, nCounter and RT-qPCR). X and Y axis are in logarithmic scale. Goodness of fit are expressed by R square. Statistical test: F-test.

To further analyze FGFR1-4 mRNA levels as a biomarker of response to rogaratinib, we developed a composite biomarker of FGFR1-4 mRNA by firstly normalizing the mRNA values (according to the highest value within the group) and then calculating the summatory of FGFR1-4, for each individual model (**Figure 31A, B**). We observed that sensitive models presented higher values of the FGFR1-4 mRNA composite biomarker. ROC curves showed very high specificity (100% in HTG and nCounter, and 87,5% in RT-qPCR) and sensitivity (88.9% in HTG, 87.5% in nCounter and 100% in RT-qPCR) for the FGFR1-4 mRNA biomarker as predictor of response to rogaratinib (**Figure 31D**). Consistently, the FGFR1-4 mRNA biomarkers generated using all 3 the platforms were able to discriminate rogaratinib sensitive *vs.* resistant PDXs.

We next analyzed if the high mRNA expression levels were concordant with the respective protein levels (**Figure 32**). We performed western blot analysis to check for FGFR1 and FGFR3 proteins and immunohistochemistry assays for FGFR2 protein levels. We could not investigate FGFR4 because of lack of specific antibodies. PDX325 express high levels of FGFR1 and PDX191 of FGFR3 protein, in agreement with their respective high mRNA values, and with these models being the only ones exhibiting PR to rogaratinib. FGFR2 protein, assessed by IHC (**Figure 32B**), showed a mild correlation with mRNA expression (r square=0.2949, **Figure 32C**), whereas FGFR1 and FGFR3 protein levels showed a very high correlation with mRNA expression (r square=0.9665 and 0.9509, respectively). In summary, overexpression of FGFR1 and FGFR3 were associated with tumor regression in PDXs and for clinical purposes it is better evaluable at the mRNA level in FFPE, since an IHC assay is not currently available for FGFR1/3 proteins.

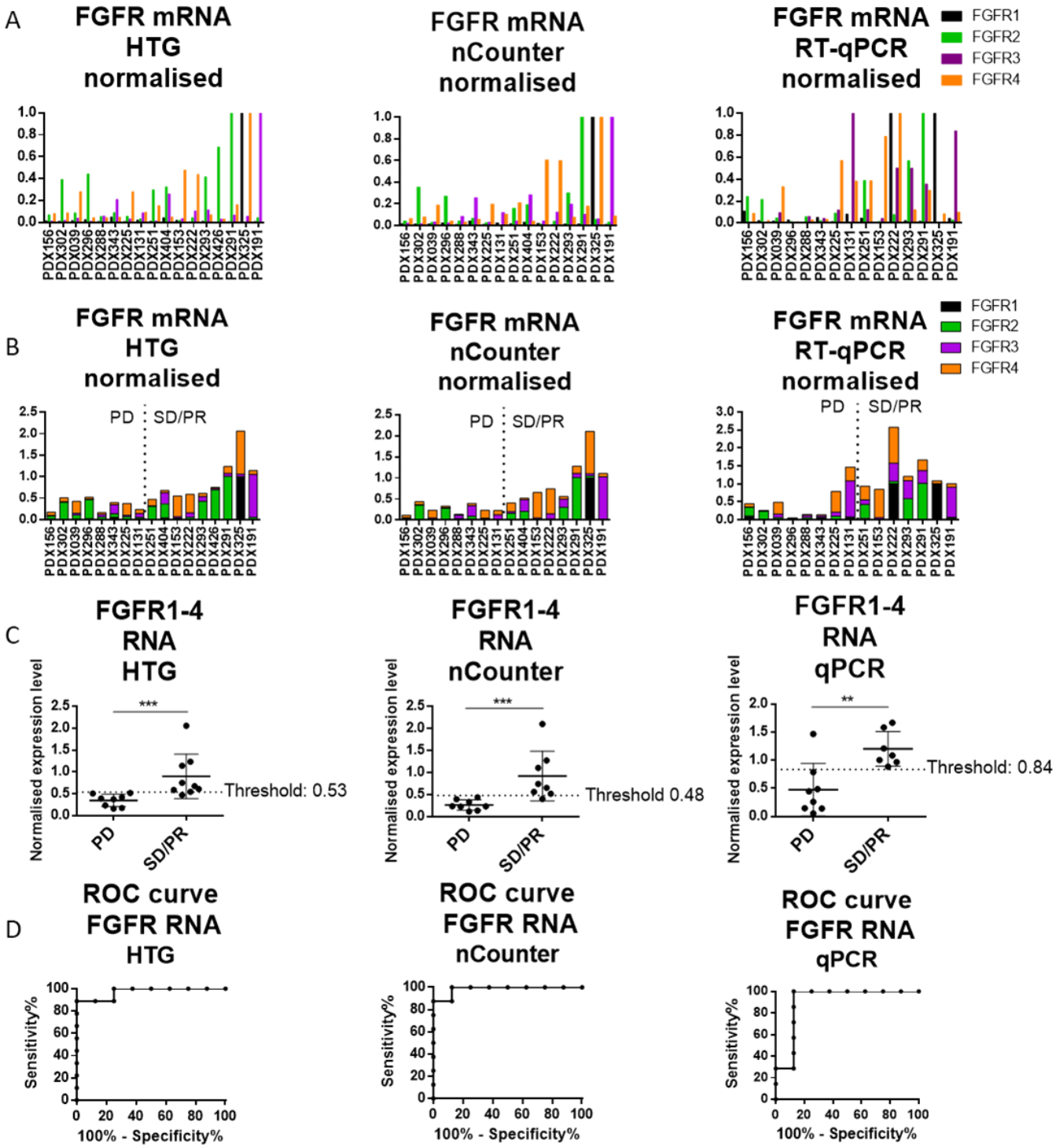

Figure 31. Total *FGFR1-4* mRNA predicts for FGFRinh response. A) mRNA levels are represented in relation to the maximum value of each model (normalized) for each platform; B) The sum of the normalized FGFR1-4 values is represented; C) FGFR1-4 sum in PD and SD/PR groups. Statistical test: Mann-Whitney U test; D) Analysis of FGFR1-4 sum as biomarker of response to rogaratinib through ROC curves by the 3 platforms, which sets a threshold at 0.53 in HTG (sensitivity 88.89%, specificity 100%), at 0.48 in nCounter (sensitivity 87.50%, specificity 100%) and at 0.84 in RT-qPCR (sensitivity 100%, specificity 87.50%).

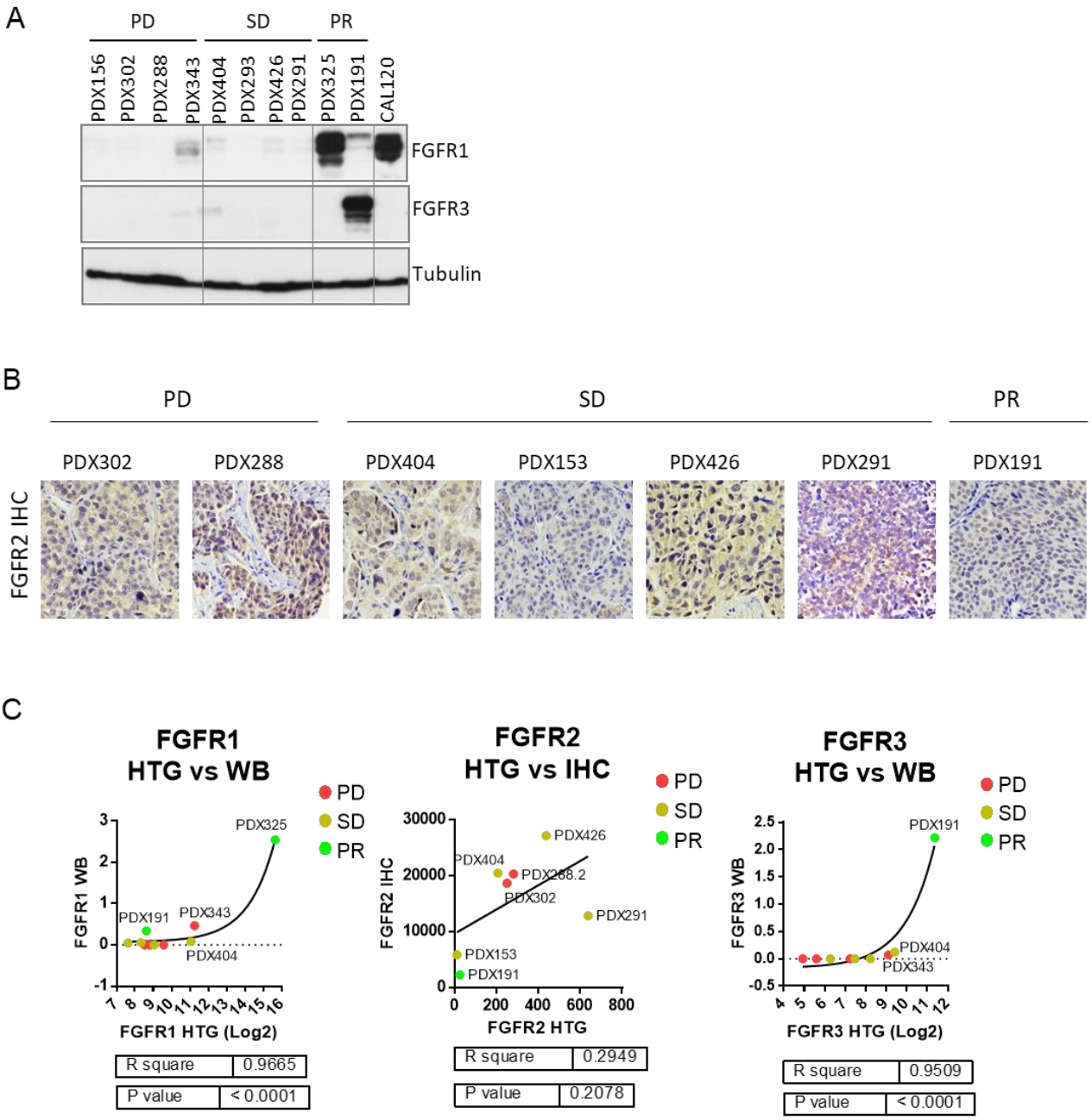

Figure 32. FGFR protein expression correlates with its respective mRNA levels with lower sensitivity. A) FGFR1 and FGFR3 protein expression in PDX models; CAL120 cell lysate is used for FGFR1 expression reference; B) Levels of FGFR2 in PDX models; C) FGFR1/2/3 mRNA *vs.* protein levels; FGFR1/3 WB quantified with ImageJ (normalized by tubulin levels) and IHC FGFR2 samples with QuPath and ImageJ. Statistical test: F-test; goodness of fit evaluated by R square.

2.3. FGF ligand levels do not predict for rogaratinib response

To test whether FGF ligand expression and/or 11q13amp could serve as biomarker of response to rogaratinib, we analyzed FGF ligand expression using two different platforms: HTG and nCounter (**Figure 33**). The HTG platform was capable to detect all FGF ligands (FGF1-10, 16-23), while the nCounter platform was restricted for the FGF ligands within the 11q13 amplicon (FGF3/4/19).

We firstly analyzed the expression levels of the FGF ligands present in the 11q13 amplicon. Data from HTG platform showed that three models with 11q amp (PDX131, PDX251 and PDX293) had high levels of either FGFR3/4/19 while the other 3 PDXs with 11q13amp (PDX156, PDX325 and PDX191) contained relative low levels of the ligands (**Figure 33A**). None of the non-11q13amp PDXs showed high levels of any of these 3 FGF ligands. Overall, the 11q13amp models expressed significant higher FGF3/4/19 ligands. However, ROC curve analysis of the overall FGF3/4/19 ligands between resistant (PD) and sensitive (SD/PR) PDXs, failed to provide high sensitivity nor specificity. The analysis of expression data using nCounter (**Figure 33B**) showed slightly different results: while PDX293 and PDX251 had equally high levels of FGF3 and FGF4, respectively, PDX131 did not show the observed expression of FGF3/19 by HTG and PDX325 presented high levels of FGF3/19. A significant difference was observed in the ligand expression between non-11q13amp and 11q13amp models. But again, ROC curve analysis of the 11q13 ligands did not provide high values of sensitivity nor specificity for prediction of FGFRinh response.

We then analyzed data from all the FGF ligands detected by the HTG platform (**Figure 33C**). The two most prominent cases were PDX156, that showed high levels of FGF2 and PDX302 with high levels of FGF7. ROC curve analysis of all ligands sum did not provide high sensitivity nor specificity. The same analysis was performed in normalized data (following the same approach as in the previous section with FGFR1-4 expression) and no tendencies were observed between PD and SD/PR models (**Figure 33D-E**).

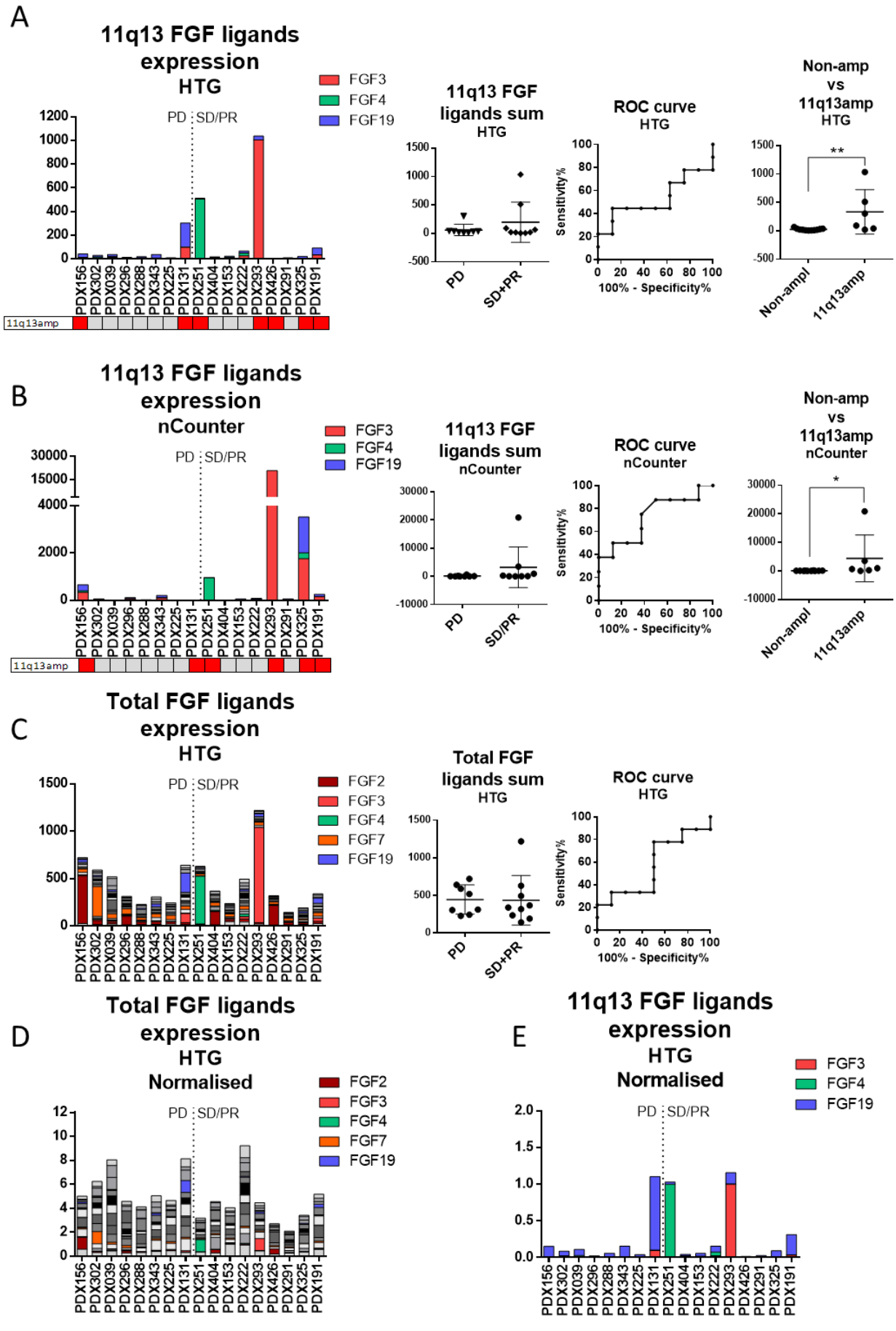
A
11q13 FGF ligands expression HTG
FGF3
FGF4
FGF19
PD
SD/PR
11q13amp
11q13 FGF ligands sum HTG
ROC curve HTG
Sensitivity%
100% - Specificity%
Non-amp vs 11q13amp HTG
Non-ampl
11q13amp
B
11q13 FGF ligands expression nCounter
11q13 FGF ligands sum nCounter
ROC curve nCounter
Non-amp vs 11q13amp nCounter
C
Total FGF ligands expression HTG
FGF2
FGF7
Total FGF ligands sum HTG
ROC curve HTG
D
Total FGF ligands expression HTG Normalised
E
11q13 FGF ligands expression HTG Normalised

Figure 33. FGF ligands expression do not predict for rogaratinib response. A) Ligands from the 11q13 amplicon (FGF3, 4 and 19) were analyzed from HTG data. B) The same analysis was performed with data from nCounter; C) Analysis of all FGF ligands in HTG platform; D) Normalized data from all FGF ligands; E) Normalized data from 11q13 FGF ligands. Statistical test: Mann-Whitney U test.

Even though FGFR ligands did not directly predict for rogaratinib response, we hypothesized that PDX293 might have responded to this inhibitor due to its high levels in FGF3, since it otherwise only expressed moderate levels of FGFR2 mRNA. To further investigate the role of FGF ligands in rogaratinib response, we selected 3 *FGFR1*amp cell line models with different levels of FGFR1 expression for drug-inhibition assays: CAL120 (TNBC), JIMT-1 (HER2+) and SUM44 (11q13 co-amp, ER+). Western blot analysis showed that CAL120 expressed high FGFR1 protein levels, alike PDX325 in **Figure 34**, and compared to SUM44 and JIMT1 (**Figure 34A**). Treatment with bFGF elicited moderate FGFR pathway activation in CAL120 cell line and in JIMT1 (**Figure 34B**).

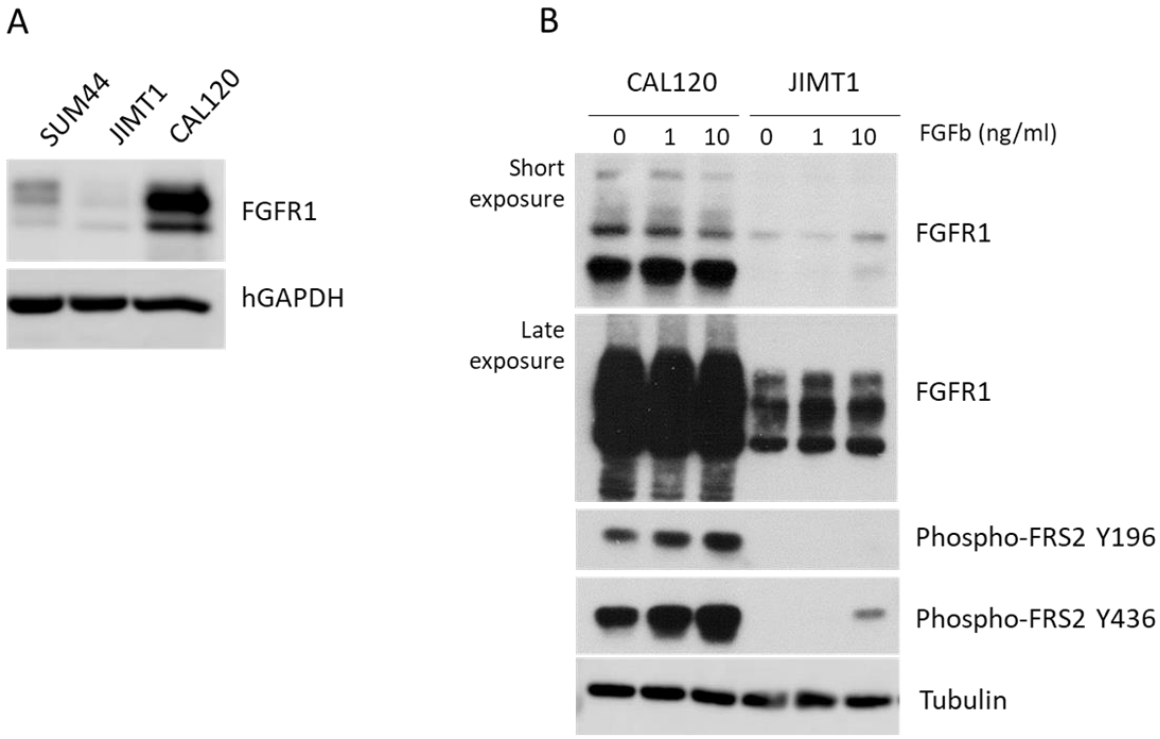

Figure 34. CAL120 expresses high levels of FGFR1 and has a highly activated FGFR pathway. A) SUM44, JIMT-1 and CAL120 relative FGFR1 protein expression; B) CAL120 and JIMT-1 cell lines were stimulated during 15 minutes with 0, 1 and 10 ng/ml of bFGF; antibodies targeting phospho-FRS2 Y436 and Y196 were used to analyze FGFR pathway activation. Gel prepared at 12% acrylamide in A) and at 10% in B).

We next dissected if FGFR pathway activation by means of high expression of FGF ligands sensitized the lowly-FGFR1-expressing cell lines to FGFRinh. Therefore, we quantified the IC_{50} of rogaratinib upon addition of bFGF or upon treatment with an FGF-trap (NSC-12), to counteract the potential effect of endogenous FGFs (**Figure 35A**). As expected, CAL120 cells were sensitive to rogaratinib and SUM44 and JIMT-1 cell lines were resistant. Media supplemented with bFGF significantly increased the growth of SUM44 cells and it moderately decreased the IC_{50}. However, the IC_{50} of the SUM44 cells treated with bFGF was much higher than the IC_{50} of the rogaratinib-sensitive cells CAL120, and therefore we could not corroborate our hypothesis with the cell line models. Similarly, the FGFtrap did not modify the IC_{50} values in these models, albeit it reduced cell growth in the JIMT1 cells.

A similar approach was used with patient-derived 3D *ex vivo* cultures (PDO) using several *FGFR1-4* and *FGF3/4/19*amp PDX models, including PDX293, the SD-model that exhibited high levels of FGF3 (**Figure 35B**). 5 models were available for this assay: PDX302 and PDX343 (PD response in *in vivo* efficacy assay), and PDX404, PDX293 and PDX291 (SD response in *in vivo* efficacy assay). Since we could not obtain PDOs from the PDXs models exhibiting a PR response, we included the CAL120 cell line as supra-sensitive FGFRinh model. All PDOs analyzed exhibited high IC_{50} values, including the models that exhibited an SD response in the *in vivo* setting, compared to CAL120 in 3D. This was unsurprising, as the *ex vivo* assay has a limited capacity to predict response for the SD models (personal communication V. Serra). Results from the addition of bFGF to the media showed a moderate reduction in IC_{50} for PDX302, a model expressing high levels of FGF7. Addition of NSC12 markedly reduced cell proliferation and IC_{50} in the same model, as observed for the JIMT-1 cells. A similar effect on IC_{50} was observed upon addition of the FGF trap in PDX404, albeit the IC_{50} values did not reach the levels of the FGFRinh-sensitive cells CAL120. In summary, these experiments could not demonstrate that high FGFR signaling by means of overexpression of FGF ligands sensitizes to FGFRinh.

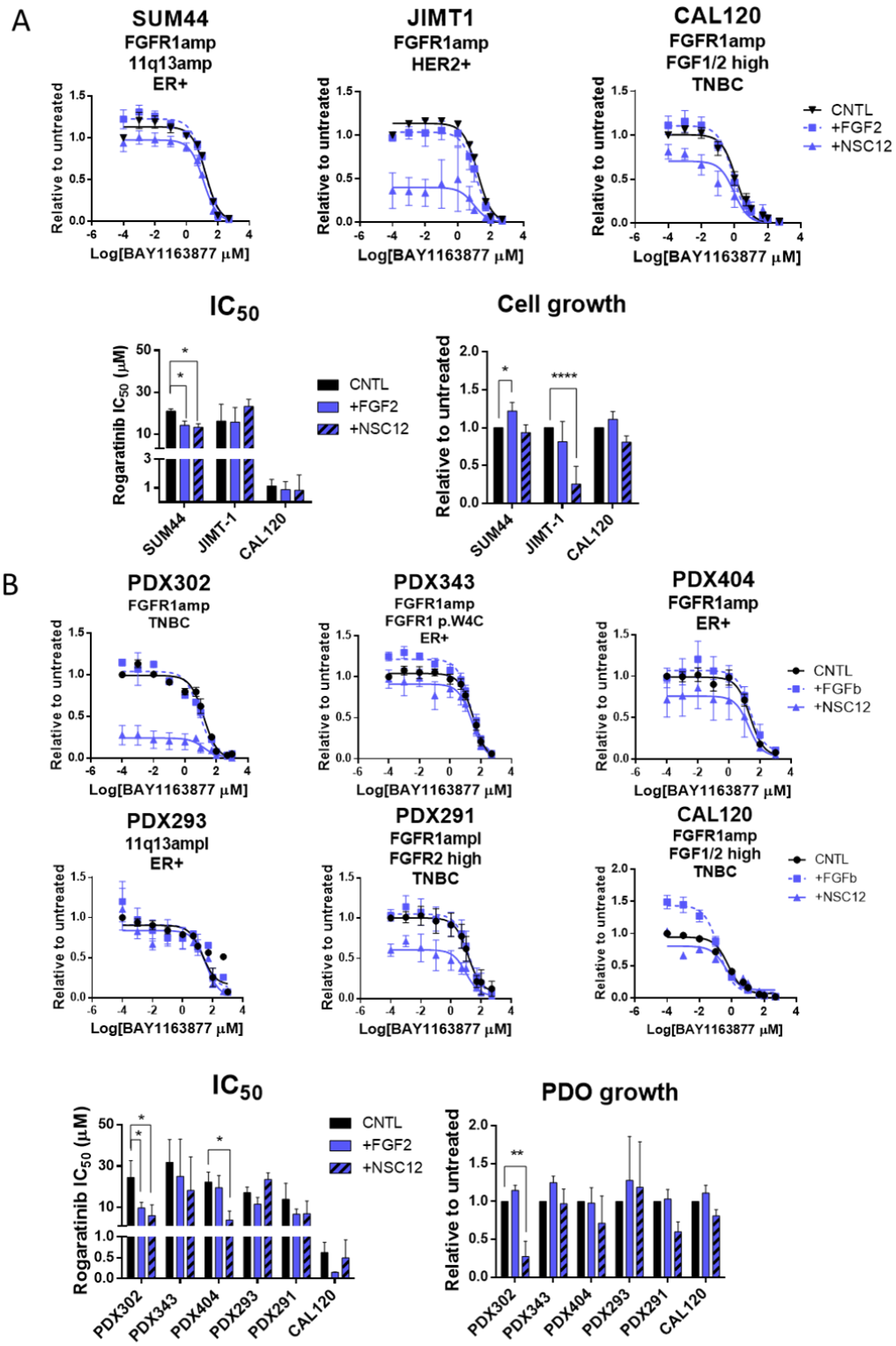

Figure 35. FGF ligands modulate the response in *FGFR1*amp cell lines and PDO models. A) Rogaratinib drug-inhibition assays in *FGFR1*amp cell lines with or without bFGF or NSC-12; B) Patient-derived Organoids (PDO) drug-inhibition assays of rogaratinib with or without bFGF or NSC-12; PDOs were cultured in Matrigel, including CAL120 cell line. Cell growth and IC_{50} determined from 3 independent experiments, except for CAL120 in PDO graph, where 2 independent experiments were performed. Statistical tests: 2-way ANOVA.

2.4. The multitarget kinase inhibitor (MTKI) lucitanib shows superior antitumor activity than the FGFR1/2/3inh rogaratinib

MTKI inhibitors showed promising activity in the clinic in FGFRamp breast cancers[177, 229]. However, when more specific FGFRinh were tested, the response rate was rather disappointing[184, 185]. For this reason, we and others hypothesized that the antiangiogenic effects of MTKI were relevant in breast cancers[181]. As a matter of fact, the anti-VEGF bevacizumab was approved for the treatment of TNBC for a period of time before discontinued after showing limited results[230]. Therefore, we compared the antitumor activity of the MTKI lucitanib with rogaratinib in seven representative PDXs: the 4 *FGFR1*amp most resistant models (PDX156, PDX302, PDX288 and PDX343) and the 3 *FGFR1*amp most sensitive models (PDX291, PDX325 and PDX191) to rogaratinib (**Figure 36**). Lucitanib showed equal or superior antitumor activity compared to rogaratinib in all the models tested, resulting in tumor growth regression (PR) or stabilization (SD) in the majority of models and only PDX156 showed a PD response. All PR models were ER+ and the rest were TNBC molecular subtype.

We analyzed the relative gene expression (HTG data) of lucitanib's targets in the PDXs, and observed that lucitanib was very efficacious (PR) in the two models with high FGFR1/3 expression. Three models that showed PD on rogaratinib treatment sensitized to lucitanib with a SD (PDX288, PDX302 and PDX343), without apparent high levels of FGFR1/2/3/4. The two most lucitanib-resistant models (PDX156 and PDX288) were devoid of FGFR1/2/3/4 expression and expressed high levels of VEGFR3 and KIT, although not as high as FGFR1/3 in PDX325 and PDX191, respectively (**Figure 36B**). This was unexpected, since lucitanib potently inhibits VEGFR3 (IC_{50}=7 nM) and, in addition, the c-KIT inhibitor imatinib did not significantly inhibit growth of PDX156 (data not shown). Therefore, we hypothesized that lucitanib's antitumor activity could be partly due to targeting the tumor vasculature. As a matter of fact, PDX343 expressed high levels of VEGFA/C and PDGFA/B/C, and VEGFC was highly expressed in the two-most sensitive models. Due to the low number of models in this substudy we did not perform ROC analyses.

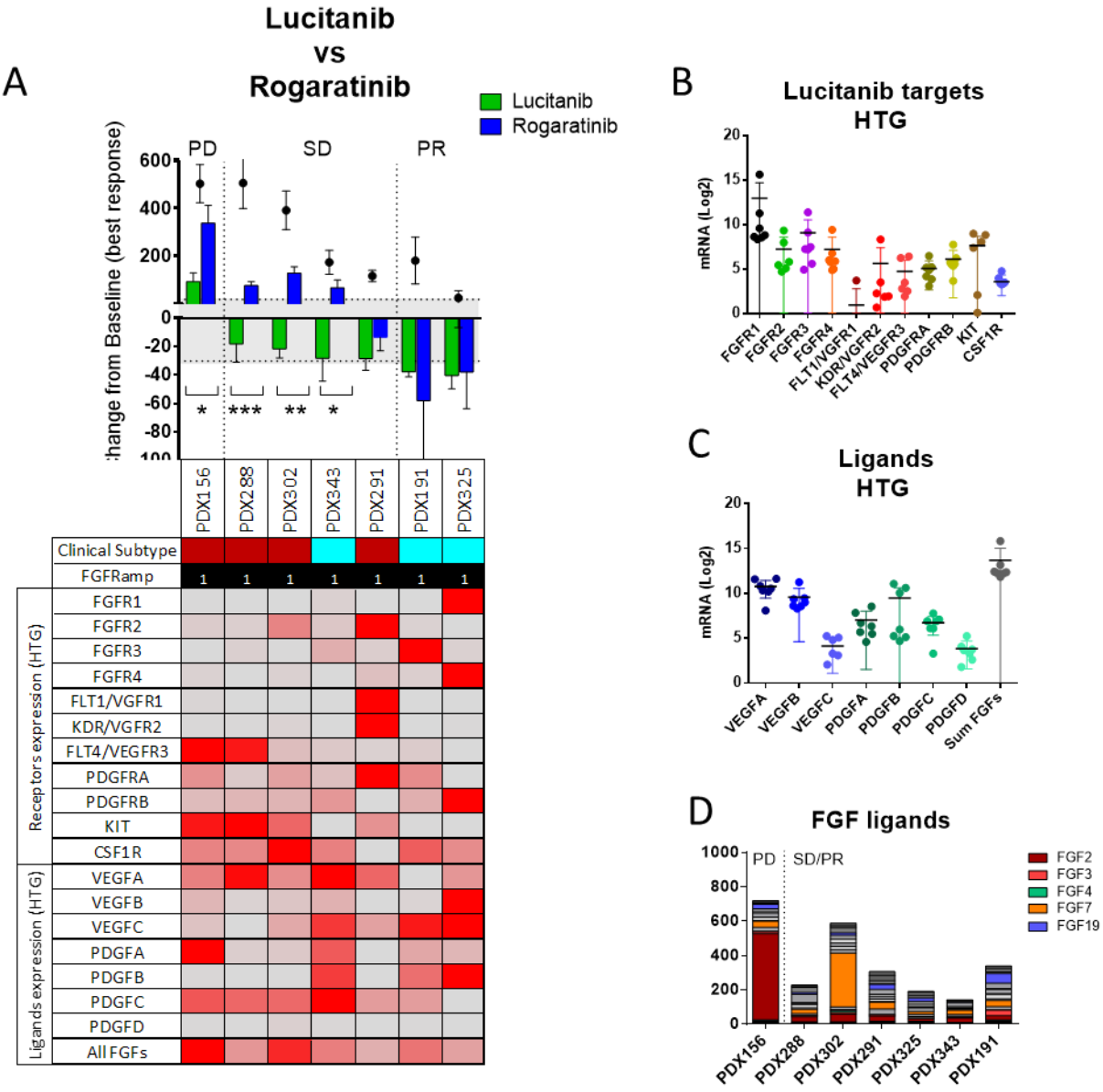

Figure 36. Lucitanib shows superior activity to rogaBratinib with no correlation with relative expression of target receptors and ligands. A) Lucitanib *vs.* rogaratinib antitumor activity (**Annex Table S4**) and relative gene expression of RTK targets of lucitanib and respective ligands (grey for low expression values and red the high expression values; data from HTG platform); B) Relative mRNA levels of lucitanib RTK targets C) Relative mRNA levels of cognate ligands; D) Depicted relative expression of each FGF ligand.

2.5. Rogaratinib and lucitanib target both proliferation and angiogenesis in sensitive PDX models

In order to dissect the mode of action of lucitanib *vs.* rogaratinib, we analyzed untreated and treated samples with both inhibitors in 5 lucitanib-sensitive PDX models (**Figure 37**) and quantified the proliferation index in tumor cells using the Ki-67 marker and the degree of vascularization by staining with the vascular endothelial cell marker CD31.

Lucitanib-treated samples showed a reduction of proliferation (Ki-67) in all models analyzed, whereas rogaratinib treatment was able to significantly reduce proliferation in exclusively in the two most sensitive models, PDX325 and PDX191.

Vascularization (CD31) was also reduced in all lucitanib-treated samples. Rogaratinib potently inhibited vascular formation in rogaratinib-sensitive PDX191, and in two rogaratinib-resistant models.

To evaluate the effect of vascularization blockade in the tumor samples, we evaluated the relative necrotic areas for each treatment. We found that lucitanib induced marked necrosis in three models (PDX288, PDX343 and PDX291), indicating that lucitanib's efficacy in these models is most likely to vascularization blockade. On the contrary, rogaratinib did not induce a marked change in necrotic areas. No necrosis was found in the FGFR-expressing models (PDX191 and PDX325), indicating that in these tumors the antitumor response was most likely due to targeting tumoral FGFR signaling.

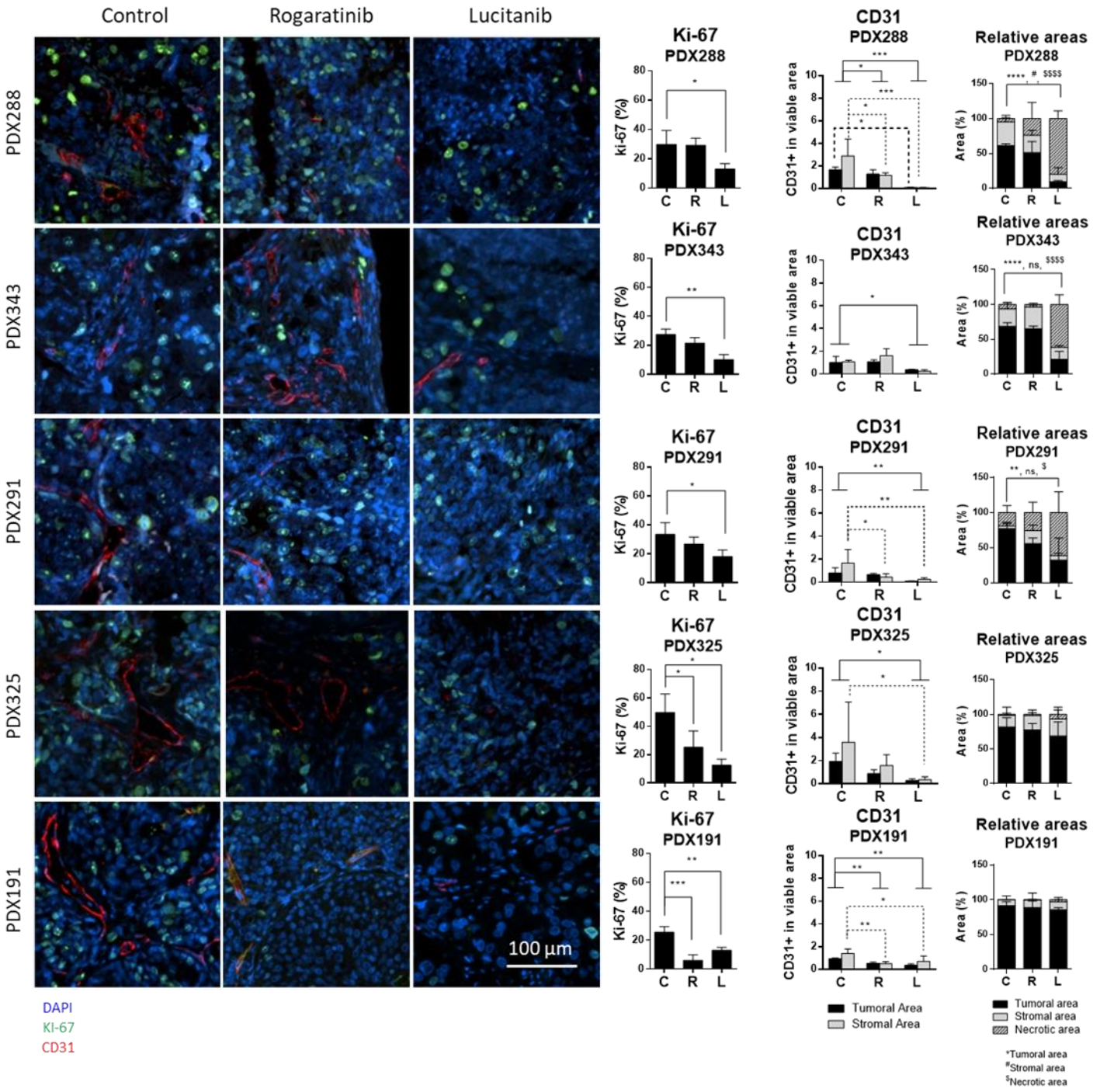

Figure 37. Rogaratinib and lucitanib treatment inhibit tumor cell proliferation and vascularization in sensitive models. Proliferation marker Ki-67 (green), vascularization marker CD31 (red) and the relative tumoral, stromal and necrotic areas were evaluated in untreated tumors (C), treated with rogaratinib (R) or lucitanib (L) in 5 PDX models. Cell nuclei are DAPI dyed (blue). Statistical tests: One-way ANOVA for Ki-67 data and 2-way ANOVA for CD31 data. 2-way ANOVA for relative areas. P-values legend: #/$, $0.01 \leq p < 0.05$; $$$$ $p < 0.0001$.

2.6. VEGF/VEGFR blockade alone is as effective as lucitanib treatment in rogaratinib-resistant models

Finally, we tested if anti-angiogenic blockade was the major phenotype in the lucitanib-sensitive models that showed marked induction of necrotic areas, and tested if the combination of rogaratinib with anti-angiogenic therapy (anti-VEGF/VEGFR) as an alternative for lucitanib, which presented limited safety in patients. For that, we performed the *in vivo* efficacy assays shown in **Figure 38**.

As anti-angiogenic therapy, we combined bevacizumab, an antibody targeting human VEGF (hVEGF); in combination with DC101, an antibody targeting murine VEGFR2 (mVEGFR2), given that bevacizumab would only block hVEGF from the tumor but not murine VEGF (mVEGF) from the stroma. Combination of DC101 and bevacizumab will assure the complete blockade of the VEGF-driven vascular signaling in the PDX models (**Figure 38A**).

In agreement with our hypothesis, both PDX models showed response to the anti-angiogenic combination treatment, and its combination with rogaratinib only offered a minor improvement in PDX288, reaching similar response levels as with lucitanib (**Figure 38B**). These results suggest that an MTKI is more effective than the combination of an anti-angiogenic and a specific FGFRinh for targeting both FGFR signaling in the tumor cells and inhibiting vascular formation.

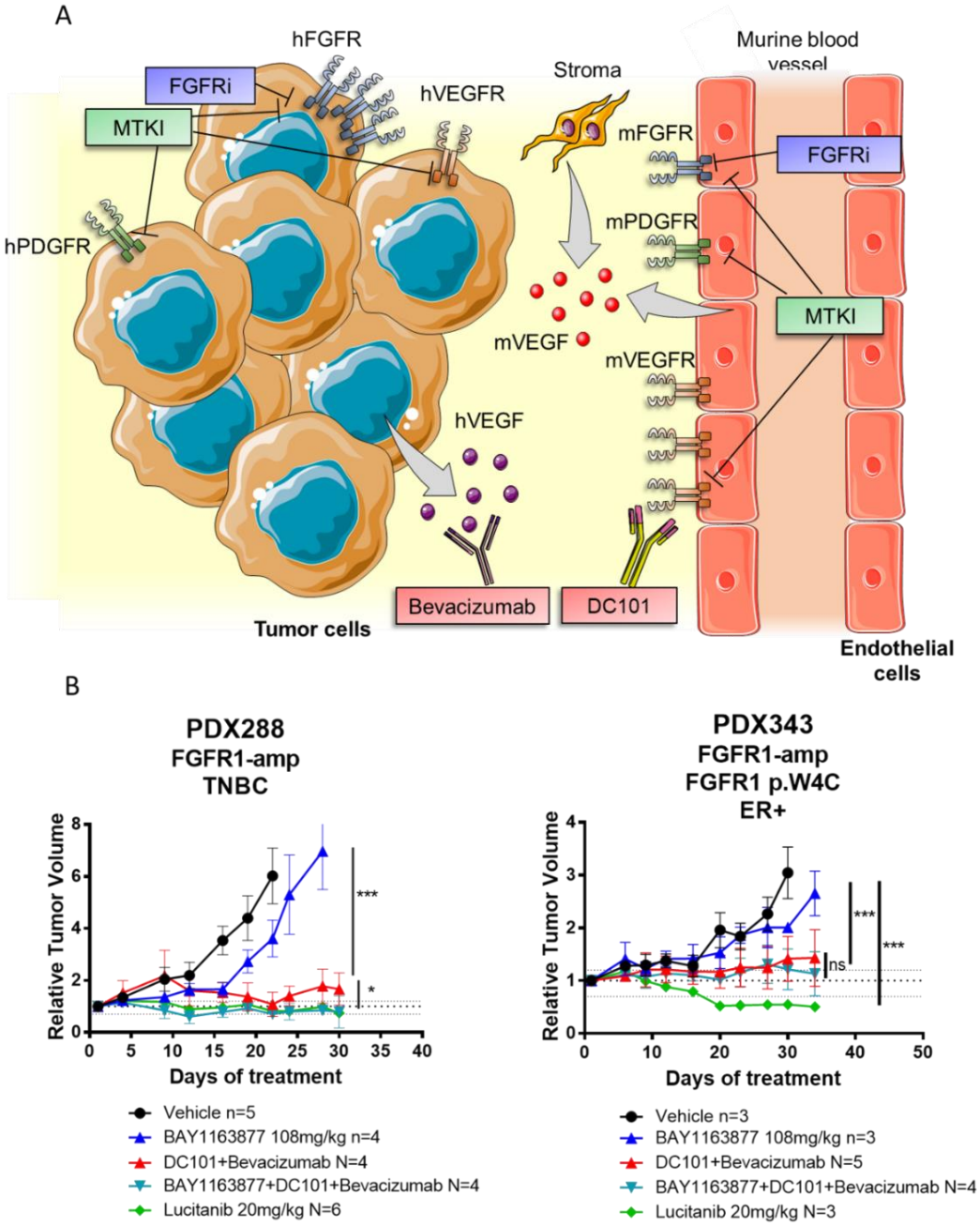

Figure 38. Rogaratinib in combination with anti-angiogenic therapy is a clinical alternative to lucitanib. A) PDX models contain two mechanisms of vascular signaling: human (from the tumor) and murine (from the mouse). Both antibodies DC101 and bevacizumab are combined in this assay in order to fully block angiogenic signaling; B) PDX288 and PDX343 *in vivo* efficacy of rogaratinib, anti-angiogenic therapy (DC101+Bevacizumab), rogaratinib in combination with anti-angiogenic therapy, *vs.* lucitanib. Statistical tests: 2-way ANOVA.

Discussion

Endocrine therapy has been the mainstay treatment for breast cancer, but innate and acquired resistance mechanisms are a problem for the treatment of patients with metastatic disease. Novel targeted agents have been developed in order to overcome resistance and three of them are currently approved: an mTORC1 allosteric inhibitor, three CDK4/6 inhibitors and a PI3Kα inhibitor. Currently, research strategies are focused in identifying novel therapeutic targets to combat endocrine (and thereof combinations) resistance and also in improving patient selection with better response biomarkers.

In this study, we aimed to identify response biomarkers and resistance mechanisms to two major therapeutic strategies for luminal breast cancer: PI3K/mTORC1/2 and FGFR inhibitors.

In part 1 of this study we tested if a clinically approved sequencing platform, the IMPACT panel, was useful to identify resistance mechanisms to PI3K inhibitors. Of note, the PI3Kα inhibitor alpelisib received approval by the FDA on May 2019 for the treatment of HER2-negative, *PIK3CA*-mutant advanced or metastatic breast cancer in combination with fulvestrant as detected by an FDA-approved test following progression on or after an endocrine-based regimen. This approval follows to over 10 years of preclinical and clinical research, demonstrating increased activity of these drugs in *PIK3CA*-mutant tumors[37, 231].

To this aim, we tested alpelisib in a set of 25 breast cancer PDXs, containing ER+, HER2 and TNBC molecular subtypes. In line with early preclinical observations, we noted that *ERBB2*-amplified / Her2-enriched tumors were likely to be sensitive to alpelisib and that TNBC / basal like tumors were resistant[232-235]. Our panel contained 7 *PIK3CA*-mutant models, two of which derived from a patient who received the PI3K inhibitor GDC-0032 plus letrozole in the clinic. In the absence of an endocrine backbone treatment, we did not observe an association between *PIK3CA* mutation and alpelisib response. This highlights the remarkable intrinsic dependence on the PI3K pathway of HER2+ tumors *vs.* ER+/*PIK3CA* mutant tumors.

This study enabled us to identify 4 groups of tumors with recurrent mutations: alterations that increase PI3K-downstream signaling, 2) alterations in the parallel MAPK signaling –both supported by an independent proteomic study-, 3) alterations in the cell cycle pathway and 4) alterations included in the 11q amplicon. Two recent studies using genomics platforms have highlighted that e.g. *TSC2* loss and *CCND1* amplification occur concomitantly to

PIK3CA mutation in metastatic tumors[236, 237] and we hypothesized that they may confer resistance to PI3K inhibitors.

To date, alterations that activate mTORC1 while generating resistance to PI3Kinh have not been yet described in breast cancer. In this study, we aimed to identify such alterations and test if they could generate sensitivity to mTORC1/2 inhibition. Previous work from our colleagues showed that PI3Kinh-resistant cell lines presented high mTORC1 activity, and thus the addition of an mTORC1inh was necessary for sensitizing the cells to a PI3Kinh[107].

We demonstrated that two out of three tumors harboring genetic alterations activating mTORC1 were more sensitive to a potent catalytic mTORC1/2inh than to a PI3K inhibitor. Nonetheless, these results lacked clinical significance, since even the combination with a novel SERD, the treatment did not result in tumor regression. We postulate several reasons for this failure: 1) the intermittent dose and schedule of the mTORC1/2inh was tolerable but inefficiently inhibiting the pathway; 2) at least one of the identified alterations might not have been relevant for activating the mTORC1 pathway (PDX251); 3) we observed high expression of PKM2/glutaminase in PDX313 and PDX039. It has been described by several studies that mTORC1 activation generates an up-regulation of PKM2[238-240], so sustained activation of the glycolytic pathway could overpass mTORC1/2 inhibition hence generating resistance[241].

The MANTA clinical study tested fulvestrant monotherapy or in combination with vistusertib or everolimus in metastatic ER+ breast cancer[116, 242]. This study showed that the combination of fulvestrant plus everolimus presented longer PFS compared with the combination of fulvestrant plus vistusertib or fulvestrant alone. Hence, the study failed to demonstrate the benefit of the dual mTORC1 and mTORC2 blockade over mTORC1 blockade alone. The trial did not recruit for patients with genetic alterations compatible with activation of the mTORC1 pathway. Nonetheless, our preclinical data suggests a limited capacity of vistusertib to induce tumor regression in biomarker-enriched tumors.

We next tested the impact of the 11q amplicon in PI3Kinh resistance. This amplification is associated with poor prognosis and endocrine therapy resistance in breast cancer[7, 243], therefore it is important to determine the impact in PI3K inhibition. Tumors with these alterations were located at the interphase between response with SD and disease

progression. Our *in vitro* models overexpressing the individual genes allowed us to conclude that overexpression of cyclin D1 results in drug resistance in two *PIK3CA*-mutant cell lines. The extent of the phenotype was more marked in the T47D cell line and this was associated with retention of phospho-Rb S807/811 upon treatment.

Other preclinical data generated in our laboratory indicate that these tumors are sensitive to the combination of a PI3Kinh plus a CDK4/6inh: PDX131, PDX191 and PDX293.1/2 were not sensitive to monotherapy CDK4/6inh but this inhibitor sensitized the three models to PI3Kinh, indicating that high cyclin D1 expression limits the activity of PI3Kinh. Of note, PDX293.1/2 harbors a *PIK3CA* mutation and would be eligible of a PI3Kinh in the clinic.

The amplification of the 11q13 locus is not the only mechanism by which cells may overexpress cyclin D1. Besides the known estrogen-induced cyclin D1 upregulation[72, 244], it has been described that activated ras and myc can lead to cyclin D1 overexpression[245, 246]. Hence, we could speculate that PI3Kinh resistance could be mediated independently of *CCND1* amplification, and detection at the protein level is important for determining the cyclin D1-overexpressing tumors.

Besides, amplifications do not always generate overexpression of the protein. As commented in this review by Jia et al[247], we tend to assume that gene amplification causes overexpression, but this assumption remains unproven until experimental verification. Here, we have shown that *CCND1*amp and *PAK1*amp showed a tendency for higher gene expression although non-significant, and *RPS6KB2*amp failed to correlate with S6K2 expression.

Of note, PDX293.2, besides the 11q13amp, it harbored an *RB1* mutation which is affecting the same cell cycle node. Rb loss of function has been described to abrogate cell cycle control and to induce abnormal proliferation[248, 249]. Thus, both alterations suggest an aberrantly activated cell cycle in this model.

We could not demonstrate that any of the other three cancer-related genes within the 11q amplicon was relevant for PI3Kinh response *per se*, albeit a marked increase in MEK/ERK signaling was observed upon treatment with FGF ligands and this resulted in PI3Kinh resistance in cyclin D1-overexpressing MCF7 cells.

The combination of cyclin D1 overexpression and addition of bFGF generated an even higher IC_{50} under PI3K inhibition, suggesting that the co-amplification (and expression) of *CCND1* with *FGF3/4/19* increase the resistance to PI3Kinh. The physical proximity of these genes in the 11q13 amplicon generates a regular co-amplification in breast cancer[65], more than with the other genes of this amplicon. This indicates that the combined effect of *CCND1* and *FGF3/4/19*amp is likely to be highly recurrent in breast cancer. We found these results extremely relevant and we are currently testing their impact on these *in vitro* models using the actual standard of care, namely the combination of alpelisib and fulvestrant.

The resistance generated by cyclin D1 and high bFGF suggests that both cell cycle and FGFR pathway activations can lead to PI3Kinh resistance. Recently, it has been published that *FGFR1*amp generates resistance to CDK4/6inh[63]. However, the 11q13amp has a difficult therapeutic strategy. This region contains several genes involved in many pathways, not necessarily actionable. It has not been yet demonstrated that cyclin D1 overexpression predicts for CDK4/6inh sensitivity[250]; high FGF ligands expression do not necessarily indicate sensitivity to FGFRinh, as shown in the second part of this thesis; PAK1 protein is a potential target, but PAKinh are poorly explored in the clinics and important toxicities might limit their efficacy[251]; and the results here presented indicate that S6K2 contributes weakly in tumor growth and/or resistance to PI3K therapy. Hence, special care must be taken and further studies need to be performed in order to give a therapeutic option for the 11q13amp cancers.

It is intriguing whether the combined effect of all the genes in the 11q13 amplicon could increase the resistance to PI3Kinh. Here we show that *CCND1*amp/cyclin D1 overexpression and addition of FGF ligand could generate resistance to PI3Kinh, but other elements present in the 11q13 region, if co-amplified, could as well participate in the resistance mechanism. Although it has been described that S6K2 can promote breast cancer survival via Akt[252], the S6K2 overexpressing cell lines generated in this thesis failed to show resistance to PI3Kinh, and we could not generate PAK1 overexpressing cell lines. Whether PAK1 overexpression and co-amplifications (and overexpression) with other 11q13 elements could participate in the resistance to PI3Kinh and endocrine combinations remains to be studied. Assays

regarding the additive effect of each gene with each other would shed light in the resistance effect of the 11q13 amplification in the current ER+ BC targeted therapy.

In part 2 of this study we aimed to identify response biomarkers to FGFRinh and hypothesized that a combination with an anti-angiogenic treatment would improve the response rate to the levels observed for MTKI. Our results highlight the importance of testing for mRNA or protein level as surrogate marker of FGFR1/2/3 expression. Copy-number alterations were not informative to predict response as: 1) they could not pinpoint which tumors were actually expressing the RTK and 2) they could not identify additional genomic alterations that resulted in high FGFR expression. This data was also informative as high expression of FGFR1/3 was associated with tumor regression (PR) and high expression of FGFR2 was associated with SD. Importantly, we can conclude that a clinically suitable Nanostring platform is capable of identifying FGFRinh-sensitive breast tumors using FFPE specimens and this is an available resource at all major hospitals.

This data is in accordance with a recent study showing higher efficacy of rogaratinib in colon and lung cancer cell lines and PDX models characterized by FGFR overexpression[207]. In fact, 3 clinical trials are currently evaluating the use of FGFR mRNA expression as a biomarker of response to FGFRinh among solid tumors (ClinicalTrials.gov Identifiers: NCT01976741, NCT02592785, NCT03410693).

Again, data showed that gene amplification does not always corresponds with overexpression. In fact, certain models without gene amplifications were showing high levels of one or more of the FGF receptors. Considering this, fusions involving the promoter of the gene or epigenetic modifications might be taking place, increasing the expression of such receptors. We presume that the tumor expressing high levels of FGFR3 (PDX191) harbor an FGFR3 fusion (such as the translocation with the IHC promoter, highly frequent in multiple myeloma[144]), and this hypothesis is being tested using a clinically approved fusion panel. Therefore, it is important to evaluate *FGFR1-4* mRNA regardless of the *FGFR1-4* gene amplification. We expect this data to stablish the rationale for future clinical trials, opening the efficacy window for FGFRinh, so other non-*FGFR1-4*amp but high *FGFR1-4* mRNA-expressing patients could benefit from this therapy.

Of note, we have evaluated *FGFR1-4* expression generating a summatory of the 4 FGF receptors, but it is important to denote that it is only valid for this cohort of PDX due to its normalization within these models (in an attempt to equal the expression levels of FGFR1 with the rest of the receptors). Therefore, we expect changes in this value if more samples are added. Hence, we think this summatory should be further validated in other cohorts, with greater sample size.

Results regarding the FGF ligands indicate that neither 11q13amp, co-amp nor high FGF expression predicts for FGFRinh. As previously stated, other genes in the 11q13, such as *CCND1*, could contribute as well on tumorigenesis, activating other pathways to overpass FGFR inhibition. However, assays with *FGFR1*amp cell lines and PDO models with higher or lower amount of ligand could slightly modulate FGFRinh response. But, in any case, higher amounts of FGF could not sensitize models which were already resistant to FGFRinh. These results might indicate that a tumor can respond to FGF stimuli, but the sensitivity to FGFRinh would be only determined by the levels of the receptor (**Figure 39**). We could speculate that if a tumor with low levels of FGFRs is stimulated with FGFs, the pathway will be activated, and it can generate resistance to certain therapies such as PI3Kinh as demonstrated in the first part of this study, but that will not determine the response to FGFRinh, because other driving mutations might be present.

We further concluded that the MTKI lucitanib is preclinically active in models overexpressing FGFR1/3 (as rogaratinib), and likely in tumors with high vascular signaling (PDX343 and PDX288, overexpressing VEGFA, an important pro-angiogenic signal[253]). Importantly, lucitanib showed greater antitumor activity than specific FGFRinh, corroborating with the favorable clinical data for MTKI[177, 182].

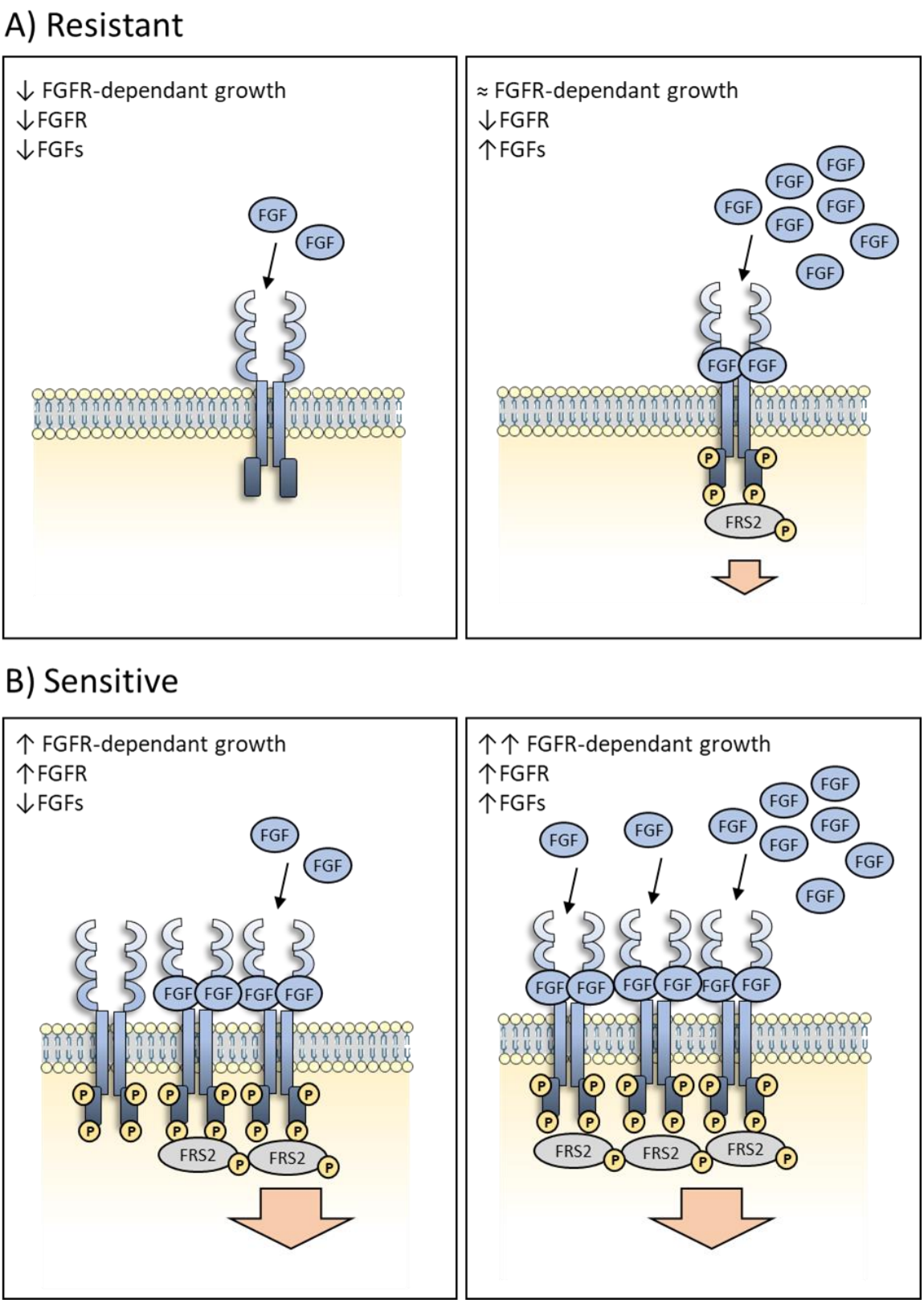

Figure 39. The molecular mechanism proposed to determine FGFRinh sensitivity. A) Resistant tumors to FGFRinh present low levels of FGFR, although they could be stimulated with FGF ligand to generate resistance to other therapies. B) Sensitive models to FGFRinh therapy harbor high levels of the receptor, and could grow faster under the stimuli of FGFs, but low levels of ligands could be enough to maintain FGFR pathway activated.

While both inhibitors blocked cell proliferation and vascularization in sensitive tumor models, lucitanib showed a greater effect. Vascularization in stromal areas was decreased in almost all models tested. This is in agreement with previous observations showing that blood vessels within the stromal area are where the tumor angiogenic response initiates[254-256]. These results show that FGFR blockade can inhibit proliferation but only when a tumor is FGFR-dependent. FGFRinh can inhibit vascularization to some extent, but not enough for antitumor response. However, lucitanib is able to highly block both proliferation and vascularization, indicating that combinatorial blockade of several RTK receptors turns into a more efficient antitumor response. Besides, the analysis of the relative areas suggests that hypoxic-driven death is the result of prolonged inhibition of angiogenesis as marked necrosis areas were observed in FGFR1/3-independent tumors.

Furthermore, our results suggest that an antibody-based anti-angiogenic approach combined with a specific FGFRinh would not result in increased response rate compared to MTKI. This is in contrast with a study that determines a synergistic anti-angiogenic treatment with the dual blockade of FGFR1 and VEGFR1[257], although only tested in a xenograft model of the *FGFR1*amp JIMT1 cell line. In this study, they identified an FGFR signalling dependent increase of VEGF secretion, suggesting that a combination of FGFRinh with anti-VEGF therapy would increase the response. However, in the context of the data presented here, this should be addressed in cancers expressing high levels of FGFR, to assure for an FGFR pathway activation.

We show that angiogenic blockade through VEGF/VEGFR inhibition is a determinant factor for antitumor response. Hence, we could speculate that the higher efficacy of MTKI observed in FGFRinh-resistant models is mainly due to targeting VEGFR1-3. However, VEGF pathway blockers, such as bevacizumab, sunitinib or sorafenib, have shown limited efficacy in breast cancer clinicals trials[92, 202, 204-206]. Further studies are needed to identify response biomarkers for angiogenesis-dependent tumors.

In summary, we have identified several biomarkers of response and mechanisms of resistance to PI3K/mTORC1/2inh and FGFRinh. Dual mTORC1/2 inhibitors presented higher efficacy than PI3Kinh in mTORC1 activated tumors, and cyclin D1 and FGF overexpression generated resistance to PI3Kinh. Furthermore, we determined that FGFR1-4 mRNA

expression predicts for FGFRinh response, and that MTKIs efficiently block proliferation and vascularization. In line with this, our data prompts the optimization of patient selection based on high expression of FGFR. Results presented in this thesis are meant to contribute in the criteria for future clinical trials for PI3Kinh, mTORC1/2inh and FGFRinh, in an attempt to improve the responses in the clinics for luminal BC.

Conclusions

PART 1

The following conclusions are derived from the first part of this thesis:

1. Her2-enriched subtype PDX models are alpelisib sensitive while Basal-like PDX models are alpelisib resistant
2. Alterations downstream PI3K and in the MAPK pathway confer resistance to alpelisib treatment.
3. mTORC1/2inh are more effective than PI3Kinh in PDX models harboring mTORC1-activating alterations such as *TSC1* deletion and *MTOR* mutation
4. Combination of mTORC1/2inh with a SERD improves the response in comparison to mTORC1/2inh monotherapy
5. High cyclin D1, high FGF and high levels of both generate resistance to PI3Kinh in models harboring *PIK3CA* activating mutation
6. 11q13amp models expressing high levels of PAK1 protein are resistant to PI3Kinh but sensitize to PAKinh

PART 2

The following conclusions are derived from the second part of this thesis:

1. High FGFR1-4 mRNA levels predict for FGFRinh response, but not gene amplification, FGF ligand amplification nor expression
2. FGFR1-4 mRNA levels can be high in absence of FGFR amplification
3. FGF ligands can modulate FGFRinh response but do not sensitize for FGFRinh
4. FGFRinh and MTKI block proliferation in sensitive models.
5. FGFRinh block angiogenesis in both sensitive and resistant models but MTKI to a greater extent
6. Antiangiogenic therapy can reach similar antitumor efficacy as with MTKI in FGFRinh-resistant models.
7. Combination of antiangiogenic therapy with FGFRinh in FGFRinh-resistant models poorly improves the efficacy of antiangiogenic agents in monotherapy

Bibliography

1. Bland KI, Copeland EM, Klimberg VS. 2 - Anatomy of the Breast, Axilla, Chest Wall, and Related Metastatic Sites. In: Bland KI, Copeland EM, Klimberg VS, Gradishar WJ, editors. The Breast (Fifth Edition): Elsevier, 2018:20-36.e22.
2. Korourian S. 10 - Infiltrating Carcinomas of the Breast: Not One Disease. In: Bland KI, Copeland EM, Klimberg VS, Gradishar WJ, editors. The Breast (Fifth Edition): Elsevier, 2018:145-155.e144.
3. Lodish H BA, Zipursky SL, et al. . Proto-Oncogenes and Tumor-Suppressor genes. Molecular Cell Biology. New York: W. H. Freeman, 2000.
4. Griffiths AJF MJ, Suzuki DT, et al. Genetic variation, An Introduction to Genetic Analysis. 7th edition ed. New York: W. H. Freeman, 2000.
5. Griffiths AJF MJ, Suzuki DT, et al. Cancer: the genetics of aberrant cell control, An Introduction to Genetic Analysis. 7th edition ed. New York: W. H. Freeman, 2000.
6. Stratton MR, Campbell PJ, Futreal PA. The cancer genome. Nature. 2009;458: 719-724.
7. Cancer Genome Atlas N. Comprehensive molecular portraits of human breast tumours. Nature. 2012;490: 61-70.
8. Foster I. Cancer: A cell cycle defect. 2008.
9. Croce CM. Oncogenes and cancer. N Engl J Med. 2008;358: 502-511.
10. Wang M, Zhao J, Zhang L, et al. Role of tumor microenvironment in tumorigenesis. J Cancer. 2017;8: 761-773.
11. Hanahan D, Weinberg RA. The hallmarks of cancer. Cell. 2000;100: 57-70.
12. Hanahan D, Weinberg RA. Hallmarks of cancer: the next generation. Cell. 2011;144: 646-674.
13. Martin TA YL, Sanders AJ, et al. . Cancer Invasion and Metastasis: Molecular and Cellular Perspective. . Austin (TX): Landes Bioscience, 2000-2013.
14. Klimberg VS, Bland KI. 9 - In Situ Carcinomas of the Breast: Ductal Carcinoma in Situ and Lobular Carcinoma in Situ. In: Bland KI, Copeland EM, Klimberg VS, Gradishar WJ, editors. The Breast (Fifth Edition): Elsevier, 2018:130-144.e134.
15. Sharma GN, Dave R, Sanadya J, Sharma P, Sharma KK. Various types and management of breast cancer: an overview. J Adv Pharm Technol Res. 2010;1: 109-126.
16. Pritzlaff M, Summerour P, McFarland R, et al. Male breast cancer in a multi-gene panel testing cohort: insights and unexpected results. Breast Cancer Res Treat. 2017;161: 575-586.
17. Jain S, Gradishar WJ. 76 - Male Breast Cancer. In: Bland KI, Copeland EM, Klimberg VS, Gradishar WJ, editors. The Breast (Fifth Edition): Elsevier, 2018:974-980.e972.
18. Kittaneh M, Montero AJ, Gluck S. Molecular profiling for breast cancer: a comprehensive review. Biomark Cancer. 2013;5: 61-70.
19. Vuong D, Simpson PT, Green B, Cummings MC, Lakhani SR. Molecular classification of breast cancer. Virchows Arch. 2014;465: 1-14.
20. Bhargava RB, J. Immunohistochemistry of the breast. In: Defrancesco K, editor. Diagnostic Immunohistochemistry: theranostic and genomic applications. United States of America: ELSEVIER SAUNDERS, 2014:710-760.
21. Wang EC, S; Rossi, M. BREAST CANCER. Available from URL: http://www.pathophys.org/breast-cancer/ [accessed July 1st, 2019].
22. Perou CM, Sorlie T, Eisen MB, et al. Molecular portraits of human breast tumours. Nature. 2000;406: 747-752.
23. Lehmann BD, Bauer JA, Chen X, et al. Identification of human triple-negative breast cancer subtypes and preclinical models for selection of targeted therapies. J Clin Invest. 2011;121: 2750-2767.

24. van 't Veer LJ, Dai H, van de Vijver MJ, et al. Gene expression profiling predicts clinical outcome of breast cancer. Nature. 2002;415: 530-536.
25. Paik S, Shak S, Tang G, et al. A multigene assay to predict recurrence of tamoxifen-treated, node-negative breast cancer. N Engl J Med. 2004;351: 2817-2826.
26. Parker JS, Mullins M, Cheang MC, et al. Supervised risk predictor of breast cancer based on intrinsic subtypes. J Clin Oncol. 2009;27: 1160-1167.
27. Prat A, Bianchini G, Thomas M, et al. Research-based PAM50 subtype predictor identifies higher responses and improved survival outcomes in HER2-positive breast cancer in the NOAH study. Clin Cancer Res. 2014;20: 511-521.
28. Filipits M, Rudas M, Jakesz R, et al. A new molecular predictor of distant recurrence in ER-positive, HER2-negative breast cancer adds independent information to conventional clinical risk factors. Clin Cancer Res. 2011;17: 6012-6020.
29. Guler EN. Gene Expression Profiling in Breast Cancer and Its Effect on Therapy Selection in Early-Stage Breast Cancer. Eur J Breast Health. 2017;13: 168-174.
30. Waks AG, Winer EP. Breast Cancer Treatment: A Review. JAMA. 2019;321: 288-300.
31. Makhoul I. 24 - Therapeutic Strategies for Breast Cancer. In: Bland KI, Copeland EM, Klimberg VS, Gradishar WJ, editors. The Breast (Fifth Edition): Elsevier, 2018:315-330.e317.
32. Tong CWS, Wu M, Cho WCS, To KKW. Recent Advances in the Treatment of Breast Cancer. Front Oncol. 2018;8: 227.
33. FDA. FDA Approves Everolimus (Afinitor) for Metastatic Breast Cancer. Available from URL: https://www.cancernetwork.com/mtor/fda-approves-everolimus-afinitor-metastatic-breast-cancer [accessed 1st July, 2019].
34. Beaver JA, Amiri-Kordestani L, Charlab R, et al. FDA Approval: Palbociclib for the Treatment of Postmenopausal Patients with Estrogen Receptor-Positive, HER2-Negative Metastatic Breast Cancer. Clin Cancer Res. 2015;21: 4760-4766.
35. Shah A, Bloomquist E, Tang S, et al. FDA Approval: Ribociclib for the Treatment of Postmenopausal Women with Hormone Receptor-Positive, HER2-Negative Advanced or Metastatic Breast Cancer. Clin Cancer Res. 2018;24: 2999-3004.
36. FDA OKs Abemaciclib for ER+, HER2- Breast Cancer. Cancer Discov. 2017;7: OF1.
37. FDA. FDA approves alpelisib for metastatic breast cancer. Available from URL: https://www.fda.gov/drugs/resources-information-approved-drugs/fda-approves-alpelisib-metastatic-breast-cancer [accessed 4th July, 2019].
38. Dixon JM. Endocrine Resistance in Breast Cancer. New Journal of Science. 2014;2014: 27.
39. FDA. FDA approves ado-trastuzumab emtansine for early breast cancer. Available from URL: https://www.fda.gov/drugs/resources-information-approved-drugs/fda-approves-ado-trastuzumab-emtansine-early-breast-cancer [accessed 04/09/2019, 2019].
40. Oliveira M, Saura C, Nuciforo P, et al. FAIRLANE, a double-blind placebo-controlled randomized phase II trial of neoadjuvant ipatasertib plus paclitaxel for early triple-negative breast cancer. Ann Oncol. 2019.
41. Kim SB, Dent R, Im SA, et al. Ipatasertib plus paclitaxel versus placebo plus paclitaxel as first-line therapy for metastatic triple-negative breast cancer (LOTUS): a multicentre, randomised, double-blind, placebo-controlled, phase 2 trial. Lancet Oncol. 2017;18: 1360-1372.
42. Rugo HS, Vidula N, Ma C. Improving Response to Hormone Therapy in Breast Cancer: New Targets, New Therapeutic Options. Am Soc Clin Oncol Educ Book. 2016;35: e40-54.
43. Li S, Shen D, Shao J, et al. Endocrine-therapy-resistant ESR1 variants revealed by genomic characterization of breast-cancer-derived xenografts. Cell Rep. 2013;4: 1116-1130.
44. Lefebvre C, Bachelot T, Filleron T, et al. Mutational Profile of Metastatic Breast Cancers: A Retrospective Analysis. PLoS Med. 2016;13: e1002201.
45. Robinson DR, Wu YM, Vats P, et al. Activating ESR1 mutations in hormone-resistant metastatic breast cancer. Nat Genet. 2013;45: 1446-1451.

46. Toy W, Shen Y, Won H, et al. ESR1 ligand-binding domain mutations in hormone-resistant breast cancer. Nat Genet. 2013;45: 1439-1445.
47. Toy W, Weir H, Razavi P, et al. Activating ESR1 Mutations Differentially Affect the Efficacy of ER Antagonists. Cancer Discov. 2017;7: 277-287.
48. Bjornstrom L, Sjoberg M. Mechanisms of estrogen receptor signaling: convergence of genomic and nongenomic actions on target genes. Mol Endocrinol. 2005;19: 833-842.
49. Ciruelos Gil EM. Targeting the PI3K/AKT/mTOR pathway in estrogen receptor-positive breast cancer. Cancer Treat Rev. 2014;40: 862-871.
50. Migliaccio A, Di Domenico M, Castoria G, et al. Tyrosine kinase/p21ras/MAP-kinase pathway activation by estradiol-receptor complex in MCF-7 cells. EMBO J. 1996;15: 1292-1300.
51. Simoncini T, Hafezi-Moghadam A, Brazil DP, Ley K, Chin WW, Liao JK. Interaction of oestrogen receptor with the regulatory subunit of phosphatidylinositol-3-OH kinase. Nature. 2000;407: 538-541.
52. Kato S, Endoh H, Masuhiro Y, et al. Activation of the Estrogen Receptor Through Phosphorylation by Mitogen-Activated Protein Kinase. Science. 1995;270: 1491-1494.
53. Campbell RA, Bhat-Nakshatri P, Patel NM, Constantinidou D, Ali S, Nakshatri H. Phosphatidylinositol 3-kinase/AKT-mediated activation of estrogen receptor alpha: a new model for anti-estrogen resistance. J Biol Chem. 2001;276: 9817-9824.
54. Yamnik RL, Digilova A, Davis DC, Brodt ZN, Murphy CJ, Holz MK. S6 kinase 1 regulates estrogen receptor alpha in control of breast cancer cell proliferation. J Biol Chem. 2009;284: 6361-6369.
55. Dowsett M. Overexpression of HER-2 as a resistance mechanism to hormonal therapy for breast cancer. Endocr Relat Cancer. 2001;8: 191-195.
56. Bose R, Kavuri SM, Searleman AC, et al. Activating HER2 mutations in HER2 gene amplification negative breast cancer. Cancer Discov. 2013;3: 224-237.
57. Smyth L, Piha-Paul S, Saura C, et al. Abstract PD3-06: Neratinib + fulvestrant for HER2-mutant, HR-positive, metastatic breast cancer: Updated results from the phase 2 SUMMIT trial. Cancer Res. 2019;79: PD3-06-PD03-06.
58. Turner N, Grose R. Fibroblast growth factor signalling: from development to cancer. Nat Rev Cancer. 2010;10: 116-129.
59. Dienstmann R, Rodon J, Prat A, et al. Genomic aberrations in the FGFR pathway: opportunities for targeted therapies in solid tumors. Ann Oncol. 2014;25: 552-563.
60. Reis-Filho JS, Simpson PT, Turner NC, et al. FGFR1 emerges as a potential therapeutic target for lobular breast carcinomas. Clin Cancer Res. 2006;12: 6652-6662.
61. Turner N, Pearson A, Sharpe R, et al. FGFR1 amplification drives endocrine therapy resistance and is a therapeutic target in breast cancer. Cancer Res. 2010;70: 2085-2094.
62. Formisano L, Stauffer KM, Young CD, et al. Correction: Association of FGFR1 with ERalpha Maintains Ligand-Independent ER Transcription and Mediates Resistance to Estrogen Deprivation in ER(+) Breast Cancer. Clin Cancer Res. 2019;25: 1433.
63. Formisano L, Lu Y, Servetto A, et al. Aberrant FGFR signaling mediates resistance to CDK4/6 inhibitors in ER+ breast cancer. Nat Commun. 2019;10: 1373.
64. Lei H, Deng C-X. Fibroblast Growth Factor Receptor 2 Signaling in Breast Cancer. Int J Biol Sci. 2017;13: 1163-1171.
65. Karlsson E, Waltersson MA, Bostner J, et al. High-resolution genomic analysis of the 11q13 amplicon in breast cancers identifies synergy with 8p12 amplification, involving the mTOR targets S6K2 and 4EBP1. Genes Chromosomes Cancer. 2011;50: 775-787.
66. deGraffenried LA, Friedrichs WE, Russell DH, et al. Inhibition of mTOR activity restores tamoxifen response in breast cancer cells with aberrant Akt Activity. Clin Cancer Res. 2004;10: 8059-8067.
67. Miller TW, Hennessy BT, Gonzalez-Angulo AM, et al. Hyperactivation of phosphatidylinositol-3 kinase promotes escape from hormone dependence in estrogen receptor-positive human breast cancer. J Clin Invest. 2010;120: 2406-2413.

68. Sanchez CG, Ma CX, Crowder RJ, et al. Preclinical modeling of combined phosphatidylinositol-3-kinase inhibition with endocrine therapy for estrogen receptor-positive breast cancer. Breast Cancer Res. 2011;13: R21.
69. Saal LH, Holm K, Maurer M, et al. PIK3CA mutations correlate with hormone receptors, node metastasis, and ERBB2, and are mutually exclusive with PTEN loss in human breast carcinoma. Cancer Res. 2005;65: 2554-2559.
70. Sherr CJ. Cancer cell cycles. Science. 1996;274: 1672-1677.
71. Butt AJ, McNeil CM, Musgrove EA, Sutherland RL. Downstream targets of growth factor and oestrogen signalling and endocrine resistance: the potential roles of c-Myc, cyclin D1 and cyclin E. Endocr Relat Cancer. 2005;12 Suppl 1: S47-59.
72. Geum D, Sun W, Paik SK, Lee CC, Kim K. Estrogen-induced cyclin D1 and D3 gene expressions during mouse uterine cell proliferation in vivo: differential induction mechanism of cyclin D1 and D3. Mol Reprod Dev. 1997;46: 450-458.
73. Thangavel C, Dean JL, Ertel A, et al. Therapeutically activating RB: reestablishing cell cycle control in endocrine therapy-resistant breast cancer. Endocr Relat Cancer. 2011;18: 333-345.
74. Wardell SE, Ellis MJ, Alley HM, et al. Efficacy of SERD/SERM Hybrid-CDK4/6 Inhibitor Combinations in Models of Endocrine Therapy-Resistant Breast Cancer. Clin Cancer Res. 2015;21: 5121-5130.
75. Walker AJ, Wedam S, Amiri-Kordestani L, et al. FDA Approval of Palbociclib in Combination with Fulvestrant for the Treatment of Hormone Receptor-Positive, HER2-Negative Metastatic Breast Cancer. Clin Cancer Res. 2016;22: 4968-4972.
76. Rane CK, Minden A. P21 activated kinase signaling in cancer. Semin Cancer Biol. 2019;54: 40-49.
77. Shrestha Y, Schafer EJ, Boehm JS, et al. PAK1 is a breast cancer oncogene that coordinately activates MAPK and MET signaling. Oncogene. 2012;31: 3397-3408.
78. Pardo OE, Seckl MJ. S6K2: The Neglected S6 Kinase Family Member. Front Oncol. 2013;3: 191.
79. Pathiraja TN, Stearns V, Oesterreich S. Epigenetic regulation in estrogen receptor positive breast cancer--role in treatment response. J Mammary Gland Biol Neoplasia. 2010;15: 35-47.
80. Yeruva SLH, Zhao F, Miller KD, et al. E2112: randomized phase iii trial of endocrine therapy plus entinostat/placebo in patients with hormone receptor-positive advanced breast cancer. NPJ Breast Cancer. 2018;4: 1.
81. Connolly RM, Rudek MA, Piekarz R. Entinostat: a promising treatment option for patients with advanced breast cancer. Future Oncol. 2017;13: 1137-1148.
82. Farabaugh SM, Boone DN, Lee AV. Role of IGF1R in Breast Cancer Subtypes, Stemness, and Lineage Differentiation. Front Endocrinol (Lausanne). 2015;6: 59.
83. Knowlden JM, Hutcheson IR, Barrow D, Gee JM, Nicholson RI. Insulin-like growth factor-I receptor signaling in tamoxifen-resistant breast cancer: a supporting role to the epidermal growth factor receptor. Endocrinology. 2005;146: 4609-4618.
84. Fox EM, Miller TW, Balko JM, et al. A kinome-wide screen identifies the insulin/IGF-I receptor pathway as a mechanism of escape from hormone dependence in breast cancer. Cancer Res. 2011;71: 6773-6784.
85. Lee AV, Jackson JG, Gooch JL, et al. Enhancement of insulin-like growth factor signaling in human breast cancer: estrogen regulation of insulin receptor substrate-1 expression in vitro and in vivo. Mol Endocrinol. 1999;13: 787-796.
86. Fagan DH, Yee D. Crosstalk between IGF1R and estrogen receptor signaling in breast cancer. J Mammary Gland Biol Neoplasia. 2008;13: 423-429.
87. Becker MA, Ibrahim YH, Cui X, Lee AV, Yee D. The IGF pathway regulates ERalpha through a S6K1-dependent mechanism in breast cancer cells. Mol Endocrinol. 2011;25: 516-528.
88. Robertson JF, Ferrero JM, Bourgeois H, et al. Ganitumab with either exemestane or fulvestrant for postmenopausal women with advanced, hormone-receptor-positive breast cancer: a randomised, controlled, double-blind, phase 2 trial. Lancet Oncol. 2013;14: 228-235.

89. Schoeffner DJ, Matheny SL, Akahane T, et al. VEGF contributes to mammary tumor growth in transgenic mice through paracrine and autocrine mechanisms. Lab Invest. 2005;85: 608-623.
90. Foekens JA, Peters HA, Grebenchtchikov N, et al. High tumor levels of vascular endothelial growth factor predict poor response to systemic therapy in advanced breast cancer. Cancer Res. 2001;61: 5407-5414.
91. Martin M, Loibl S, von Minckwitz G, et al. Phase III trial evaluating the addition of bevacizumab to endocrine therapy as first-line treatment for advanced breast cancer: the letrozole/fulvestrant and avastin (LEA) study. J Clin Oncol. 2015;33: 1045-1052.
92. Sasich LD, Sukkari SR. The US FDAs withdrawal of the breast cancer indication for Avastin (bevacizumab). Saudi pharmaceutical journal : SPJ : the official publication of the Saudi Pharmaceutical Society. 2012;20: 381-385.
93. Pardoll DM. The blockade of immune checkpoints in cancer immunotherapy. Nat Rev Cancer. 2012;12: 252-264.
94. Muenst S, Schaerli AR, Gao F, et al. Expression of programmed death ligand 1 (PD-L1) is associated with poor prognosis in human breast cancer. Breast Cancer Res Treat. 2014;146: 15-24.
95. Alley EW, Lopez J, Santoro A, et al. Clinical safety and activity of pembrolizumab in patients with malignant pleural mesothelioma (KEYNOTE-028): preliminary results from a non-randomised, open-label, phase 1b trial. Lancet Oncol. 2017;18: 623-630.
96. Vanhaesebroeck B, Guillermet-Guibert J, Graupera M, Bilanges B. The emerging mechanisms of isoform-specific PI3K signalling. Nat Rev Mol Cell Biol. 2010;11: 329-341.
97. Shimoi T, Hamada A, Yamagishi M, et al. PIK3CA mutation profiling in patients with breast cancer, using a highly sensitive detection system. Cancer Sci. 2018;109: 2558-2566.
98. Di Cosimo S, Baselga J. Phosphoinositide 3-Kinase Mutations in Breast Cancer: A “Good” Activating Mutation? Clinical Cancer Research. 2009;15: 5017-5019.
99. Karakas B, Bachman KE, Park BH. Mutation of the PIK3CA oncogene in human cancers. Br J Cancer. 2006;94: 455-459.
100. Ikenoue T, Kanai F, Hikiba Y, et al. Functional analysis of PIK3CA gene mutations in human colorectal cancer. Cancer Res. 2005;65: 4562-4567.
101. Liu P, Gan W, Inuzuka H, et al. Sin1 phosphorylation impairs mTORC2 complex integrity and inhibits downstream Akt signalling to suppress tumorigenesis. Nat Cell Biol. 2013;15: 1340-1350.
102. Liu P, Gan W, Inuzuka H, et al. Author Correction: Sin1 phosphorylation impairs mTORC2 complex integrity and inhibits downstream Akt signalling to suppress tumorigenesis. Nat Cell Biol. 2019;21: 662-663.
103. Lee JJ, Loh K, Yap YS. PI3K/Akt/mTOR inhibitors in breast cancer. Cancer Biol Med. 2015;12: 342-354.
104. Hardie DG, Ross FA, Hawley SA. AMPK: a nutrient and energy sensor that maintains energy homeostasis. Nat Rev Mol Cell Biol. 2012;13: 251-262.
105. Fernandez P, Carretero J, Medina PP, et al. Distinctive gene expression of human lung adenocarcinomas carrying LKB1 mutations. Oncogene. 2004;23: 5084-5091.
106. Green AS, Chapuis N, Lacombe C, Mayeux P, Bouscary D, Tamburini J. LKB1/AMPK/mTOR signaling pathway in hematological malignancies: From metabolism to cancer cell biology. Cell Cycle. 2011;10: 2115-2120.
107. Elkabets M, Vora S, Juric D, et al. mTORC1 inhibition is required for sensitivity to PI3K p110alpha inhibitors in PIK3CA-mutant breast cancer. Sci Transl Med. 2013;5: 196ra199.
108. Yang J, Nie J, Ma X, Wei Y, Peng Y, Wei X. Targeting PI3K in cancer: mechanisms and advances in clinical trials. Molecular cancer. 2019;18: 26-26.
109. Li J, Kim SG, Blenis J. Rapamycin: one drug, many effects. Cell Metab. 2014;19: 373-379.
110. Feldman ME, Apsel B, Uotila A, et al. Active-site inhibitors of mTOR target rapamycin-resistant outputs of mTORC1 and mTORC2. PLoS biology. 2009;7: e38-e38.

111. Wolff AC, Lazar AA, Bondarenko I, et al. Randomized phase III placebo-controlled trial of letrozole plus oral temsirolimus as first-line endocrine therapy in postmenopausal women with locally advanced or metastatic breast cancer. J Clin Oncol. 2013;31: 195-202.
112. Baselga J, Campone M, Piccart M, et al. Everolimus in postmenopausal hormone-receptor-positive advanced breast cancer. N Engl J Med. 2012;366: 520-529.
113. Guichard SM, Curwen J, Bihani T, et al. AZD2014, an Inhibitor of mTORC1 and mTORC2, Is Highly Effective in ER+ Breast Cancer When Administered Using Intermittent or Continuous Schedules. Mol Cancer Ther. 2015;14: 2508-2518.
114. Yu CC, Huang HB, Hung SK, et al. AZD2014 Radiosensitizes Oral Squamous Cell Carcinoma by Inhibiting AKT/mTOR Axis and Inducing G1/G2/M Cell Cycle Arrest. PLoS One. 2016;11: e0151942.
115. Kim ST, Kim SY, Klempner SJ, et al. Rapamycin-insensitive companion of mTOR (RICTOR) amplification defines a subset of advanced gastric cancer and is sensitive to AZD2014-mediated mTORC1/2 inhibition. Ann Oncol. 2017;28: 547-554.
116. Schmid P, Zaiss M, Harper-Wynne C, et al. Abstract GS2-07: MANTA - A randomized phase II study of fulvestrant in combination with the dual mTOR inhibitor AZD2014 or everolimus or fulvestrant alone in estrogen receptor-positive advanced or metastatic breast cancer. Cancer Res. 2018;78: GS2-07-GS02-07.
117. FDA. The therascreen PIK3CA RGQ PCR Kit - P190001 and P190004. Available from URL: https://www.fda.gov/medical-devices/recently-approved-devices/therascreen-pik3ca-rgq-pcr-kit-p190001-and-p190004 [accessed 05/09/2019, 2019].
118. Baselga J, Im SA, Iwata H, et al. Buparlisib plus fulvestrant versus placebo plus fulvestrant in postmenopausal, hormone receptor-positive, HER2-negative, advanced breast cancer (BELLE-2): a randomised, double-blind, placebo-controlled, phase 3 trial. Lancet Oncol. 2017;18: 904-916.
119. Krop IE, Mayer IA, Ganju V, et al. Pictilisib for oestrogen receptor-positive, aromatase inhibitor-resistant, advanced or metastatic breast cancer (FERGI): a randomised, double-blind, placebo-controlled, phase 2 trial. Lancet Oncol. 2016;17: 811-821.
120. Baselga J, Dent SF, Cortés J, et al. Phase III study of taselisib (GDC-0032) + fulvestrant (FULV) v FULV in patients (pts) with estrogen receptor (ER)-positive, PIK3CA-mutant (MUT), locally advanced or metastatic breast cancer (MBC): Primary analysis from SANDPIPER. Journal of Clinical Oncology. 2018;36: LBA1006-LBA1006.
121. Andre F, Campone M, Ciruelos EM, et al. SOLAR-1: A phase III study of alpelisib + fulvestrant in men and postmenopausal women with HR+/HER2– advanced breast cancer (BC) progressing on or after prior aromatase inhibitor therapy. Journal of Clinical Oncology. 2016;34: TPS618-TPS618.
122. Andre F, Ciruelos E, Rubovszky G, et al. Alpelisib for PIK3CA-Mutated, Hormone Receptor-Positive Advanced Breast Cancer. N Engl J Med. 2019;380: 1929-1940.
123. Castel P, Scaltriti M. Mechanisms of Resistance to PI3K and AKT Inhibitors. In: Yarden Y, Elkabets M, editors. Resistance to Anti-Cancer Therapeutics Targeting Receptor Tyrosine Kinases and Downstream Pathways. Cham: Springer International Publishing, 2018:117-146.
124. Juric D, Castel P, Griffith M, et al. Convergent loss of PTEN leads to clinical resistance to a PI(3)Kα inhibitor. Nature. 2015;518: 240-244.
125. Jia S, Liu Z, Zhang S, et al. Essential roles of PI(3)K-p110beta in cell growth, metabolism and tumorigenesis. Nature. 2008;454: 776-779.
126. Chakrabarty A, Sanchez V, Kuba MG, Rinehart C, Arteaga CL. Feedback upregulation of HER3 (ErbB3) expression and activity attenuates antitumor effect of PI3K inhibitors. Proc Natl Acad Sci U S A. 2012;109: 2718-2723.
127. Chandarlapaty S, Sawai A, Scaltriti M, et al. AKT inhibition relieves feedback suppression of receptor tyrosine kinase expression and activity. Cancer Cell. 2011;19: 58-71.
128. Serra V, Scaltriti M, Prudkin L, et al. PI3K inhibition results in enhanced HER signaling and acquired ERK dependency in HER2-overexpressing breast cancer. Oncogene. 2011;30: 2547-2557.

129. Castel P, Ellis H, Bago R, et al. PDK1-SGK1 Signaling Sustains AKT-Independent mTORC1 Activation and Confers Resistance to PI3Kalpha Inhibition. Cancer Cell. 2016;30: 229-242.
130. Le X, Antony R, Razavi P, et al. Systematic Functional Characterization of Resistance to PI3K Inhibition in Breast Cancer. Cancer Discov. 2016;6: 1134-1147.
131. Bosch A, Li Z, Bergamaschi A, et al. PI3K inhibition results in enhanced estrogen receptor function and dependence in hormone receptor-positive breast cancer. Sci Transl Med. 2015;7: 283ra251.
132. Tenbaum SP, Ordóñez-Morán P, Puig I, et al. β-catenin confers resistance to PI3K and AKT inhibitors and subverts FOXO3a to promote metastasis in colon cancer. Nature Medicine. 2012;18: 892.
133. Costa C, Ebi H, Martini M, et al. Measurement of PIP3 levels reveals an unexpected role for p110beta in early adaptive responses to p110alpha-specific inhibitors in luminal breast cancer. Cancer Cell. 2015;27: 97-108.
134. Juric D, Castel P, Griffith M, et al. Convergent loss of PTEN leads to clinical resistance to a PI(3)Kalpha inhibitor. Nature. 2015;518: 240-244.
135. Muellner MK, Uras IZ, Gapp BV, et al. A chemical-genetic screen reveals a mechanism of resistance to PI3K inhibitors in cancer. Nat Chem Biol. 2011;7: 787-793.
136. Liu P, Cheng H, Santiago S, et al. Oncogenic PIK3CA-driven mammary tumors frequently recur via PI3K pathway-dependent and PI3K pathway-independent mechanisms. Nature Medicine. 2011;17: 1116-1120.
137. Serra V, Eichhorn PJ, Garcia-Garcia C, et al. RSK3/4 mediate resistance to PI3K pathway inhibitors in breast cancer. J Clin Invest. 2013;123: 2551-2563.
138. Courjal F, Cuny M, Simony-Lafontaine J, et al. Mapping of DNA Amplifications at 15 Chromosomal Localizations in 1875 Breast Tumors: Definition of Phenotypic Groups. Cancer Res. 1997;57: 4360-4367.
139. Reis-Filho JS, Simpson PT, Turner NC, et al. FGFR1 Emerges as a Potential Therapeutic Target for Lobular Breast Carcinomas. Clinical Cancer Research. 2006;12: 6652-6662.
140. Kunii K, Davis L, Gorenstein J, et al. FGFR2-Amplified Gastric Cancer Cell Lines Require FGFR2 and Erbb3 Signaling for Growth and Survival. Cancer Res. 2008;68: 2340-2348.
141. Dutt A, Salvesen HB, Chen T-H, et al. Drug-sensitive FGFR2 mutations in endometrial carcinoma. Proceedings of the National Academy of Sciences. 2008;105: 8713-8717.
142. Cappellen D, De Oliveira C, Ricol D, et al. Frequent activating mutations of FGFR3 in human bladder and cervix carcinomas. Nature Genetics. 1999;23: 18-20.
143. Avet-Loiseau H, Li J-Y, Facon T, et al. High Incidence of Translocations t(11;14)(q13;q32) and t(4;14)(p16;q32) in Patients with Plasma Cell Malignancies. Cancer Res. 1998;58: 5640-5645.
144. Chesi M, Nardini E, Brents LA, et al. Frequent translocation t(4;14)(p16.3;q32.3) in multiple myeloma is associated with increased expression and activating mutations of fibroblast growth factor receptor 3. Nature Genetics. 1997;16: 260-264.
145. Babina IS, Turner NC. Advances and challenges in targeting FGFR signalling in cancer. Nat Rev Cancer. 2017;17: 318-332.
146. FDA. FDA approves first targeted therapy for metastatic bladder cancer. Available from URL: https://www.fda.gov/news-events/press-announcements/fda-approves-first-targeted-therapy-metastatic-bladder-cancer [accessed June 29th, 2019].
147. Yun Y-R, Won JE, Jeon E, et al. Fibroblast Growth Factors: Biology, Function, and Application for Tissue Regeneration. Journal of Tissue Engineering. 2010;1: 218142.
148. Holzmann K, Grunt T, Heinzle C, et al. Alternative Splicing of Fibroblast Growth Factor Receptor IgIII Loops in Cancer. J Nucleic Acids. 2012;2012: 950508.
149. Eswarakumar VP, Lax I, Schlessinger J. Cellular signaling by fibroblast growth factor receptors. Cytokine Growth Factor Rev. 2005;16: 139-149.

150. Sarabipour S, Hristova K. Mechanism of FGF receptor dimerization and activation. Nature Communications. 2016;7: 10262.
151. Presta M, Dell'Era P, Mitola S, Moroni E, Ronca R, Rusnati M. Fibroblast growth factor/fibroblast growth factor receptor system in angiogenesis. Cytokine Growth Factor Rev. 2005;16: 159-178.
152. Kandel J, Bossy-Wetzel E, Radvanyi F, Klagsbrun M, Folkman J, Hanahan D. Neovascularization is associated with a switch to the export of bFGF in the multistep development of fibrosarcoma. Cell. 1991;66: 1095-1104.
153. Werner S, Grose R. Regulation of wound healing by growth factors and cytokines. Physiol Rev. 2003;83: 835-870.
154. Casanovas O, Hicklin DJ, Bergers G, Hanahan D. Drug resistance by evasion of antiangiogenic targeting of VEGF signaling in late-stage pancreatic islet tumors. Cancer Cell. 2005;8: 299-309.
155. Kerbel RS. Therapeutic implications of intrinsic or induced angiogenic growth factor redundancy in tumors revealed. Cancer Cell. 2005;8: 269-271.
156. Zhong C, Saribekyan G, Liao C-P, Cohen MB, Roy-Burman P. Cooperation between FGF8b Overexpression and PTEN Deficiency in Prostate Tumorigenesis. Cancer Res. 2006;66: 2188-2194.
157. Tomlinson DC, Lamont FR, Shnyder SD, Knowles MA. Fibroblast growth factor receptor 1 promotes proliferation and survival via activation of the mitogen-activated protein kinase pathway in bladder cancer. Cancer Res. 2009;69: 4613-4620.
158. Nomura S, Yoshitomi H, Takano S, et al. FGF10/FGFR2 signal induces cell migration and invasion in pancreatic cancer. Br J Cancer. 2008;99: 305.
159. Welm BE, Freeman KW, Chen M, Contreras A, Spencer DM, Rosen JM. Inducible dimerization of FGFR1. development of a mouse model to analyze progressive transformation of the mammary gland. 2002;157: 703-714.
160. Acevedo VD, Gangula RD, Freeman KW, et al. Inducible FGFR-1 activation leads to irreversible prostate adenocarcinoma and an epithelial-to-mesenchymal transition. Cancer Cell. 2007;12: 559-571.
161. Kang Y, Massague J. Epithelial-mesenchymal transitions: twist in development and metastasis. Cell. 2004;118: 277-279.
162. Cappellen D, De Oliveira C, Ricol D, et al. Frequent activating mutations of FGFR3 in human bladder and cervix carcinomas. Nat Genet. 1999;23: 18-20.
163. van Rhijn BW, van Tilborg AA, Lurkin I, et al. Novel fibroblast growth factor receptor 3 (FGFR3) mutations in bladder cancer previously identified in non-lethal skeletal disorders. Eur J Hum Genet. 2002;10: 819-824.
164. di Martino E, L'Hote CG, Kennedy W, Tomlinson DC, Knowles MA. Mutant fibroblast growth factor receptor 3 induces intracellular signaling and cellular transformation in a cell type- and mutation-specific manner. Oncogene. 2009;28: 4306-4316.
165. Xiao S, Nalabolu SR, Aster JC, et al. FGFR1 is fused with a novel zinc-finger gene, ZNF198, in the t(8;13) leukaemia/lymphoma syndrome. Nat Genet. 1998;18: 84-87.
166. Yagasaki F, Wakao D, Yokoyama Y, et al. Fusion of ETV6 to fibroblast growth factor receptor 3 in peripheral T-cell lymphoma with a t(4;12)(p16;p13) chromosomal translocation. Cancer Res. 2001;61: 8371-8374.
167. Gallo LH, Nelson KN, Meyer AN, Donoghue DJ. Functions of Fibroblast Growth Factor Receptors in cancer defined by novel translocations and mutations. Cytokine Growth Factor Rev. 2015;26: 425-449.
168. Avet-Loiseau H, Li JY, Facon T, et al. High incidence of translocations t(11;14)(q13;q32) and t(4;14)(p16;q32) in patients with plasma cell malignancies. Cancer Res. 1998;58: 5640-5645.
169. Chesi M, Nardini E, Brents LA, et al. Frequent translocation t(4;14)(p16.3;q32.3) in multiple myeloma is associated with increased expression and activating mutations of fibroblast growth factor receptor 3. Nat Genet. 1997;16: 260-264.

170. Meredith SD, Levine PA, Burns JA, et al. Chromosome 11q13 Amplification in Head and Neck Squamous Cell Carcinoma: Association With Poor Prognosis. JAMA Otolaryngology–Head & Neck Surgery. 1995;121: 790-794.
171. Schuuring E. The involvement of the chromosome 11q13 region in human malignancies: cyclin D1 and EMS1 are two new candidate oncogenes--a review. Gene. 1995;159: 83-96.
172. Ormandy CJ, Musgrove EA, Hui R, Daly RJ, Sutherland RL. Cyclin D1, EMS1 and 11q13 amplification in breast cancer. Breast Cancer Res Treat. 2003;78: 323-335.
173. Sawey ET, Chanrion M, Cai C, et al. Identification of a therapeutic strategy targeting amplified FGF19 in liver cancer by Oncogenomic screening. Cancer Cell. 2011;19: 347-358.
174. Zhang K, Chu K, Wu X, et al. Amplification of FRS2 and activation of FGFR/FRS2 signaling pathway in high-grade liposarcoma. Cancer Res. 2013;73: 1298-1307.
175. Luo LY, Kim E, Cheung HW, et al. The Tyrosine Kinase Adaptor Protein FRS2 Is Oncogenic and Amplified in High-Grade Serous Ovarian Cancer. Mol Cancer Res. 2015;13: 502-509.
176. He X, Pang Z, Zhang X, et al. Consistent Amplification of FRS2 and MDM2 in Low-grade Osteosarcoma: A Genetic Study of 22 Cases With Clinicopathologic Analysis. Am J Surg Pathol. 2018;42: 1143-1155.
177. Andre F, Bachelot T, Campone M, et al. Targeting FGFR with dovitinib (TKI258): preclinical and clinical data in breast cancer. Clin Cancer Res. 2013;19: 3693-3702.
178. Angevin E, Lopez-Martin JA, Lin CC, et al. Phase I study of dovitinib (TKI258), an oral FGFR, VEGFR, and PDGFR inhibitor, in advanced or metastatic renal cell carcinoma. Clin Cancer Res. 2013;19: 1257-1268.
179. Motzer RJ, Porta C, Vogelzang NJ, et al. Dovitinib versus sorafenib for third-line targeted treatment of patients with metastatic renal cell carcinoma: an open-label, randomised phase 3 trial. Lancet Oncol. 2014;15: 286-296.
180. Musolino A, Campone M, Neven P, et al. Phase II, randomized, placebo-controlled study of dovitinib in combination with fulvestrant in postmenopausal patients with HR(+), HER2(-) breast cancer that had progressed during or after prior endocrine therapy. Breast Cancer Res. 2017;19: 18.
181. Soria JC, DeBraud F, Bahleda R, et al. Phase I/IIa study evaluating the safety, efficacy, pharmacokinetics, and pharmacodynamics of lucitanib in advanced solid tumors. Ann Oncol. 2014;25: 2244-2251.
182. Hui R, Pearson A, Cortes Castan J, et al. Lucitanib for the treatment of HR+ HER2- metastatic breast cancer (MBC) patients (pts): results from the multicohort phase II FINESSE trial. Ann Oncol. 2018;29: 289PD.
183. Bono P, Massard C, Peltola K, et al. 420PPhase I/II study of ODM-203, a selective dual FGFR/VEGFR inhibitor, in patients with advanced solid tumours. Annals of Oncology. 2018;29.
184. Paik PK, Shen R, Berger MF, et al. A Phase Ib Open-Label Multicenter Study of AZD4547 in Patients with Advanced Squamous Cell Lung Cancers. Clin Cancer Res. 2017;23: 5366-5373.
185. Smyth EC, Turner NC, Peckitt C, et al. Phase II multicenter proof of concept study of AZD4547 in FGFR amplified tumours. Journal of Clinical Oncology. 2015;33: 2508-2508.
186. Bang Y-J, Cutsem EV, Mansoor W, et al. A randomized, open-label phase II study of AZD4547 (AZD) versus Paclitaxel (P) in previously treated patients with advanced gastric cancer (AGC) with Fibroblast Growth Factor Receptor 2 (FGFR2) polysomy or gene amplification (amp): SHINE study. Journal of Clinical Oncology. 2015;33: 4014-4014.
187. Nogova L, Sequist LV, Perez Garcia JM, et al. Evaluation of BGJ398, a Fibroblast Growth Factor Receptor 1-3 Kinase Inhibitor, in Patients With Advanced Solid Tumors Harboring Genetic Alterations in Fibroblast Growth Factor Receptors: Results of a Global Phase I, Dose-Escalation and Dose-Expansion Study. J Clin Oncol. 2017;35: 157-165.
188. Kelly CM, Shoushtari AN, Qin LX, et al. A phase Ib study of BGJ398, a pan-FGFR kinase inhibitor in combination with imatinib in patients with advanced gastrointestinal stromal tumor. Invest New Drugs. 2019;37: 282-290.

189. Javle M, Lowery M, Shroff RT, et al. Phase II Study of BGJ398 in Patients With FGFR-Altered Advanced Cholangiocarcinoma. J Clin Oncol. 2018;36: 276-282.
190. Tabernero J, Bahleda R, Dienstmann R, et al. Phase I Dose-Escalation Study of JNJ-42756493, an Oral Pan-Fibroblast Growth Factor Receptor Inhibitor, in Patients With Advanced Solid Tumors. J Clin Oncol. 2015;33: 3401-3408.
191. Bahleda R, Italiano A, Hierro C, et al. Multicenter Phase I Study of Erdafitinib (JNJ-42756493), Oral Pan-Fibroblast Growth Factor Receptor Inhibitor, in Patients with Advanced or Refractory Solid Tumors. Clin Cancer Res. 2019.
192. Michael M, Bang YJ, Park YS, et al. A Phase 1 Study of LY2874455, an Oral Selective pan-FGFR Inhibitor, in Patients with Advanced Cancer. Target Oncol. 2017;12: 463-474.
193. Goyal L, Bahleda R, Furuse J, et al. FOENIX-101: A phase II trial of TAS-120 in patients with intrahepatic cholangiocarcinoma harboring FGFR2 gene rearrangements. Journal of Clinical Oncology. 2019;37: TPS468-TPS468.
194. Voss MH, Hierro C, Heist RS, et al. A Phase I, Multicenter, Dose-Escalation Study of the Oral Selective FGFR inhibitor Debio 1347 in Patients with Advanced Solid Tumors Harboring FGFR Gene Alterations. Clin Cancer Res. 2019.
195. Joerger M, Soo RA, Cho BC, et al. 379PA novel mRNA-based patient selection strategy identifies fibroblast growth factor receptor (FGFR) inhibitor-sensitive tumors: Results from rogaratinib Phase-1 study. Annals of Oncology. 2017;28.
196. Bendell JC, Rogers S, Xiang H, et al. FPA144-001: A first in human study of FPA 144, an ADCC-enhanced, FGFR2b isoform-selective monoclonal antibody in patients with advanced solid tumors. Journal of Clinical Oncology. 2016;34: 140-140.
197. Odonnell P, Goldman JW, Gordon MS, et al. 621 A Phase I Dose-escalation Study of MFGR1877S, a Human Monoclonal Anti-fibroblast Growth Factor Receptor 3 (FGFR3) Antibody, in Patients (pts) with Advanced Solid Tumors. Eur J Cancer. 2012;48: 191-192.
198. Harding TC, Long L, Palencia S, et al. Blockade of nonhormonal fibroblast growth factors by FP-1039 inhibits growth of multiple types of cancer. Sci Transl Med. 2013;5: 178ra139.
199. Tolcher AW, Papadopoulos KP, Patnaik A, et al. A phase I, first in human study of FP-1039 (GSK3052230), a novel FGF ligand trap, in patients with advanced solid tumors. Ann Oncol. 2016;27: 526-532.
200. Bronte G, Andreis D, Bravaccini S, et al. Sorafenib for the treatment of breast cancer. Expert Opin Pharmacother. 2017;18: 621-630.
201. FDA. FDA approves bevacizumab in combination with chemotherapy for ovarian cancer. Available from URL: https://www.fda.gov/drugs/resources-information-approved-drugs/fda-approves-bevacizumab-combination-chemotherapy-ovarian-cancer [accessed June 29th, 2019].
202. Dickler MN, Barry WT, Cirrincione CT, et al. Phase III Trial Evaluating Letrozole As First-Line Endocrine Therapy With or Without Bevacizumab for the Treatment of Postmenopausal Women With Hormone Receptor-Positive Advanced-Stage Breast Cancer: CALGB 40503 (Alliance). J Clin Oncol. 2016;34: 2602-2609.
203. FDA. FDA approves sunitinib malate for adjuvant treatment of renal cell carcinoma. Available from URL: https://www.fda.gov/drugs/resources-information-approved-drugs/fda-approves-sunitinib-malate-adjuvant-treatment-renal-cell-carcinoma [accessed June 29th, 2019].
204. Crown JP, Dieras V, Staroslawska E, et al. Phase III trial of sunitinib in combination with capecitabine versus capecitabine monotherapy for the treatment of patients with pretreated metastatic breast cancer. J Clin Oncol. 2013;31: 2870-2878.
205. Baselga J, Zamagni C, Gómez P, et al. RESILIENCE: Phase III Randomized, Double-Blind Trial Comparing Sorafenib With Capecitabine Versus Placebo With Capecitabine in Locally Advanced or Metastatic HER2-Negative Breast Cancer. Clin Breast Cancer. 2017;17: 585-594.e584.

206. Decker T, Overkamp F, Rosel S, et al. A randomized phase II study of paclitaxel alone versus paclitaxel plus sorafenib in second- and third-line treatment of patients with HER2-negative metastatic breast cancer (PASO). BMC Cancer. 2017;17: 499.
207. Grunewald S, Politz O, Bender S, et al. Rogaratinib: A potent and selective pan-FGFR inhibitor with broad antitumor activity in FGFR-overexpressing preclinical cancer models. Int J Cancer. 2019.
208. Fritsch C, Huang A, Chatenay-Rivauday C, et al. Characterization of the novel and specific PI3Kalpha inhibitor NVP-BYL719 and development of the patient stratification strategy for clinical trials. Mol Cancer Ther. 2014;13: 1117-1129.
209. Hudson K, Hancox UJ, Trigwell C, et al. Intermittent High-Dose Scheduling of AZD8835, a Novel Selective Inhibitor of PI3Kalpha and PI3Kdelta, Demonstrates Treatment Strategies for PIK3CA-Dependent Breast Cancers. Mol Cancer Ther. 2016;15: 877-889.
210. Weir HM, Bradbury RH, Lawson M, et al. AZD9496: An Oral Estrogen Receptor Inhibitor That Blocks the Growth of ER-Positive and ESR1-Mutant Breast Tumors in Preclinical Models. Cancer Res. 2016;76: 3307-3318.
211. Bello E, Colella G, Scarlato V, et al. E-3810 is a potent dual inhibitor of VEGFR and FGFR that exerts antitumor activity in multiple preclinical models. Cancer Res. 2011;71: 1396-1405.
212. Falcon BL, Chintharlapalli S, Uhlik MT, Pytowski B. Antagonist antibodies to vascular endothelial growth factor receptor 2 (VEGFR-2) as anti-angiogenic agents. Pharmacol Ther. 2016;164: 204-225.
213. Papadopoulos N, Martin J, Ruan Q, et al. Binding and neutralization of vascular endothelial growth factor (VEGF) and related ligands by VEGF Trap, ranibizumab and bevacizumab. Angiogenesis. 2012;15: 171-185.
214. Gao H, Korn JM, Ferretti S, et al. High-throughput screening using patient-derived tumor xenografts to predict clinical trial drug response. Nature Medicine. 2015;21: 1318.
215. Therasse P, Arbuck SG, Eisenhauer EA, et al. New guidelines to evaluate the response to treatment in solid tumors. European Organization for Research and Treatment of Cancer, National Cancer Institute of the United States, National Cancer Institute of Canada. J Natl Cancer Inst. 2000;92: 205-216.
216. Cheng DT, Mitchell TN, Zehir A, et al. Memorial Sloan Kettering-Integrated Mutation Profiling of Actionable Cancer Targets (MSK-IMPACT): A Hybridization Capture-Based Next-Generation Sequencing Clinical Assay for Solid Tumor Molecular Oncology. J Mol Diagn. 2015;17: 251-264.
217. Zehir A, Benayed R, Shah RH, et al. Mutational landscape of metastatic cancer revealed from prospective clinical sequencing of 10,000 patients. Nat Med. 2017;23: 703-713.
218. Prat A, Navarro A, Pare L, et al. Immune-Related Gene Expression Profiling After PD-1 Blockade in Non-Small Cell Lung Carcinoma, Head and Neck Squamous Cell Carcinoma, and Melanoma. Cancer Res. 2017;77: 3540-3550.
219. Gopal YN, Deng W, Woodman SE, et al. Basal and treatment-induced activation of AKT mediates resistance to cell death by AZD6244 (ARRY-142886) in Braf-mutant human cutaneous melanoma cells. Cancer Res. 2010;70: 8736-8747.
220. Deng W, Gopal YN, Scott A, Chen G, Woodman SE, Davies MA. Role and therapeutic potential of PI3K-mTOR signaling in de novo resistance to BRAF inhibition. Pigment Cell Melanoma Res. 2012;25: 248-258.
221. Kielkowska A, Niewczas I, Anderson KE, et al. A new approach to measuring phosphoinositides in cells by mass spectrometry. Adv Biol Regul. 2014;54: 131-141.
222. Ong CC, Gierke S, Pitt C, et al. Small molecule inhibition of group I p21-activated kinases in breast cancer induces apoptosis and potentiates the activity of microtubule stabilizing agents. Breast Cancer Res. 2015;17: 59.
223. Pearce LR, Alton GR, Richter DT, et al. Characterization of PF-4708671, a novel and highly specific inhibitor of p70 ribosomal S6 kinase (S6K1). Biochem J. 2010;431: 245-255.
224. Ronca R, Giacomini A, Di Salle E, et al. Long-Pentraxin 3 Derivative as a Small-Molecule FGF Trap for Cancer Therapy. Cancer Cell. 2015;28: 225-239.

225. Rudolph M, Anzeneder T, Schulz A, et al. AKT1 (E17K) mutation profiling in breast cancer: prevalence, concurrent oncogenic alterations, and blood-based detection. BMC Cancer. 2016;16: 622.
226. Grabiner BC, Nardi V, Birsoy K, et al. A diverse array of cancer-associated MTOR mutations are hyperactivating and can predict rapamycin sensitivity. Cancer Discov. 2014;4: 554-563.
227. Fedele CG, Ooms LM, Ho M, et al. Inositol polyphosphate 4-phosphatase II regulates PI3K/Akt signaling and is lost in human basal-like breast cancers. Proc Natl Acad Sci U S A. 2010;107: 22231-22236.
228. Pearson A, Smyth E, Babina IS, et al. High-Level Clonal FGFR Amplification and Response to FGFR Inhibition in a Translational Clinical Trial. Cancer Discov. 2016;6: 838-851.
229. Soria JC, DeBraud F, Bahleda R, et al. Phase I/IIa study evaluating the safety, efficacy, pharmacokinetics, and pharmacodynamics of lucitanib in advanced solid tumors. Ann Oncol. 2014;25: 2244-2251.
230. Rose S. FDA pulls approval for avastin in breast cancer. Cancer Discov. 2011;1: Of1-2.
231. Juric D, Janku F, Rodon J, et al. Alpelisib Plus Fulvestrant in PIK3CA-Altered and PIK3CA-Wild-Type Estrogen Receptor-Positive Advanced Breast Cancer: A Phase 1b Clinical Trial. JAMA Oncol. 2018: e184475.
232. Xu Y-C, Wang X, Chen Y, et al. Integration of Receptor Tyrosine Kinases Determines Sensitivity to PI3Kα-selective Inhibitors in Breast Cancer. Theranostics. 2017;7: 974-986.
233. Zhang C, Xu B, Liu P. Addition of the p110α inhibitor BYL719 overcomes targeted therapy resistance in cells from Her2-positive-PTEN-loss breast cancer. Tumor Biology. 2016;37: 14831-14839.
234. Gordon V, Banerji S. Molecular Pathways: PI3K Pathway Targets in Triple-Negative Breast Cancers. Clinical Cancer Research. 2013;19: 3738-3744.
235. Yuan Y, Wen W, Yost SE, et al. Combination therapy with BYL719 and LEE011 is synergistic and causes a greater suppression of p-S6 in triple negative breast cancer. Sci Rep. 2019;9: 7509-7509.
236. Razavi P, Chang MT, Xu G, et al. The Genomic Landscape of Endocrine-Resistant Advanced Breast Cancers. Cancer Cell. 2018;34: 427-438.e426.
237. Lefebvre C, Bachelot T, Filleron T, et al. Mutational Profile of Metastatic Breast Cancers: A Retrospective Analysis. PLoS Med. 2016;13: e1002201-e1002201.
238. Sun Q, Chen X, Ma J, et al. Mammalian target of rapamycin up-regulation of pyruvate kinase isoenzyme type M2 is critical for aerobic glycolysis and tumor growth. Proceedings of the National Academy of Sciences. 2011;108: 4129-4134.
239. Xiaoyu H, Yiru Y, Shuisheng S, et al. The mTOR Pathway Regulates PKM2 to Affect Glycolysis in Esophageal Squamous Cell Carcinoma. Technology in cancer research & treatment. 2018;17: 1533033818780063-1533033818780063.
240. He C-L, Bian Y-Y, Xue Y, et al. Pyruvate Kinase M2 Activates mTORC1 by Phosphorylating AKT1S1. Sci Rep. 2016;6: 21524.
241. Yasumizu Y, Hongo H, Kosaka T, et al. PKM2 under hypoxic environment causes resistance to mTOR inhibitor in human castration resistant prostate cancer. Oncotarget. 2018;9: 27698-27707.
242. Schmid P, Zaiss M, Harper-Wynne C, et al. Fulvestrant Plus Vistusertib vs Fulvestrant Plus Everolimus vs Fulvestrant Alone for Women With Hormone Receptor–Positive Metastatic Breast Cancer: The MANTA Phase 2 Randomized Clinical Trial. JAMA Oncology. 2019.
243. Bostner J, Ahnstrom Waltersson M, Fornander T, Skoog L, Nordenskjold B, Stal O. Amplification of CCND1 and PAK1 as predictors of recurrence and tamoxifen resistance in postmenopausal breast cancer. Oncogene. 2007;26: 6997-7005.
244. Mawson A, Lai A, Carroll JS, Sergio CM, Mitchell CJ, Sarcevic B. Estrogen and insulin/IGF-1 cooperatively stimulate cell cycle progression in MCF-7 breast cancer cells through differential regulation of c-Myc and cyclin D1. Mol Cell Endocrinol. 2005;229: 161-173.
245. Filmus J, Robles AI, Shi W, Wong MJ, Colombo LL, Conti CJ. Induction of cyclin D1 overexpression by activated ras. Oncogene. 1994;9: 3627-3633.

246. Daksis JI, Lu RY, Facchini LM, Marhin WW, Penn LJ. Myc induces cyclin D1 expression in the absence of de novo protein synthesis and links mitogen-stimulated signal transduction to the cell cycle. Oncogene. 1994;9: 3635-3645.
247. Jia Y, Chen L, Jia Q, Dou X, Xu N, Liao DJ. The well-accepted notion that gene amplification contributes to increased expression still remains, after all these years, a reasonable but unproven assumption. Journal of carcinogenesis. 2016;15: 3-3.
248. Mayhew CN, Carter SL, Fox SR, et al. RB Loss Abrogates Cell Cycle Control and Genome Integrity to Promote Liver Tumorigenesis. Gastroenterology. 2007;133: 976-984.
249. Harrington EA, Bruce JL, Harlow E, Dyson N. pRB plays an essential role in cell cycle arrest induced by DNA damage. Proc Natl Acad Sci U S A. 1998;95: 11945-11950.
250. Finn R, Jiang Y, Rugo H, et al. Biomarker analyses from the phase 3 PALOMA-2 trial of palbociclib (P) with letrozole (L) compared with placebo (PLB) plus L in postmenopausal women with ER + /HER2– advanced breast cancer (ABC). Annals of Oncology. 2016;27.
251. Semenova G, Chernoff J. Targeting PAK1. Biochem Soc Trans. 2017;45: 79-88.
252. Sridharan S, Basu A. S6 kinase 2 promotes breast cancer cell survival via Akt. Cancer Res. 2011;71: 2590-2599.
253. Claesson-Welsh L, Welsh M. VEGFA and tumour angiogenesis. Journal of Internal Medicine. 2013;273: 114-127.
254. Brown LF, Guidi AJ, Schnitt SJ, et al. Vascular Stroma Formation in Carcinoma in Situ, Invasive Carcinoma, and Metastatic Carcinoma of the Breast. Clinical Cancer Research. 1999;5: 1041.
255. Agrawal V, Kim DY, Kwon Y-G. Hhip regulates tumor-stroma-mediated upregulation of tumor angiogenesis. Experimental & molecular medicine. 2017;49: e289-e289.
256. Asano K, Nelson CM, Nandadasa S, et al. Stromal Versican Regulates Tumor Growth by Promoting Angiogenesis. Sci Rep. 2017;7: 17225-17225.
257. Golfmann K, Meder L, Koker M, et al. Synergistic anti-angiogenic treatment effects by dual FGFR1 and VEGFR1 inhibition in FGFR1-amplified breast cancer. Oncogene. 2018;37: 5682-5693.

Annex

Table S1. Tumor measurements from alpelisib waterfall

PDX	Day measurment	Alpelisib-treated tumors										Average	SD
PDX347	35	517,1	838,3									677,7	227,2
PDX313	35	354,5	760,3	1121,3	1103,3	1240,7	464,5	158,4	668,0	382,9	125,7	638,0	407,9
PDX244	35	700,0	449,9	174,4	559,2	391,3	101,6					396,1	227,0
STG201	35	349,7	332,6									341,1	12,1
PDX039	35	28,9	336,1	21,0	583,1	344,3						262,7	238,6
PDX284	35	114,4	182,5	32,1	269,2	138,7	45,4					130,4	88,5
PDX270	35	242,7	96,9	139,3	160,1	45,6	57,1					123,6	73,5
PDX098	35	174,5	239,0	179,8	1,8	30,2	45,1	140,7	134,8	114,4		117,8	78,2
PDX350	35	127,9	23,0									75,5	74,1
PDX293.1	35	25,9	-100,0	91,3		43,8	153,3	127,4	152,6			70,6	90,4
PDX225	35	-28,8	66,4	17,0	-29,0	104,9						26,1	59,1
PDX191	35	37,7	-9,3	67,5		58,2	55,4	-100,0	67,3			25,2	61,3
PDX450	35	-72,7	118,7									23,0	135,3
PDX251	35	9,2		-4,0	215,3	-74,5	-46,7					19,9	114,3
PDX293.2	35	103,5	-59,0	-33,2								3,8	87,3
PDX131	35	20,9	0,0	-1,5	-0,3	16,4	-48,2	28,2	2,5			2,2	23,3
PDX222	35	-28,8	56,2	-3,3	-58,4	51,1	-37,9					-3,5	47,7
PDX173	35	14,0	41,2		-75,5							-6,8	61,1
PDX251J	35	-24,4	-28,0									-26,2	2,6
PDX004	35	-84,9	14,0									-35,4	70,0
PDX399	35	-52,2	-18,9									-35,5	23,6
PDX118	35	15,7	-53,0	-75,0								-37,4	47,3
STG195	35	-30,1	-59,7	-44,4								-44,7	14,8
PDX153	35	-78,4	-61,5	-88,1	-100,0	-48,8	-100,0	-57,0	-44,9			-72,3	22,3

PDX	Day measurment	Non-treated tumors															Average	SD
PDX347	35	745,3	696,8														721,0	34,4
PDX313	35	1170,9	710,4	1160,0	515,7	1253,5	2420,8	1275,5	765,4	712,8	721,8						1070,7	547,4
PDX244	35	1328,7	864,4	619,0	483,2												823,8	371,7
STG201	35	696,4															696,4	0,0
PDX039	35	522,7	114,1	676,9													437,9	290,8
PDX284	35	862,4	905,5	255,4	1158,5	230,4	108,7										586,8	440,4
PDX270	35	1039,1	432,9	536,1	356,1												591,0	307,6
PDX098	35	366,1	462,3	1110,8	362,2	331,2	218,8	1253,7	653,8	168,7							547,5	387,3
PDX350	35	-50,7	27,4	-26,9	79,5	98,5											25,5	64,8
PDX293.1	35	62,8	107,4	183,4	398,7	177,6											186,0	129,1
PDX225	35	1328,7	864,4	619,0	483,2												823,8	371,7
PDX191	35	374,4	295,7	277,1	805,3	301,4	351,2	253,7	501,6								395,1	183,1
PDX450	35	697,7	722,2	-22,5	628,1												506,4	354,9
PDX251	35	78,9		143,2	301,1	73,1	72,9										133,9	98,1
PDX293.2	35	112,7	233,3														173,0	85,3
PDX131	35	170,9	192,5	73,1	413,4	131,5	65,2	327,8									196,3	130,2
PDX222	35	83,0	13,0	116,0	60,7												68,2	43,2
PDX173	35	226,1	168,8	370,5													255,1	103,9
PDX251J	35	260,4	166,6														213,5	66,3
PDX004	35	99,0	410,7	443,1													317,6	190,0
PDX399	35	138,4	148,5	180,6	312,1												194,9	80,2
PDX118	35	171,2	81,7	196,3	133,0	16,0											119,6	72,3
STG195	35	134,7	87,7	126,1	112,4	-12,7	335,0										130,5	113,6
PDX153	35	-78,4	117,8	139,4	-48,8	535,1	410,4	312,4	198,6	121,9	312,4	80,3	280,1	67,6	172,5	124,1	183,0	164,4

Table S2. MSKCC genetic alterations

		Clinical subtype	PAM50	Gene	Alteration	VAF	FC	Functional significance
1	PDX347	TNBC	Basal-like	*TSC2*	p.R1706H	0,4861		Unknown
				TP53	p.E286*	0,99367		STOP codon; probably deleterious
2	PDX313	ER+	Basal-like	*AKT1*	p.E17K	1		Activating
				MTOR	p.W1456G	0,45848		Hotspot; probably activating
				RPTOR	Amp		2,969	
				STK11	p.K191E	0,99568		Unknown
				NF1	p.L375V	0,49315		Unknown
				CCND2	Amp		4,417102	
3	PDX244	ER+	Luminal B	*ESR1*	p.Y537S	0,33046		Activating
				PTEN	DeepDel		-7,799	
				CDKN2A-p16	DeepDel		-10,2447	
				CDKN2A-p14	DeepDel		-10,2447	
				CDKN2B-p15	DeepDel		-10,2447	
				TP53	p.C176R	0,99701		Unknown
4	STG201	ER+	Basal-like	*PTEN*	p.G165fs	0,79348		Freameshift; probably deleterious
				AKT1	Amp		2,972	
				CDKN2A-p16	DeepDel		-24,4218	
				CDKN2A-p14	DeepDel		-24,4218	
				CDKN2B-p15	DeepDel		-24,4218	
				TP53	p.M237I	0,99046		Unknown
5	PDX039	ER+	Luminal B	*TSC1*	DeepDel		-134,559	
				TP53	p.V157I	0,50283		Unknown
6	PDX284	TNBC	Basal-like	*KRAS*	Amp		3,174215	
				CDKN1B	Amp		4,152269	
				CDKN2A-p16	DeepDel		-18,6043	
				CDKN2A-p14	DeepDel		-70,8797	
				CDKN2B-p15	DeepDel		-70,8797	
				CCND2	Amp		4,152269	
				TP53	p.R110P	0,99429		Unknown
				CCND1	p.D289N	0,98916		Unknown
7	PDX270	TNBC	Basal-like	*AKT3*	Amp		3,185	
				TP53	p.S241A	0,99771		Unknown
8	PDX098	ER+	Basal-like	*STK11*	p.E256*	0,99081		STOP codon; probably deleterious
				RB1	p.F721fs	0,95278		Freameshift; probably deleterious
9	PDX343	ER+	Luminal B	*PIK3CA*	Amp		3,460307	
				FGFR1	Amp		8,996102	
				PAK1	Amp		6,893325	
10	PDX350	ER+	Luminal B	*PIK3CA*	p.E545K	0,47625		Activating
				PIK3CA	p.G106R	0,50833		Activating
				TP53	p.V274D	1		Unknown
11	PDX293.1	ER+	Luminal B	*PIK3CA*	p.H1047R	0,46503		Activating
				CCND1	Amp		7,592632	
				FGF19	Amp		6,891573	
				FGF4	Amp		5,677674	
				FGF3	Amp		5,677674	
				PAK1	Amp		12,53335	
12	PDX225	ER+	Her2-enriched	*AKT1*	p.E17K	0,7426		Activating
				TP53	p.Q167*	0,98134		STOP codon; probably deleterious
13	PDX191	ER+	Luminal B	*FGFR1*	Amp		6,596039	
				CCND1	Amp		7,872381	
				FGF19	Amp		7,872381	
				FGF4	Amp		7,872381	
				FGF3	Amp		7,872381	
				PAK1	Amp		4,240987	
14	PDX450	ER+	Luminal B	*PIK3CA*	p.E545K	0,28878		Activating
				ESR1	p.D538G	0,33333		Activating
				PTEN	DeepDel		-7,16445	
				MAP3K1	p.S939C	0,48		
				MAPK3	p.E13_P14ins	0,23077		

15	PDX251	ER+	Luminal B	*PIK3CA*	p.E545K	0,63889		Activating
				STK11	p.R297S	0,9926		Unknown
				TP53	p.Y236C	1		Unknown
16	PDX293.2	ER+	Luminal B	*PIK3CA*	p.H1047R	0,5		Activating
				RB1	p.K810N	0,25333		Unknown
				RPS6KB2	Amp		3,241811	
				CCND1	Amp		10,26456	
				FGF19	Amp		10,26456	
				FGF4	Amp		10,26456	
				FGF3	Amp		10,26456	
				PAK1	Amp		10,26456	
17	PDX131	ER+	Luminal B	*ESR1*	p.Y537S	0,47716		Activating
				RPS6KB2	Amp		4,069918	
				CCND1	Amp		12,59344	
				FGF19	Amp		12,59344	
				FGF4	Amp		12,59344	
				FGF3	Amp		12,59344	
18	PDX222	HER2+	Her2-enriched	*ERBB2*	Amp		10,89051	
				TP53	p.R280G	0,98004		Unknown
19	PDX173	ER+/HER2+	Her2-enriched	*ERBB2*	Amp		14,34888	
20	PDX251J	ER+/HER2+	Her2-enriched	*ERBB2*	Amp		13,03212	
				TP53	p.E287*	0,99615		STOP codon; probably deleterious
21	PDX004	ER+	Luminal B					
22	PDX118	HER2+	Her2-enriched	*ERBB2*	Amp		11,43841	
23	PDX399	ER+	Luminal B	*PIK3CA*	p.H1047R	0,51463		Activating
24	STG195	ER+	Luminal B	*ERBB2*	Amp		7,923841	
				IGF1R	Amp		8,1173	
				ESR1	p.Y537S	0,51501		Activating
25	PDX153	HER2+	Her2-enriched	*PIK3CA*	p.K111E	0,6506		Activating
				ERBB2	Amp		21,6786	

VAF=Variant Allele Frequency

FC=Fold change

PD
SD
PR

Table S3. Tumor measurements from rogaratinib waterfall

PDX	Day measurment	Rogaratinib-treated tumors								Average	SD
PDX156	15	228,0	780,0	166,0	446,0	276,0	459,0	206,0	170,0	341,4	211,4
PDX302	21	175,1	68,6	177,3	169,0	63,4				130,7	59,2
PDX039	21	257,0	19,0	43,0						106,3	131,0
PDX288.2	11	82,0	23,4	209,6						105,0	95,2
PDX288	12	126,0	105,0	67,0	45,0	46,0				77,8	36,3
PDX343	21	35,8	100,8							68,3	46,0
PDX225	19	36,9	81,2							59,0	31,3
PDX131	21	39,0	94,0	-31,0	13,0					28,8	52,2
PDX251	36	-42,1	15,9	84,1	-16,6					10,3	54,6
PDX404	35	-17,0	17,0							0,0	24,0
PDX153	21	8,7	-9,4							-0,3	12,8
PDX222	21	-2,5	-9,8							-6,2	5,2
PDX293	32	-33,0	-21,0		18,0					-12,0	26,7
PDX426	21	-48,2	22,3							-13,0	49,8
PDX291	21	13,1	-38,0	-42,0	10,4	1,4	-39,0			-15,7	26,6
PDX325	43	-63,5	-12,0							-37,8	36,4
PDX191	12	-100,0	-16,0							-58,0	59,4

PDX	Day measurment	Non-treated tumors							Average	SD
PDX156	15	542,0	342,0	612,0	254,0	267,0	341,0	438,0	399,4	136,9
PDX302	21	390,0	284,0	614,0	262,0				387,5	161,0
PDX039	21	140,0	336,0						238,0	138,6
PDX288.2	11	294,4	221,4	268,4					261,4	37,0
PDX288	12	59,0	282,2	141,1	204,5	153,0	79,0		153,1	82,2
PDX343	21	236,1	130,2						183,2	74,9
PDX225	19	102,9	101,1						102,0	1,2
PDX131	21	309,0	96,0	104,0					169,7	120,7
PDX251	36	116,8	301,1	73,1	72,9	364,0	25,0		158,8	139,1
PDX404	35	201,2	103,4						152,3	69,2
PDX153	21	245,0	335,0						290,0	63,6
PDX222	21	121,0	39,0	141,0	140,0				110,3	48,4
PDX293	32	404,0	432,0	342,0	293,0				367,8	62,4
PDX426	21	100,9	23,1						62,0	55,0
PDX291	21	34,2	37,7	94,9	137,3	116,6			84,1	46,5
PDX325	43	89,2	67,3						78,3	15,5
PDX191	12	117,0	93,0	215,0	68,0				123,3	64,4

Table S4. Tumor measurements from lucitanib waterfall

PDX	Day measurment	Lucitanib-treated tumors								Average	SD
PDX156	22	-18,0	100,0	78,0	81,0	260,0	64,0			94,2	91,1
PDX288	22	32,0	-49,0	-32,0	-28,0	9,0	-40,0			-18,0	31,5
PDX302	21	-42,0	-6,0	-24,0	-25,0	-11,0				-21,6	14,0
PDX343	22	-53,0	-36,8	41,8	-36,8	41,8	-43,3	-61,9	-77,0	-28,2	45,2
PDX291	22	-47,0	-55,3	11,5	-24,3	-18,6	-25,5	-38,6		-28,3	21,9
PDX191	19	-31,0	-42,0	-40,0						-37,7	5,9
PDX325	22	-57,9	-26,3	-36,6						-40,3	16,1

PDX	Day measurment	Non-treated tumors										Average	SD
PDX156	22	455,0	605,0	420,0	741,0	275,0						499,2	179,0
PDX288	22	152,0	382,0	766,0	631,0	578,0						501,8	239,3
PDX302	21	390,0	284,0	614,0	262,0							387,5	161,0
PDX343	22	29,6	129,9	300,6	88,4	120,6	107,7	460,3	124,9			170,2	140,2
PDX291	22	34,2	37,7	94,9	206,0	238,0	137,3	116,6	85,0	66,0		112,8	70,8
PDX191	19	275,0	80,0									177,5	137,9
PDX325	22	-11,6	-56,5	82,8	95,3	0,0						22,0	64,9